Analytical Strategies for Quantitative Accuracy in Nontargeted Lipidomics

By

Lauren Bishop

A DISSERTATION

Submitted in partial satisfaction of the requirements for the degree of

DOCTOR OF PHILOSOPHY

in

Chemistry and Chemical Biology

in the

OFFICE OF GRADUATE STUDIES

of the

UNIVERSITY OF CALIFORNIA

DAVIS

Approved:

Oliver Fiehn, Chair

Carlito Lebrilla

Justin Siegel

Committee in Charge

2024

## Acknowledgements

First and foremost, I would like to thank my advisor Prof. Oliver Fiehn for his mentorship throughout my Ph.D. studies. I appreciate his passion and dedication to good science, and I am forever grateful for the freedom he gave me to explore and develop my own scientific interests. I would also like to thank Dr. Tong Shen and Dr. Uri Keshet for their continued support and guidance, which have been invaluable to my development as an analytical chemist. I want to also extend my gratitude to the past and present Fiehn lab members for their scientific support and, more importantly, their friendship. It has been a privilege to work alongside you all for the last five years. Finally, none of this would have been possible without the love and encouragement of my family, my partner, and all of the friends I have made throughout this journey – thank you all sincerely.

## Abstract

Nontargeted lipidomics enables both hypothesis-testing studies and discovery-driven projects in biology. However, classic nontargeted lipidomics analyses do not provide accurate concentration levels of the hundreds of annotated lipids, inhibiting comparison and integration of datasets across studies. Improvements in nontargeted lipidomics relies on developing more robust and standardized workflows that can provide reproducible, high-throughput quantification of diverse lipid species. Ultimately, achieving accurate quantification would ensure that results are reproducible and transferable across laboratories, thus enhancing the reliability of lipidomics as a tool for clinical and research applications. Hence, we explore strategies for sample preparation, data curation, and the integration of novel workflows to improve quantitative output in nontargeted analyses.

Chapter one evaluates the effectiveness of volumetric microsampling devices for nontargeted lipidomic profiling by liquid chromatography-high resolution tandem mass spectrometry (LC-HRMS/MS). With the promise of accessibility for larger studies, the commercial plasma separation card is thoroughly analyzed by standard method validation protocols and compared dually to dried blood spots and traditional venipuncture plasma. This includes tests of repeatability, recovery, and stability, as well as comparing the overall lipidome coverage offered by each approach. We found that the plasma separation card provides acceptable coverage for its low volume and correlates well to standard plasma responses, ultimately outperforming dried blood spots on nearly all criterion. Despite certain class-dependent limitations, we conclude that plasma separation cards represent the most reliable method for quantification in microsampling applications to lipidomic profiling.

Chapter two focuses on the curation of nontargeted lipidomic datasets, specifically in regards to the handling of multiple adduct forms of individual lipid species. Data analysis is

traditionally done using the primary or most abundant ion species per analyte. However, certain types of lipids, most notably neutral lipids, will form multiple adduct ions that can vary in relative abundance by up to 70% depending on chemical structure and/or ionization conditions. Here, we systematically evaluate adduct formation trends in diacylglycerols (DAG) across eight different biological matrices. First, the consistency of ratios between four established adduct forms of DAGs were reviewed for inter-sample variability, inter-class variability, and variations between study matrices. Next, several factors were investigated to better understand the variance, including acyl chain length, degree of unsaturation, and signal intensity. Lastly, different combinations of these adduct forms were tried to determine the impact of adduct joining on lipid quantification. Our findings emphasize the need for regular adduct evaluation within data processing methods to properly account for response variations that contribute to quantitative inaccuracies.

Chapter three provides a novel approach to absolute quantification within the classical nontargeted lipidomics workflow. Typical single-point calibrations are hindered by mismatched ionization effects between the internal standards and endogenous species, thus leading to quantitative inaccuracies when left uncorrected. Current acquisitions of large-scale data are capable of quantifying these effects with minimal intervention to the workflow. To this end, we propose the use of pooled QC dilutions to determine the extent of matrix effects in a given retention time window to better inform the alignment and subsequent matching of internal standards for quantitation. Additionally, we calculate response factors from the intensities of subclass-specific internal standards which can be further extrapolated to correct for large disparities in structure-based ionization efficiencies. This information is then used to inform subclass-specific approaches to internal standard selection for absolute quantification. This method demonstrates greater accuracy when compared to traditional single-point calibrations and can be readily applied to most nontargeted workflows.

# Table of Contents

# Chapter 1: Comprehensive Lipidomic Profiling by Plasma Separation Cards

*Reproduced from "Comprehensive Lipidomic Profiling by Plasma Separation Cards" by Lauren M. Bishop and Oliver Fiehn in Analytical and Bioanalytical Chemistry (2023).*

## 1.1 Abstract

Large-scale lipidomic analyses have been limited by the cost and accessibility of traditional venipuncture sampling. Microsampling techniques offer a less-invasive and more accessible alternative. From a single drop of blood, plasma separation cards (PSC) deliver two volumetric dried plasma samples which are studied here for profiling endogenous blood lipids. Six lots of EDTA-treated human whole blood were used to compare PSC, dried blood spot analyses (DBS), and classic wet plasma extractions. Six replicate extractions were performed for each lot. Nontargeted lipidomics was performed by liquid chromatography-high resolution tandem mass spectrometry. Lipids were annotated by accurate mass/retention time matching and MS/MS spectral library matching using peak intensities for quantitation. Four hundred ninety-eight compounds covering 24 lipid subclasses were annotated. Inter-lot repeatability was evaluated by the percent relative standard deviation (%RSD) for each lot, giving median %RSD values across the lots at 14.6% for PSC, 9.3% for DBS, and 8.6% for wet plasma. Strong correlations of lipid peak intensities between wet plasma and PSCs were observed, but less for DBS. Lipid recovery and stability were comparable between the PSC and DBS samples, with roughly 60% of annotated lipids stable at room temperature after 28 days. Overall, PSCs provide a better alternative for quantitative blood lipidomic analyses compared to dried blood spots. However, problems with lipid stability for samples handled and shipped at room temperature are currently unavoidable outside of a clinical setting. Data transferability and comparability to standard plasma is lipid and lipid class dependent.

## 1.2 Introduction

Lipidomics focuses on the high-throughput profiling and quantification of lipids. As essential molecules, lipids participate in many biological functions, and the analysis of these endogenous lipids serves to expand our understanding of disease pathologies [1]. Nontargeted lipidomic assays are becoming more robust by liquid-chromatography-high-resolution tandem mass spectrometry (LC-HRMS/MS), with possible applications in clinical research such as Alzheimer's disease and cardiovascular diseases [2,3,4].

For clinical applications, traditional venipuncture sampling and analysis of blood specimen (plasma or serum) are mostly used. However, classic clinical and epidemiological studies face multiple obstacles. Recruitments and retention of patients is time-consuming and costly, especially for healthy controls that are less likely to present at a clinic. Secondly, populations that live in remote areas, have reason to mistrust institutions, or people in adverse socioeconomic circumstances are difficult to convince to undertake the efforts necessary to participate. Third, longitudinal studies and studies with homebound patients are increasingly challenging to perform in classic clinical settings.

For these reasons, subject participation should be empowered by at-home blood sampling. Here, microsampling techniques have provided a less invasive, more accessible, and cheaper alternative. Whole blood microsampling is most commonly used, involving minimally invasive techniques such as finger-prick or heel-stick. Dried blood spots (DBS) are the most common form of microsampling devices. While they have served as a mainstay in newborn screening for the last several decades, recent applications of dried blood spots have included therapeutic drug monitoring, targeted metabolite screenings, and lipidomic analyses [5,6,7]. Nontargeted lipidomics by DBS has been generally successful; however, significant challenges remain to meet

the demands for accurate quantification [8]. The most notable disadvantage of DBS is hematocrit, or the ratio of red blood cells in whole blood, which can vary between subjects and impact the quantity of specific lipids. Although there have been efforts to measure and correct for hematocrit variations, there are still no standardized approaches to overcoming this issue [9]. Additionally, the non-volumetric aspect of DBS impedes straightforward translation to in vivo concentrations, which is an important prerequisite for clinical application [10].

In response to these limitations, several volumetric microsampling devices have been introduced, though the complexity of whole blood remains a concern. Telimmune Plasma Separation Cards (PSC), formerly Noviplex, were introduced in 2012 [11] and produce two, 3.2-μL-volume dried plasma spot samples that are highly reproducible and stable at ambient temperatures. Figure 1 illustrates the principle schema of such plasma separation cards. PSC devices have shown promising results in their application to toxicological studies and targeted metabolite quantitation [11, 12]. Considering the independence from hematocrit and volumetric compatibility to traditional venipuncture plasma, application of the PSC is an exciting prospect for the advancement of human blood lipidomic analyses. The primary goal of our work is to validate PSCs as an acceptable alternative to venipuncture plasma for nontargeted lipidomic profiling. Following standard lipidomics workflows for sample preparation and data analysis [8, 13], evaluations of inter-subject repeatability, intensity correlations, analyte recovery, and storage stability are made to assess the performance of the sampling methods. Additionally, we here compare the PSC devices to DBS samples to determine whether they offer an improved approach to quantitative lipidomics.

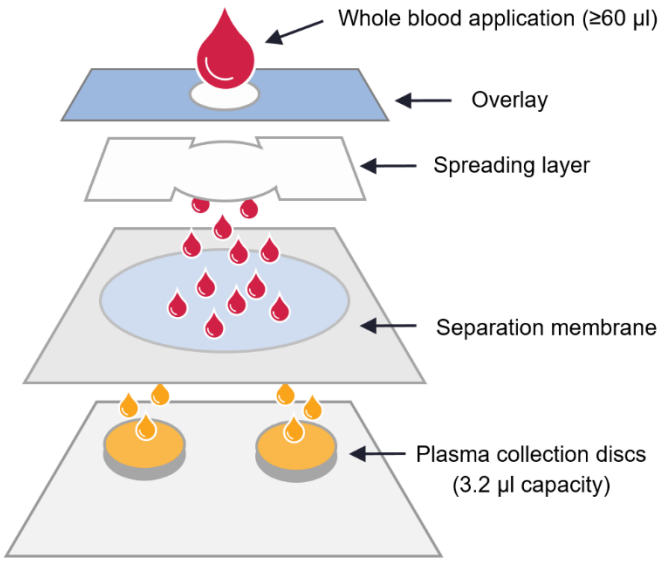


**Figure 1.1:** Illustration of a commercial plasma separation card.

## 1.3 Materials and Methods

### 1.3.1 Materials

UltimateSPLASH ONE lipidomic standards and supplemental standards of oleic acid-D9, arachidonic acid-D11, cholesterol-D7, and C17-sphingosine were purchased from Avanti Polar Lipids. Additional supplement standards of decanoyl-L-carnitine-D3, dodecanoyl-L-carnitine-D3, and octadecanoyl-L-carnitine-D3 were purchased from Cambridge Isotope Laboratories, and palmitic acid-D3 was purchased from CDN Isotopes. All reagents used were of LC-MS grade.

Telimmune DUO plasma separation cards were obtained from Novilytic, now Telimmune. Whatman® 903 Protein saver cards purchased from Sigma-Aldrich were used for dried blood spot sampling. Human whole blood was obtained through BioIVT. Six individual matrix lots treated with K2EDTA and another lot treated with 3.8% sodium citrate were used for the initial analysis. An additional lot of K2EDTA-treated human whole blood was purchased from BioIVT to evaluate storage stability.

### 1.3.2 Sample Preparation for Lipidomic Analyses

Seventy-five microliter of human whole blood was applied by pipette to each Telimmune DUO Plasma Separation Card. After 3 min, the top layer of the plasma separation card was removed, exposing two collection discs each containing 3.2 μL of the plasma fraction. The collection discs were dried for approximately 15 min and placed into the original packaging with desiccant for later extraction. Similarly, 75 μL of K2EDTA-treated whole blood was added onto Whatman® 903 Protein saver cards for each individual dried blood spot. The cards were dried for approximately 3 h and stored with desiccant in an air-tight bag. The remaining whole blood was left at room temperature for 45 min and centrifuged at 3400 rpm for 15 min to isolate the wet plasma. No hemolysis was observed. All samples were stored overnight at −20°C before extraction.

To evaluate recovery, a spiked solution was prepared using the following internal standards: 1 mL of UltimateSPLASH ONE mix, 0.5 μL decanoyl-L-carnitine-D3, 1.0 μL dodecanoyl-L-carnitine-D3, 1.5 μL octadecanoyl-L-carnitine-D3, 75 μL palmitic acid-D3, 25 μL arachidonic acid-D11, and 50 μL each of oleic acid-D9, cholesterol-D7, and C17-sphingosine. All supplemental standards were pulled from a 1 mg/mL stock solution. The mix was then dried down and resuspended with 1 mL of methanol. Two microliter of the standard solution was aliquoted directly onto the dried spots, dried for approximately 20 min, and extracted immediately.

For sample extraction, one collection disc containing 3.2 μL of dried plasma was placed in a 1.5-mL polypropylene tube. Dried blood spot samples were collected using a 6-mm punch to replicate the diameter of the plasma separation card disc. Additionally, 3.2 μL aliquots of wet plasma were used to maximize comparability between the sample types. Blank spots in replicates of six from both the PSC and DBS cards were used in addition to extraction method blanks to

evaluate potential contaminants. All samples were suspended in 225 µL of -20°C cold methanol treated with the UltimateSPLASH ONE and supplemental standards. 225 µL of internal standard-free methanol was used to suspend the recovery samples. 750 µL of -20°C cold methyl-tert-butyl ether (MTBE) containing a cholesteryl ester 22:1 standard was added to each sample and then vortexed for 10 minutes. Next, 188 µL of LC-MS grade water was added and vortexed for 5 minutes to induce a phase separation. Samples were centrifugated for 2 minutes at 14,000 x g before 700 µL of the upper non-polar layer was collected and dried. The remaining fractions of matrix-containing samples were combined to form pooled QC samples. Samples were resuspended using 50 µL of methanol/toluene (9:1, v/v) with 50ng/mL of 12-[(cyclohexylamine) carbonyl]amino]-dodecanoic acid (CUDA) and stored at -20°C until analysis.

### 1.3.3 Sample Preparation for Storage Stability Evaluation

Briefly, an additional lot of K2EDTA-treated whole blood was used to prepare samples to evaluate short-term storage stability at room temperature and −20°C conditions. Following the sample preparation protocols previously stated, samples were prepared in replicates of six for time points of 1 day, 7 days, and 28 days for each storage condition. Plasma separation card and dried blood spot samples were stored in air-tight bags with desiccant, while wet plasma samples were pre-aliquoted into 1.5-mL polypropylene tubes. Day zero and blank card samples were extracted on the same day of preparation to provide baseline data. Method blank and bioreclamation plasma samples were also extracted at each time point to provide quality control. All stability test samples were extracted and prepared for analysis as described above.

### 1.3.4 LC-MS/MS Data Acquisition

For nontargeted lipidomic analysis, 5 μL of the resuspended non-polar phase was injected into a Thermo Fisher Scientific Vanquish UHPLC+ liquid chromatography system coupled to a Q-Exactive HF orbital ion trap mass spectrometer. The LC system was equipped with a Waters Acquity UPLC CSH C18 column (100 mm × 2.1 mm; 1.7 μm) and Waters Acquity VanGuard CSH C18 precolumn (5 mm × 2.1 mm; 1.7 μm). The column compartment and mobile phase preheater were set at 65°C, and the mobile phase flow rate was 0.6 mL/min. As demonstrated previously [14], different mobile phases were employed for positive mode and negative mode analysis to improve lipid coverage. The positive mobile phase A was acetonitrile/water (60/40, v/v) with 0.1% formic acid and 10 mM ammonium formate as modifiers and mobile phase B consisted of isopropanol/acetonitrile (90:10, v/v) with 0.1% formic acid and 10 mM ammonium formate. Mobile phase A for negative mode analysis was prepared using acetonitrile/water (60/40, v/v) with 10 mM ammonium acetate, while mobile phase B consisted of isopropanol/acetonitrile (90/10, v/v) with 10 mM ammonium acetate. Both modes shared the same gradient with B started at 15%, increasing to 30% between 0 and 2 min. B was brought from 30 to 48% between 2 and 2.5 min, 48 to 82% between 2.5 and 11 min, and 82 to 99% from 11 to 11.5 min. 99% B was maintained between 11.5 and 12 min and then brought back to 15% between 12 and 12.1 min and held there between 12.1 and 14.2 min for re-equilibration. The injection needle was washed for 10 s before and after each injection with isopropanol.

Positive mode and negative mode electrospray ionization (ESI) used a spray voltage of 3.6 kV, capillary temperature of 300°C, sheath gas flow rate of 60 units nitrogen, and auxiliary gas flow rate of 25 units nitrogen. Data were collected from 0 to 13 min of the LC gradient in scan range 120–1700 m/z using data-dependent acquisition (DDA) with the top four ions from each

MS1 scan being selected for MS/MS fragmentation. DDA MS/MS was acquired with a stepped normalized collision energy of 20%, 30%, and 40%. MS1 spectra were collected with a resolving power setting of 60,000, and MS/MS spectra were collected at a resolving power setting of 15,000. To increase the total number of MS/MS spectra, five consecutive runs were made using the R package "IE-Omics" [15] for both positive and negative electrospray conditions. All spectra were stored in centroid, ".raw" format.

### 1.3.5 Data Analysis

The data were converted from ".raw" format into ".abf" format using the Analysis Base File converter. Deconvolution, peak picking, alignment, and compound identification were completed through open source software MS-DIAL v4.60 [16]. Compounds were annotated by matching retention times, accurate precursor masses, and MS/MS fragmentation patterns against the LipidBlast library [17]. The primary result data matrix was processed with MS-FLO software to identify ion adducts, duplicate peaks, and isotopic features [18]. Peak height was used as spectral intensity for all data analysis. Samples were normalized first by CUDA internal standard intensities followed by Systematic Error Removal by Random Forest (SERRF) [19] to correct for instrument signal drifts. Internal standards added during extraction were used to assess injection quality and demonstrated a relative standard deviation of less than 6% across all matrix-containing samples after normalization. For lipids that were detected in both acquisition modes, values with the lowest relative standard deviation in quality control samples were kept. The quantitative results of lipids were calculated using the peak heights and the known concentrations of the spiked internal standards and then normalized to sample volume.

## 1.4 Results

### 1.4.1 Lipidome Coverage

We identified 498 unique lipids with 237 of these knowns characterized by accurate mass, retention time, and MS/MS spectral matching. These annotations are detailed as 357 lipid species and 67 labeled internal standards confidently detected and characterized in ESI positive mode, compared to 306 known compounds and 54 labeled internal standards annotated in ESI negative mode. Roughly 80% of the known compounds were found in all three sample types. The remaining 20% of annotations were either unique to a specific sample type or were measured at contaminant levels in one of the microsampling devices. A complete list of the classifications can be found in Supplemental Table S1. To compare the analytical performance of each sample type, 315 compounds that were found in at least 95% of matrix-containing samples were utilized for data analysis. As shown in Fig. 2, these lipids are represented by 17 subclasses of 5 main lipid classes [20]: 10% fatty acyls (FA), 16% glycerolipids (GL), 50% glycerophospholipids (GP), 21% sphingolipids (SP), and 3% sterol lipids (ST).

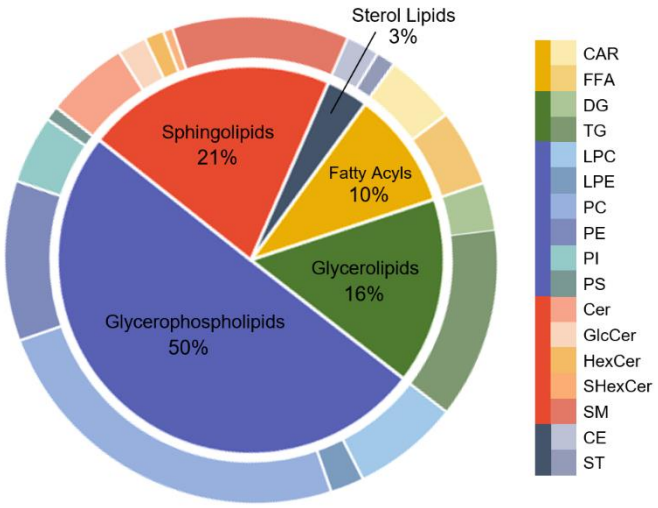


**Figure 1.2:** Classification of lipids found in ≥95% of samples (n=315).

### 1.4.2 Data Comparability

The performance of the PSC and DBS sampling devices were evaluated qualitatively through inter-subject repeatability and quantitatively by average lipid peak intensities as compared to wet plasma. Median percent relative standard deviation (%RSD) was calculated for each of the 315 lipids using 6 replicates prepared from the same whole blood lot. For the EDTA-treated samples, the median %RSD of the six individual lots were used to visualize overall repeatability in the three sample types, as shown in Fig. 3a. The median %RSD across all lipids for the wet plasma, PSC, and DBS samples is 8.6%, 14.6%, and 9.3% respectively. The PSC samples show elevated variability in contrast to the other sampling methods due to notably increased variation of three lipid subclasses: free fatty acids (FFA), diglycerides (DG), and ceramides (Cer). We therefore investigated whether this increase was due to the citrate anticoagulant used in PSCs or if the variation was being influenced by blood separation mechanisms during PSC usage. We did not find major differences between the standard wet plasma and PSC-treated samples that were prepared using BioIVT citrated whole blood, but in both cases, we found the same trend of increased lipid subclasses (Fig. 3b) compared to EDTA plasma. This finding suggests that citrate anticoagulants induce this difference in lipid subclass abundance compared to EDTA-plasma rather than the mechanisms of separation within the PSC itself. Indeed, the same three lipid subclasses largely contributed to the increase in median %RSD observed between PSCs and wet plasma or DBS (Fig. 3a). When comparing EDTA- and citrate-derived plasma samples, the median %RSD increased by an average of 7.8% for free fatty acids, diglycerides, and ceramide lipids.

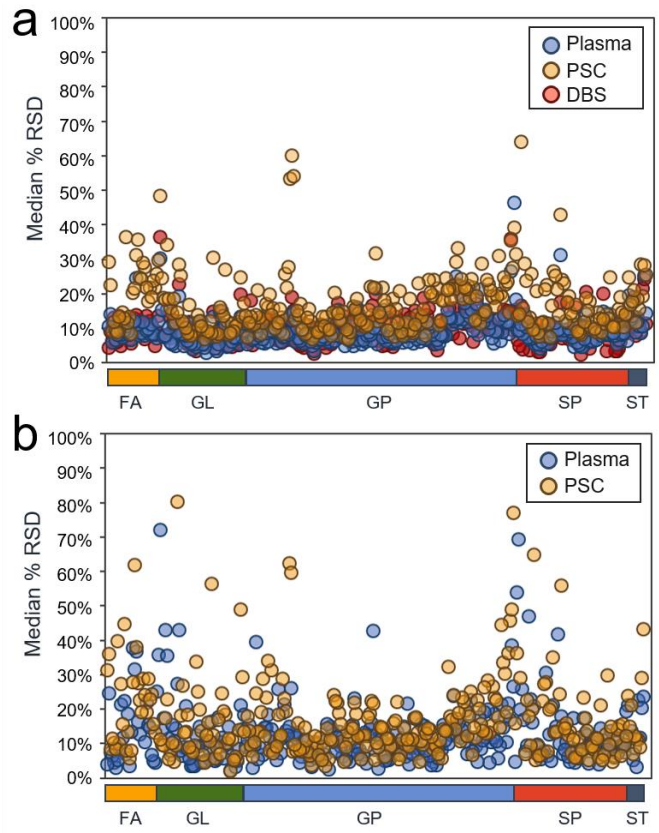


**Figure 1.3: a** Median percent relative standard deviation (%RSD) values across all annotated lipids for EDTA-treated samples. Median %RSD for plasma, PSC, and DBS samples is 8.6%, 14.6%, and 9.3%, respectively. **B** Median %RSD of individual lipids for citrate-treated samples. Overall %RSD is 10.5% and 13.6% for plasma and PSC samples, respectively.

Quantitative potential was evaluated through correlations between average lipid peak intensities, or peak heights, and were assessed by one-to-one comparisons of the microsampling devices to wet plasma. Figure 4a shows the correlations of lipid intensities between the wet plasma and PSC samples derived from EDTA-treated whole blood. With an R2=0.9851, these two sample types show a very strong correlation across all lipid classes, although the PSC samples presented an overall median percent change of −34% in peak intensities compared to the wet plasma extracts of the same volume. A weaker linear correlation was observed at R2=0.9115 in the comparison of wet plasma and DBS intensities, as shown in Fig. 4b. Interestingly, the change in median lipid

intensities was more than twice as high at 118% (Supplemental Table S2). This observation was expected due to the additional red blood components present in whole blood (as used for DBS) compared to wet plasma, in addition to different volumes used between DBS and PSC methods. It is important to note that fatty acyls, glycerophospholipids, and sphingolipids species were significantly increased in the DBS samples compared to PSC and standard plasma (Fig. 4b), making direct comparisons of DBS data to clinical human cohort data difficult. In Fig. 4c, the average intensities from the citrate-treated samples are compared. Similar to Fig. 4a, the citrate-treated PSC and wet plasma samples are strongly correlated across all lipid classes with a median percent change of −26%. This value is consistent across most lipid subclasses, with an exception of diglyceride species which exhibit average intensities 46% higher in the PSC samples than the citrate-treated plasma samples.

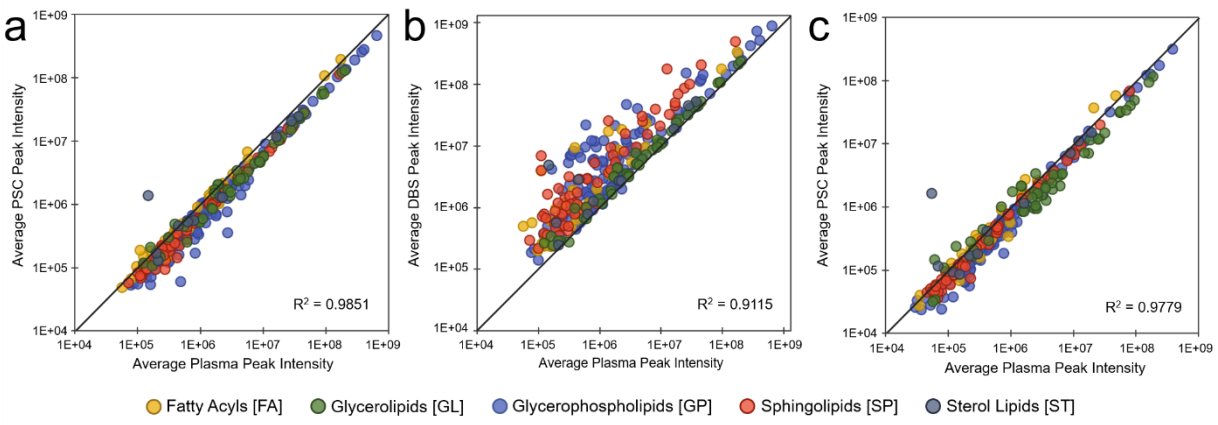


**Figure 1.4: a** Correlation between average peak intensities in EDTA-treated PSC and EDTA plasma samples. **b** Correlation between average peak intensities in EDTA-treated DBS and EDTA plasma samples. **c** Correlation between average peak intensities in citrate-treated PSC and citrate plasma samples. The median percent changes of lipid intensities for the three sample types in comparison to plasma are −34%, +118%, and −26%, respectively.

Additionally, the quantitative performance of each sampling method was evaluated through absolute quantitation by labeled internal standards. Twenty-eight endogenous lipids were selected and paired with a matching deuterated internal standard. Using the known concentrations

of the standards and the peak heights obtained during analysis, concentrations in nmol/mL were calculated for all three sample types and compared between the microsampling devices and wet plasma (Supplemental Fig. 1). The PSCs show strong correlation in absolute concentration for all 28 lipids without any additional corrections; however, the DBS samples require further volume normalization for direct comparison to wet plasma. The internal standard levels were not adjusted for recovery values in the PSC and DBS samples.

### 1.4.3 Recovery

Recovery experiments were performed by extracting an internal standard solution directly from the dried card samples. Upon evaluation of 61 representative internal standards, peak intensities decreased by an average of 1.42-fold in PSC recovery samples and 1.34-fold in DBS recovery samples. The change in internal standard response for the PSC samples is illustrated in Fig. 5a. While the 1.42-fold change is a representative average of the responses, the fold changes measured in the PSC recovery samples were calculated for each specific lipid subclass represented by the added internal standards (Fig. 5b). When applying these fold change values as correction factors to the corresponding classes of the endogenous lipids, much of the previously observed deviation in the PSC samples with respect to wet plasma was absolved, with an improved median percent change of -6% and an R2=0.993 (Fig. 5c).

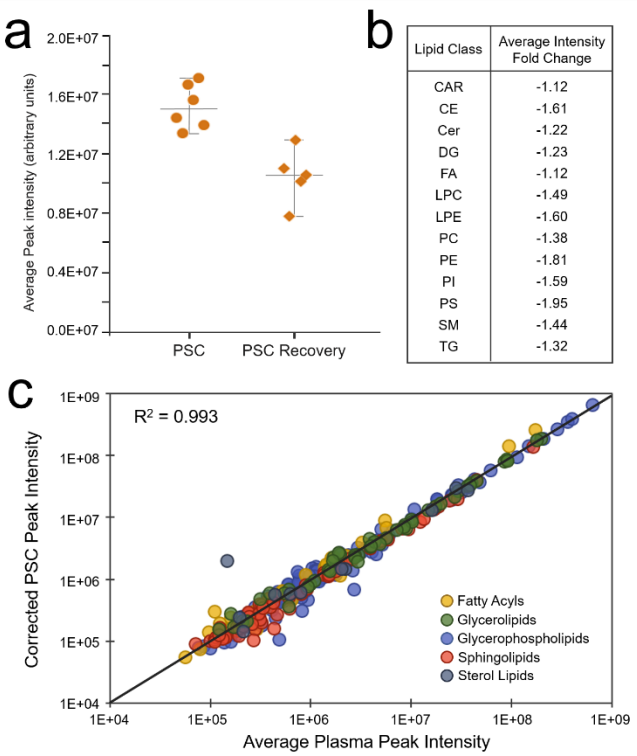


**Figure 1.5: a** Differences in peak intensities of regularly extracted lipid internal standards versus internal standards directly spotted onto the sample. **b** Intensity fold changes for each lipid class represented by the internal standards. c The fold changes applied as correction factors to the individual lipid intensities, improving the median percent change of PSCs to plasma to −6%.

### 1.4.4 Stability

Short-term stability was evaluated for room temperature and −20°C storage conditions at 1 day, 7 days, and 28 days after initial sample preparation. In this experiment, we annotated 554 unique lipid species. Three hundred forty-four lipids were present in at least 5 of 6 replicates at each time point at < 30%RSD on average for each sample type. These 344 lipids were used to evaluate stability. Stable compounds were defined as having < 30% change in average peak intensity from the baseline. Figure 6a shows the proportions of stable compounds across both microsampling devices at −20°C and room temperature as compared to the standard plasma at −20°C. Samples stored at −20°C proved most stable, with 95.9%, 92.2%, and 94.5% of the

compounds stable after 28 days for wet plasma, PSC, and DBS, respectively. For samples kept at room temperature, only 58.7% of compounds were stable after 28 days in PSC samples, and 55.5% in DBS samples. Trends between the PSC and DBS samples were overall consistent at room temperature conditions with both sample types identifying 72.7% of compounds as stable after 7 days.

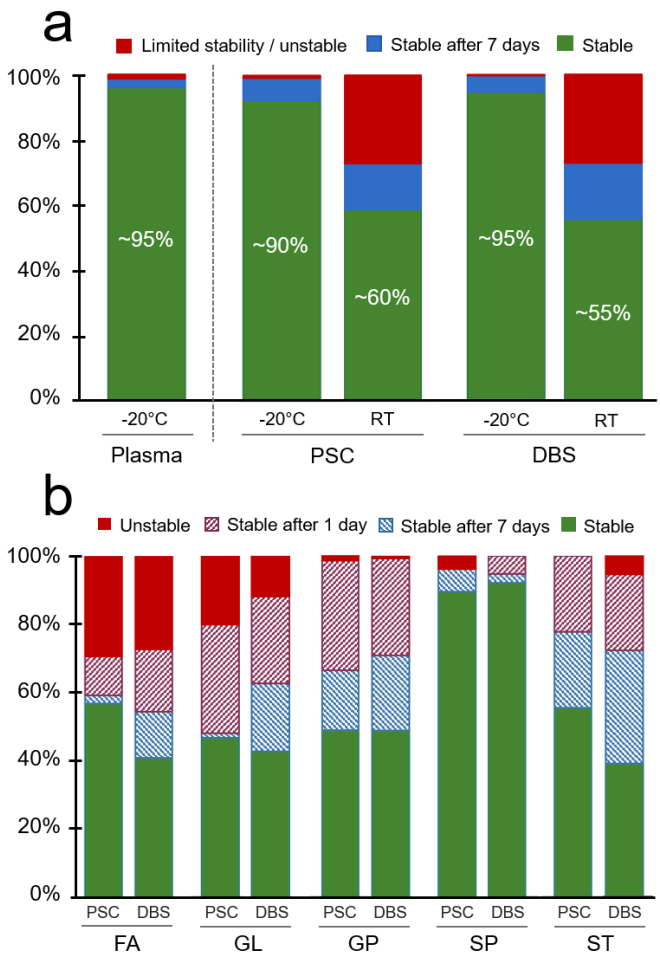


**Figure 1.6: a** Proportion of lipids at each temperature assigned to each stability category (n=344). Green indicates stability across days 1–28, blue indicates stability after 7 days of storage, and red indicates limited or no stability over the 28-day storage period. **b** Frequency of stability category per lipid class for PSC and DBS samples stored at room temperature.

After a detailed investigation of the performance of each lipid class within the PSC and DBS samples at room temperature, we found that free fatty acids were the least stable lipid subclass for both sampling devices (Fig. 6b). While 18 of 27 free fatty acids from DBS samples were stable after one day, only 5 of 27 remained stable after the 28-day time point. Similarly, only 14 of 27 free fatty acids were stable after one day at room temperature in the PSC samples, decreasing to 10 species determined as stable after 28 days of storage under room temperature. Each free fatty acid species labeled as unstable in PSCs showed an increase in intensity between day 0 and day 28, with 6 compounds exhibiting greater than a 3-fold change, including oleic acid (FA 18:1), linoleic acid (FA 18:2), and arachidonic acid (FA 20:4). This finding supports the notion that increases in free fatty acids are likely caused by lipase activities in blood samples, but not by oxidation through exposure to residual air during storage. From the glycerolipids, 11 diglyceride species were unstable at each time point in the PSC samples with all but one showing intensities between 2- and 3-fold higher than the baseline extracts. Consistent decrease in intensity was observed across all time points for nearly half of the annotated glycerophospholipids with, most notably, all 14 phosphatidylethanolamine (PE) species labeled as unstable following the day 1 time point for both PSC and DBS. In contrast, roughly 90% of sphingolipids remained stable through 28 days at room temperature for both sample types.

## 1.5 Discussion

Plasma sampling by venipuncture remains the gold standard for nontargeted lipidomic analyses. However, the detection and characterization of nearly 500 unique lipids by plasma separation cards indicates a promising future for accessible lipidomic profiling. While the overall data quality of the PSCs fared well against wet plasma, the use of citrate anticoagulant and its impact on specific lipid subclasses is a concern. Our observations of increased variability in the

free fatty acids, diglycerides, and ceramide lipids are supported by previous findings that the higher pH and ionic strength of sodium citrate can influence the ability to reliably measure specific lipids [21]. Conversely, other work has shown that citrate improves inter-subject repeatability for glycerophospholipids and sphingolipids [22]. From a quantitative perspective, diglycerides were the only subclass significantly impacted by the citrate additive with substantially elevated responses throughout the PSC samples. The high ionic strength of citrate is known to promote lipid release from lipoproteins and is likely a factor in the ion enhancement of specific lipids, such as the diglycerides in our analysis [21]. Nevertheless, most lipids extracted from PSCs appeared unaffected by the citrate and shared comparable repeatability and intensity levels to the control wet plasma.

Overall, we established that recovery was the largest contributing factor in data comparability to traditional wet plasma. Similar to most microsampling devices, both PSC and DBS sampling methods must overcome challenges in analyte recovery in order to provide accurate data. Previous studies have acknowledged the limitations of extracting dried spot samples with traditional methods, especially in the addition of internal standards during extraction [10]. However, treating dried matrix spots directly with internal standards is a time-consuming and often tedious task. Nonetheless, our analysis of directly applied internal standards and the implementation of subclass-specific correction factors was effective in amending deviation caused by lipid recovery. We recommend similar methods be employed to evaluate recovery in future applications of PSCs to ensure quantitative accuracy.

The quantitative compatibility and performance of PSCs proved superior to DBS with most lipid classes showing exceptional correlation to plasma peak intensities. While the comparison of wet plasma and DBS also yielded a positive correlation, the difference in matrix constitution

prevented true assessment of the quantitative performance of DBS. Attempts of improving quantitative analysis by DBS have included normalization by hemoglobin, automated hematocrit analysis, and use of reference standards though further validation of these methods is needed before regular application [6, 23,24,25]. With the larger goals of accessibility and clinical utility, our analysis shows the volumetric and hematocrit-independent PSC provides quantitative lipidomic results without the additional corrections that are required for DBS analyses.

While PSCs appear to be suitable for lipidomic analyses, regular implementation of microsampling devices continues to be limited by analyte stability. Our results revealed deficient stability following storage at room temperature with less than 60% of annotations remaining stable through 28 days for both PSC and DBS samples. Other studies have also encountered difficulty retaining endogenous compounds when dried samples are left unattended at ambient temperatures, with cumulative degradation attributed to enzymatic reactions, chemical hydrolysis, and oxidation [26,27,28]. For example, degradation of glycerolipids and glycerophospholipids during sample handling has been associated with phospholipase activity promoting the hydrolysis of glycerol backbones, leading to elevated levels of lysoglycerophospholipids and free fatty acids [29]. Additionally, the enzyme-catalyzed hydrolysis of triglycerides could explain our observations of elevated diglycerides and free fatty acid species. Successful efforts to overcome residual enzyme activity in dried matrix samples have included heat-treatments and flash freezing, though these methods are not accessible outside of a laboratory setting [29, 30]. New strategies for increasing stability of at-home sampling devices at room temperature have focused extensively on additives. Sample pretreatments of non-specific enzyme inhibitors and antioxidants such as phenylmethanesulfonyl fluoride (PMSF) and butylated hydroxytoluene (BHT) have proved effective in reducing the degradation of specific lipids [31, 32]. Obstacles remain with

incorporating additives to microsampling methodologies, but their usage could potentially improve the stability of PSCs in nonoptimal conditions. Moreover, in its current state we recommend storage at −20°C for PSC samples kept for longer than 7 days.

## 1.6 Conclusions

From our analysis, we can conclude that the plasma separation cards are an acceptable alternative to traditional venipuncture plasma for nontargeted lipidomic analyses. Nevertheless, complete data transferability and comparability with standard plasma is lipid and lipid class dependent. When compared to DBS, the overall data quality was consistent for both sampling devices; however, there are clear quantitative advantages to using PSCs, especially in clinical settings. The volumetric capabilities, independence from hematocrit variation, and commercial availability indicate a promising path forward for these plasma microsampling cards in lipidomic analyses. Further validation with clinical cohorts is recommended before regular clinical application.

## 1.7 References


(1) Stephenson DJ, Hoeferlin LA, Chalfant CE. Lipidomics in translational research and the clinical significance of lipid-based biomarkers. Transl Res 2017;189:13-29. https://doi.org/10.1016/j.trsl.2017.06.006

(2) Naudí A, Cabré R, Jové M, Ayala V, Gonzalo H, Portero-Otín M, et al. Lipidomics of human brain aging and Alzheimer's disease pathology. Int. Rev. Neurobiol. 2015;122:133-89. https://doi.org/10.1016/bs.irn.2015.05.008

(3) Meikle PJ, Wong G, Barlow CK, Kingwell BA. Lipidomics: potential role in risk prediction and therapeutic monitoring for diabetes and cardiovascular disease. Pharmacol. Ther. 2014;143:12-23. https://doi.org/10.1016/j.pharmthera.2014.02.001

(4) Lv J, Zhang L, Yan F, Wang X. Clinical lipidomics: a new way to diagnose human diseases. Clin Transl Med 2018;7:12. https://doi.org/10.1186/s40169-018-0190-9

(5) Poetto AS, Posocco B, Gagno S, Orleni M, Zanchetta M, Iacuzzi V, et al. A new dried blood spot LC-MS/MS method for therapeutic drug monitoring of palbociclib, ribociclib, and letrozole in patients with cancer. J Chromatogr B 2021;1185:122985. https://doi.org/10.1016/j.jchromb.2021.122985

(6) Yu M, Dolios G, Yong-Gonzalez V, Bjorkqvist O, Colicino E, Halfvarson J, Petrick L. Untargeted metabolomics profiling and hemoglobin normalization for archived newborn dried blood spots from a refrigerated biorepository. J Pharm Biomed Anal 2020;191:113574. https://doi.org/10.1016/j.jpba.2020.113574

(7) Koulman A, Prentice P, Yong MCY, Matthews L, Bond NJ, Eiden M, et. al. The development and validation of a fast and robust dried blood spot based lipid profiling

method to study infant metabolism. Metabolomics 2014;10:1018-1025. https://doi.org/10.1007/s11306-014-0628-z

(8) Lam SM, Tian H, Shui G. Lipidomics, en route to accurate quantitation. Biochim Biophys Acta Mol Cell Biol Lipids 2017;1862:752-761. doi.org/10.1016/j.bbalip.2017.02.008

(9) Velghe S, Delahaye L, Stove CP. Is the hematocrit still an issue in quantitative dried blood spot analysis? J Pharm Biomed Anal 2019;163:188-196. https://doi.org/10.1016/j.jpba.2018.10.010

(10) Meikle TG, Huynh K, Giles C, Meikle PJ. Clinical lipidomics: realizing the potential of lipid profiling. J Lipid Res 2021;62:100127. https://doi.org/10.1016/j.jlr.2021.100127

(11) Kim J, Woenker T, Adamec J, Regnier FE. Simple, miniaturized blood plasma extraction method. Anal Chem 2013;85:11501-11508. https://doi.org/10.1021/ac402735y

(12) Li Y, Jiang Y, Cao H, Lin H, Ren W, Huang J, Zhang J. Therapeutic drug monitoring of valproic acid using a dried plasma spot sampling device. J Mass Spectrom 2021;56:4603. https://doi.org/10.1002/jms.4603

(13) Long NP, Park S, Anh NH, Kim SJ, Kim HM, Yoon SJ, Lim J, Kwon SW. Advances in liquid chromatography-mass spectrometry-based lipidomics: a look ahead. J Anal Test 2020;4:183-197. https://doi.org/10.1007/s41664-020-00135-y

(14) Cajka T, Fiehn O. Increasing lipidomic coverage by selecting optimal mobile-phase modifiers in LC–MS of blood plasma. Metabolomics 2016;12:34. https://doi.org/10.1007/s11306-015-0929-x

(15) Koelmel JP, Kroeger NM, Gill EL, Ulmer CZ, Bowden JA, Patterson RE, et al. Expanding lipidome coverage using LC–MS/MS data-dependent acquisition with automated

exclusion list generation. J Am Soc Mass Spectrom 2017;28:908-917. https://doi.org/10.1007/s13361-017-1608-0

(16) Tsugawa H, Cajka T, Kind T, Ma Y, Higgins B, Ikeda K, et al. MS-DIAL: Data-independent MS/MS deconvolution for comprehensive metabolome analysis. Nat Methods 2015;12:523-26. https://doi.org/10.1038/nmeth.3393

(17) Kind T, Liu K, Lee DY, DeFelice B, Meissen JK, Fiehn O. LipidBlast in silico tandem mass spectrometry data-base for lipid identification. Nat Methods 2013;10:755–58. https://doi.org/10.1038/nmeth.2551

(18) DeFelice BC, Mehta SS, Samra S, Cajka T, Wancewicz B, Fahrmann JF, Fiehn O. Mass spectral feature list optimizer (MS-FLO): a tool to minimize false positive peak reports in untargeted liquid chromatography-mass spectroscopy (LC–MS) data processing. Anal Chem 2017;89:3250-55. https://doi.org/10.1021/acs.analchem.6b04372

(19) Fan S, Kind T, Cajka T, Hazen SL, Tang WHW, Kaddurah-Daouk R, et al. Systematic error removal using random forest for normalizing large-scale untargeted lipidomics data. Anal Chem 2019;91:3590–96. https://doi.org/10.1021/acs.analchem.8b05592

(20) Liebisch G, Fahy E, Aoki J, Dennis EA, Durand T, Ejsing CS, et al. Update on LIPID MAPS classification, nomenclature, and shorthand notation for MS-derived lipid structures. J Lipid Res 2020;61:1539-55. https://doi.org/10.1194/jlr.S120001025

(21) Gonzalez-Covarrubias V, Dane A, Hankemeier T, Vreeken RJ. The influence of citrate, EDTA, and heparin anticoagulants to human plasma LC–MS lipidomic profiling. Metabolomics 2013;9:337–48. https://doi.org/10.1007/s11306-012-0450-4

(22) Paglia G, Del Greco FM, Sigurdsson BB, Rainer J, Volani C, Hicka AA, et al. Influence

of collection tubes during quantitative targeted metabolomics studies in human blood samples. Clin Chim Acta 2018;486:320-28. https://doi.org/10.1016/j.cca.2018.08.014

(23) Luginbuhl M, Gaugler S. Addressing new possibilities and new challenges: automated nondestructive hematocrit normalization for dried blood spots. Ther Drug Monit 2021;43:346-50. https://doi.org/10.1097/FTD.0000000000000887

(24) Luginbuhl M, Stoth F, Weinmann W, Gaugler S. Fully automated correction for the hematocrit bias of non-volumetric dried blood spot phosphatidylethanol analysis. Alcohol 2021;94:17-23. https://doi.org/10.1016/j.alcohol.2021.04.002

(25) Chepyala D, Kuo H, Su K, Liao H, Wang S, Chepyala SR, et al. Improved dried blood spot-based metabolomics analysis by a postcolumn infused-internal standard assisted liquid chromatography-electrospray ionization mass spectrometry method. Anal Chem 2019;91:10702-12. https://doi.org/10.1021/acs.analchem.9b02050

(26) Di Marino C, De Marco A, Pisanti A, Romanucci V. Effects of dried blood spot storage on lipidomic analysis. Molecules 2018;28:403. https://doi.org/10.3390/molecules23020403

(27) Prentice PM, Turner C, Wong MCY, Dalton RN. Stability of metabolites in dried blood spots stored at different temperatures over a 2-year period. Bioanalysis 2013;5:1507-14. https://doi.org/10.4155/bio.13.121

(28) Faller A, Richter B, Kluge M, Koenig P, Seitz HK, Skopp G. Stability of phosphatidylethanol species in spiked and authentic whole blood and matching dried blood spots. Int J Legal Med 2013;127:603-10. https://doi.org/10.1007/s00414-012-0799-y

(29) Ulmer CZ, Koelmel JP, Jones CM, Garrett TJ, Aristizabal-Henao JJ, Vesper HW, Bowden JA. A review of efforts to improve lipid stability during sample preparation and

standardization efforts to ensure accuracy in the reporting of lipid measurements. Lipids 2021;56:3-16. https://doi.org/10.1002/lipd.12263

(30) Koelmel JP, Jones CM, Ulmer CZ, Garrett TJ, Yost RA, Schock TB, Bowden JA. Examining heat treatment for stabilization of the lipidome. Bioanalysis 2018;10:291-305. https://doi.org/10.4155/bio-2017-0209

(31) Wang X, Gu X, Song H, Song Q, Gao X, Lu Y, Chen H. Phenylmethanesulfonyl fluoride pretreatment stabilizes plasma lipidome in lipidomic and metabolomic analysis. Anal Chim Acta 2015;893:77-83. https://doi.org/10.1016/j.aca.2015.08.049

(32) Liu G, Muehlhauser S, Gibson RA. A method for long term stabilization of long chain polyunsaturated fatty acids in dried blood spots and its clinical application. Prostaglandins Leukot Essent Fatty Acids 2014;91:251-60. https://doi.org/10.1016/j.plefa.2014.09.009 Wishart, D. S.; Feunang, Y. D.; Marcu, A.; Guo, A. C.; Liang, K.; Vázquez-Fresno, R.;

## 1.8 Supplemental Information

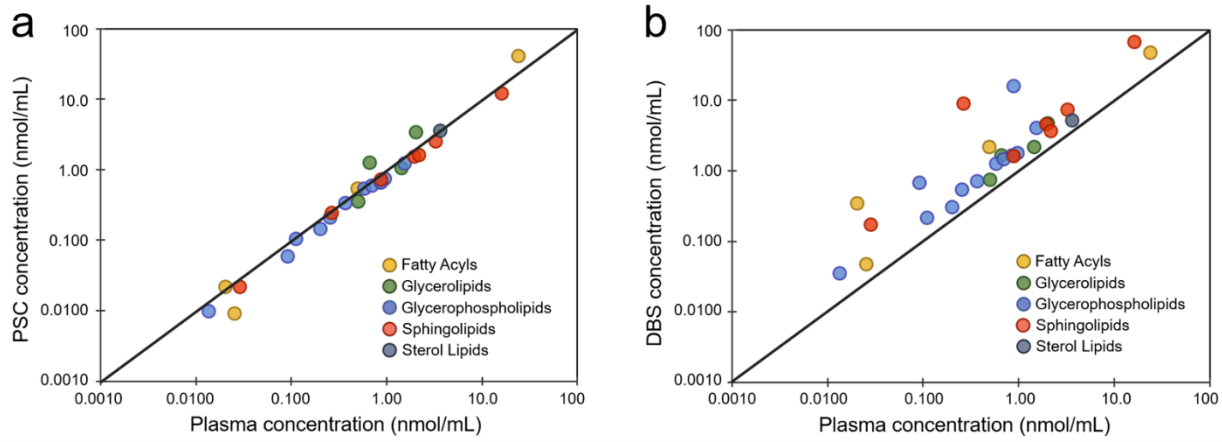


**Figure S1: a** Correlation between absolute concentrations of 28 endogenous lipids measured in plasma and PSC samples, respectively. **b** Correlation between the absolute concentrations of 28 endogenous lipids measured in plasma and DBS samples, respectively.

**Table S1:** Classification of all annotated lipids

| Lipid Name | Lipid Class | Lipid Subclass | ESI mode | Annotation level* | Sample Type Designation** | Fill (%) *** |
|---|---|---|---|---|---|---|
| CAR 8:1 | FA | Acyl Carnitine | pos | mzRT | All | 100% |
| CAR 10:0 | FA | Acyl Carnitine | pos | mzRT | All | 100% |
| CAR 10:1 | FA | Acyl Carnitine | pos | mzRT | All | 73% |
| CAR 12:0 | FA | Acyl Carnitine | pos | mzRT MS2 | All | 85% |
| CAR 14:0 | FA | Acyl Carnitine | pos | mz MS2 | All | 100% |
| CAR 14:1 | FA | Acyl Carnitine | pos | mzRT MS2 | All | 93% |
| CAR 16:0 | FA | Acyl Carnitine | pos | mzRT MS2 | All | 100% |
| CAR 16:1 | FA | Acyl Carnitine | pos | mz MS2 | All | 100% |
| CAR 18:0 | FA | Acyl Carnitine | pos | mzRT MS2 | All | 100% |
| CAR 18:1 | FA | Acyl Carnitine | pos | mzRT MS2 | All | 100% |
| CAR 18:2 | FA | Acyl Carnitine | pos | mzRT MS2 | All | 100% |
| CAR 18:3 | FA | Acyl Carnitine | pos | mzRT MS2 | All | 92% |
| CAR 20:1 | FA | Acyl Carnitine | pos | mz MS2 | All | 100% |
| CAR 20:2 | FA | Acyl Carnitine | pos | mz MS2 | All | 100% |
| CAR 20:5 | FA | Acyl Carnitine | pos | mz MS2 | All | 41% |
| CAR 20:3 | FA | Acyl Carnitine | pos | mz MS2 | All | 100% |
| CAR 20:4 | FA | Acyl Carnitine | pos | mz MS2 | All | 97% |
| CAR 22:4 | FA | Acyl Carnitine | pos | mz MS2 | All | 75% |
| CAR 22:6 | FA | Acyl Carnitine | pos | mz MS2 | All | 46% |
| CAR 24:0 | FA | Acyl Carnitine | pos | mz MS2 | All | 100% |
| CAR 26:0 | FA | Acyl Carnitine | pos | mz MS2 | All | 100% |
| CAR 26:1 | FA | Acyl Carnitine | pos | mz MS2 | All | 100% |
| CE 16:0 | ST | Cholesteryl Ester | pos | mzRT | All | 94% |
| CE 16:1 | ST | Cholesteryl Ester | pos | mzRT | All | 99% |
| CE 18:2 | ST | Cholesteryl Ester | pos | mzRT MS2 | All | 100% |
| CE 18:3 | ST | Cholesteryl Ester | pos | mzRT | All | 100% |
| CE 20:3 | ST | Cholesteryl Ester | pos | mzRT | All | 100% |
| CE 20:4 | ST | Cholesteryl Ester | pos | mzRT MS2 | All | 100% |
| CE 20:5 | ST | Cholesteryl Ester | pos | mzRT | All | 94% |
| CE 22:5 | ST | Cholesteryl Ester | pos | MS2 | All | 100% |
| CE 22:6 | ST | Cholesteryl Ester | pos | mzRT | All | 100% |
| Cer d32:1 | SP | Ceramide | neg | mzRT MS2 | All | 88% |
| Cer d34:0 | SP | Ceramide | neg | mzRT MS2 | All | 99% |
| Cer d34:1 | SP | Ceramide | pos | mzRT MS2 | All | 100% |
| Cer d36:0 | SP | Ceramide | neg | mz MS2 | All | 93% |
| Cer d36:1 | SP | Ceramide | pos | mzRT MS2 | All | 98% |
| Cer d38:0 | SP | Ceramide | neg | mz MS2 | All | 96% |
| Cer d38:1 | SP | Ceramide | pos | mzRT MS2 | All | 100% |
| Cer d39:1 | SP | Ceramide | neg | mzRT MS2 | All | 97% |
| Cer d40:0 | SP | Ceramide | pos | mz MS2 | All | 100% |
| Cer d40:1 | SP | Ceramide | pos | mzRT MS2 | All | 100% |
| Cer d40:2 | SP | Ceramide | pos | mz MS2 | All | 100% |
| Cer d41:0 | SP | Ceramide | pos | mz MS2 | All | 100% |
| Cer d41:1 | SP | Ceramide | pos | mzRT MS2 | All | 100% |
| Cer d41:2 | SP | Ceramide | pos | mz MS2 | All | 99% |
| Cer d42:0 | SP | Ceramide | pos | mz MS2 | All | 100% |
| Cer d42:1 | SP | Ceramide | pos | mzRT MS2 | All | 100% |
| Cer d42:2 | SP | Ceramide | pos | mzRT MS2 | All | 100% |
| Cer d43:1 | SP | Ceramide | pos | mz MS2 | All | 99% |
| Cer d43:2 | SP | Ceramide | neg | mz MS2 | All | 84% |
| Cer d44:1 | SP | Ceramide | pos | mz MS2 | All | 85% |
| Cholesterol | ST | Sterol Lipid | pos | mzRT | All | 100% |
| CoQ10 | Other | Other | pos | mz MS2 | All | 94% |
| DG 32:0 | GL | Diglyceride | pos | mz MS2 | All | 81% |
| DG 32:1 | GL | Diglyceride | pos | mzRT MS2 | All | 100% |
| DG 34:1 | GL | Diglyceride | pos | mzRT MS2 | All | 100% |
| DG 34:2 | GL | Diglyceride | pos | mzRT MS2 | All | 100% |
| DG 34:3 | GL | Diglyceride | pos | mzRT | All | 100% |
| DG 36:1 | GL | Diglyceride | pos | mzRT MS2 | All | 100% |
| DG 36:2 | GL | Diglyceride | pos | mzRT MS2 | All | 100% |

| | | | | | | |
|---|---|---|---|---|---|---|
| DG 36:3 | GL | Diglyceride | pos | mzRT MS2 | All | 100% |
| DG 36:4 | GL | Diglyceride | pos | mzRT MS2 | All | 100% |
| DG 38:4 | GL | Diglyceride | pos | mz MS2 | All | 81% |
| DG 38:5 | GL | Diglyceride | pos | mzRT MS2 | All | 100% |
| DG 38:6 | GL | Diglyceride | pos | mzRT MS2 | All | 100% |
| DG 40:5 | GL | Diglyceride | pos | mz MS2 | All | 64% |
| FA 16:3 | FA | Free Fatty Acid | neg | mz MS2 | All | 98% |
| FA 18:1 (oleic acid) | FA | Free Fatty Acid | neg | mzRT MS2 | All | 100% |
| FA 18:2 (linoleic acid) | FA | Free Fatty Acid | neg | mzRT MS2 | All | 100% |
| FA 18:3 (linolenic acid) | FA | Free Fatty Acid | neg | mzRT MS2 | All | 100% |
| FA 18:4 | FA | Free Fatty Acid | neg | mz MS2 | All | 96% |
| FA 20:2 | FA | Free Fatty Acid | neg | mzRT MS2 | All | 100% |
| FA 20:4 (arachidonic acid) | FA | Free Fatty Acid | neg | mzRT MS2 | All | 100% |
| FA 20:5 | FA | Free Fatty Acid | neg | mzRT MS2 | All | 100% |
| FA 22:4 | FA | Free Fatty Acid | neg | mz MS2 | All | 100% |
| FA 22:5 | FA | Free Fatty Acid | neg | mz MS2 | All | 100% |
| FA 22:6 | FA | Free Fatty Acid | neg | mzRT MS2 | All | 100% |
| FA 23:0 | FA | Free Fatty Acid | neg | mz MS2 | All | 100% |
| FA 25:0 | FA | Free Fatty Acid | neg | mz MS2 | All | 100% |
| FA 26:0 (cerotic acid) | FA | Free Fatty Acid | neg | mzRT MS2 | All | 100% |
| FA 26:4 | FA | Free Fatty Acid | neg | mz MS2 | All | 98% |
| GlcCer d34:1 | SP | Glucosylceramide | pos | mzRT MS2 | All | 100% |
| GlcCer d38:1 | SP | Glucosylceramide | neg | mzRT | All | 82% |
| GlcCer d40:1 | SP | Glucosylceramide | neg | mzRT MS2 | All | 100% |
| GlcCer d41:1 | SP | Glucosylceramide | neg | mzRT MS2 | All | 100% |
| GlcCer d42:1 | SP | Glucosylceramide | pos | mzRT MS2 | All | 100% |
| GlcCer d42:2 | SP | Glucosylceramide | pos | mzRT MS2 | All | 100% |
| GM3 34:1 | Other | Other | neg | mz MS2 | All | 100% |
| GM3 36:1 | Other | Other | neg | mz MS2 | All | 88% |
| Hex2Cer 34:1;2O | SP | Hexosylceramide | neg | mz MS2 | All | 100% |
| Hex3Cer 34:1;2O | SP | Hexosylceramide | pos | MS2 | All | 100% |
| HexCer 34:1;2O | SP | Hexosylceramide | neg | mz MS2 | All | 100% |
| HexCer 41:1;2O | SP | Hexosylceramide | pos | mz MS2 | All | 100% |
| Hex2Cer 42:1;2O | SP | Hexosylceramide | neg | mz MS2 | All | 76% |
| Hex3Cer 42:1;2O | SP | Hexosylceramide | neg | mz MS2 | All | 45% |
| Lactosylceramide d42:2 | SP | Lactosylceramide | pos | mzRT | All | 79% |
| LPC 14:0 | GP | Lysophosphatidylcholine | pos | mzRT MS2 | All | 94% |
| LPC 15:0 | GP | Lysophosphatidylcholine | pos | mzRT MS2 | All | 100% |
| LPC 16:0 | GP | Lysophosphatidylcholine | pos | mzRT MS2 | All | 100% |
| LPC 16:1 | GP | Lysophosphatidylcholine | pos | mzRT MS2 | All | 100% |
| LPC 17:0 | GP | Lysophosphatidylcholine | pos | mz MS2 | All | 100% |
| LPC 18:0 | GP | Lysophosphatidylcholine | pos | mzRT MS2 | All | 100% |
| LPC 18:1 | GP | Lysophosphatidylcholine | pos | mzRT MS2 | All | 100% |
| LPC 18:2 | GP | Lysophosphatidylcholine | pos | mzRT MS2 | All | 100% |
| LPC 18:3 | GP | Lysophosphatidylcholine | pos | mzRT MS2 | All | 94% |
| LPC 19:0 | GP | Lysophosphatidylcholine | pos | mz MS2 | All | 100% |
| LPC 20:0 | GP | Lysophosphatidylcholine | pos | mzRT | All | 100% |
| LPC 20:1 | GP | Lysophosphatidylcholine | pos | mzRT MS2 | All | 100% |
| LPC 20:2 | GP | Lysophosphatidylcholine | pos | mzRT MS2 | All | 100% |
| LPC 20:3 | GP | Lysophosphatidylcholine | pos | mzRT MS2 | All | 100% |
| LPC 20:4 | GP | Lysophosphatidylcholine | pos | mzRT MS2 | All | 100% |
| LPC 20:5 | GP | Lysophosphatidylcholine | pos | mzRT MS2 | All | 90% |
| LPC 22:4 | GP | Lysophosphatidylcholine | pos | mzRT MS2 | All | 100% |
| LPC 22:5 | GP | Lysophosphatidylcholine | pos | mzRT MS2 | All | 100% |
| LPC 22:6 | GP | Lysophosphatidylcholine | pos | mzRT MS2 | All | 100% |
| LPC 24:0 | GP | Lysophosphatidylcholine | pos | mz MS2 | All | 100% |
| LPC O-16:0 | GP | Lysophosphatidylcholine | pos | mzRT MS2 | All | 100% |
| LPC O-16:1 | GP | Lysophosphatidylcholine | pos | mzRT MS2 | All | 100% |
| LPC O-18:1 | GP | Lysophosphatidylcholine | pos | mzRT MS2 | All | 100% |
| LPC O-18:2 | GP | Lysophosphatidylcholine | pos | mz MS2 | All | 92% |
| LPC O-20:0 | GP | Lysophosphatidylcholine | pos | mz MS2 | All | 100% |
| LPC O-24:0 | GP | Lysophosphatidylcholine | pos | mz MS2 | All | 100% |
| LPE 16:0 | GP | Lysophosphatidylethanolamine | pos | mz MS2 | All | 100% |
| LPE 18:0 | GP | Lysophosphatidylethanolamine | pos | mzRT MS2 | All | 94% |
| LPE 18:1 | GP | Lysophosphatidylethanolamine | neg | mz MS2 | All | 100% |

| | | | | | | |
|---|---|---|---|---|---|---|
| LPE 18:2 | GP | Lysophosphatidylethanolamine | neg | mzRT MS2 | All | 100% |
| LPE 20:4 | GP | Lysophosphatidylethanolamine | neg | mzRT MS2 | All | 100% |
| LPE 22:6 | GP | Lysophosphatidylethanolamine | neg | mzRT MS2 | All | 100% |
| LPE O-16:1 | GP | Lysophosphatidylethanolamine | neg | mz MS2 | All | 99% |
| LPE O-18:1 | GP | Lysophosphatidylethanolamine | neg | mz MS2 | All | 99% |
| LPE O-18:2 | GP | Lysophosphatidylethanolamine | neg | mz MS2 | All | 83% |
| LPI 18:0 | GP | Lysophosphatidylinositol | neg | mz MS2 | All | 94% |
| LPI 18:1 | GP | Lysophosphatidylinositol | neg | mz MS2 | All | 79% |
| NAE 18:1 | FA | N-acyl Ethanolamine | pos | MS2 | All | 91% |
| O1_Cer d40:0 | SP | Ceramide (Ox) | neg | mz MS2 | All | 95% |
| O1_Cer d42:0 | SP | Ceramide (Ox) | pos | mz MS2 | All | 93% |
| O1_FA 18:2 | FA | Free Fatty Acid (Ox) | neg | mz MS2 | All | 100% |
| O2_FA 18:2 | FA | Free Fatty Acid (Ox) | neg | mz MS2 | All | 68% |
| O1_PC 34:1 | GP | Phosphatidylcholine (Ox) | neg | mz MS2 | All | 91% |
| O1_SHexCer 34:1 | SP | Sulfatide (Ox) | neg | mz MS2 | All | 100% |
| O1_SM 42:1 | SP | Sphingomyelin (Ox) | neg | mz MS2 | All | 99% |
| O1_SM d34:0 | SP | Sphingomyelin (Ox) | pos | MS2 | All | 100% |
| O1_SM d34:1 | SP | Sphingomyelin (Ox) | pos | mz MS2 | All | 100% |
| PC 21:4 | GP | Phosphatidylcholine | pos | mz MS2 | All | 92% |
| PC 28:0 | GP | Phosphatidylcholine | pos | mzRT MS2 | All | 89% |
| PC 29:0 | GP | Phosphatidylcholine | pos | mz MS2 | All | 60% |
| PC 30:0 | GP | Phosphatidylcholine | pos | mzRT MS2 | All | 100% |
| PC 301 | GP | Phosphatidylcholine | neg | mz MS2 | All | 60% |
| PC 31:0 | GP | Phosphatidylcholine | pos | mzRT MS2 | All | 100% |
| PC 31:1 | GP | Phosphatidylcholine | pos | mzRT MS2 | All | 87% |
| PC 32:0 | GP | Phosphatidylcholine | pos | mzRT MS2 | All | 100% |
| PC 32:1 | GP | Phosphatidylcholine | pos | mzRT MS2 | All | 100% |
| PC 32:2 | GP | Phosphatidylcholine | pos | mzRT MS2 | All | 100% |
| PC 33:0 | GP | Phosphatidylcholine | pos | mzRT MS2 | All | 100% |
| PC 33:1 | GP | Phosphatidylcholine | pos | mzRT MS2 | All | 100% |
| PC 33:2 | GP | Phosphatidylcholine | pos | mzRT MS2 | All | 100% |
| PC 33:3 | GP | Phosphatidylcholine | pos | mz MS2 | All | 100% |
| PC 34:0 | GP | Phosphatidylcholine | pos | mzRT MS2 | All | 100% |
| PC 34:1 | GP | Phosphatidylcholine | pos | mzRT MS2 | All | 100% |
| PC 34:2 | GP | Phosphatidylcholine | pos | mzRT MS2 | All | 100% |
| PC 34:3 | GP | Phosphatidylcholine | pos | mzRT MS2 | All | 100% |
| PC 34:4 | GP | Phosphatidylcholine | pos | mzRT MS2 | All | 100% |
| PC 34:5 | GP | Phosphatidylcholine | pos | mz MS2 | All | 72% |
| PC 35:0 | GP | Phosphatidylcholine | pos | mz MS2 | All | 61% |
| PC 35:1 | GP | Phosphatidylcholine | pos | mzRT MS2 | All | 100% |
| PC 35:2 | GP | Phosphatidylcholine | pos | mzRT MS2 | All | 100% |
| PC 35:3 | GP | Phosphatidylcholine | pos | mzRT MS2 | All | 100% |
| PC 35:4 | GP | Phosphatidylcholine | pos | mzRT MS2 | All | 100% |
| PC 35:5 | GP | Phosphatidylcholine | pos | mz MS2 | All | 73% |
| PC 36:1 | GP | Phosphatidylcholine | pos | mzRT MS2 | All | 100% |
| PC 36:2 | GP | Phosphatidylcholine | pos | mzRT MS2 | All | 100% |
| PC 36:3 | GP | Phosphatidylcholine | pos | mzRT MS2 | All | 100% |
| PC 36:4 | GP | Phosphatidylcholine | pos | mzRT MS2 | All | 100% |
| PC 36:5 | GP | Phosphatidylcholine | pos | mzRT MS2 | All | 100% |
| PC 36:6 | GP | Phosphatidylcholine | pos | mzRT MS2 | All | 100% |
| PC 37:2 | GP | Phosphatidylcholine | pos | mzRT MS2 | All | 100% |
| PC 37:3 | GP | Phosphatidylcholine | pos | mzRT MS2 | All | 100% |
| PC 37:4 | GP | Phosphatidylcholine | pos | mzRT MS2 | All | 100% |
| PC 37:5 | GP | Phosphatidylcholine | pos | mzRT MS2 | All | 100% |
| PC 37:6 | GP | Phosphatidylcholine | pos | mzRT | All | 100% |
| PC 38:1 | GP | Phosphatidylcholine | pos | mzRT MS2 | All | 100% |
| PC 38:2 | GP | Phosphatidylcholine | pos | mzRT MS2 | All | 100% |
| PC 38:3 | GP | Phosphatidylcholine | pos | mzRT MS2 | All | 100% |
| PC 38:4 | GP | Phosphatidylcholine | pos | mzRT MS2 | All | 100% |
| PC 38:5 | GP | Phosphatidylcholine | pos | mzRT MS2 | All | 100% |
| PC 38:6 | GP | Phosphatidylcholine | pos | mzRT MS2 | All | 100% |
| PC 38:7 | GP | Phosphatidylcholine | pos | mzRT MS2 | All | 100% |
| PC 39:5 | GP | Phosphatidylcholine | pos | mz MS2 | All | 100% |
| PC 39:6 | GP | Phosphatidylcholine | pos | mzRT MS2 | All | 100% |
| PC 40:3 | GP | Phosphatidylcholine | pos | mz MS2 | All | 76% |

| | | | | | | |
|---|---|---|---|---|---|---|
| PC 40:4 | GP | Phosphatidylcholine | pos | mzRT MS2 | All | 100% |
| PC 40:5 | GP | Phosphatidylcholine | pos | mzRT MS2 | All | 100% |
| PC 40:6 | GP | Phosphatidylcholine | pos | mzRT MS2 | All | 100% |
| PC 40:7 | GP | Phosphatidylcholine | pos | mzRT MS2 | All | 100% |
| PC 40:8 | GP | Phosphatidylcholine | pos | mzRT MS2 | All | 100% |
| PC 42:10 | GP | Phosphatidylcholine | pos | mzRT MS2 | All | 100% |
| PC 42:5 | GP | Phosphatidylcholine | pos | mzRT MS2 | All | 100% |
| PC 42:6 | GP | Phosphatidylcholine | pos | mzRT MS2 | All | 86% |
| PC 42:7 | GP | Phosphatidylcholine | pos | mz MS2 | All | 72% |
| PC 42:8 | GP | Phosphatidylcholine | pos | mz MS2 | All | 100% |
| PC O-30:0 | GP | Phosphatidylcholine | pos | mz MS2 | All | 100% |
| PC O-31:0 | GP | Phosphatidylcholine | pos | mz MS2 | All | 77% |
| PC O-32:0 | GP | Phosphatidylcholine | pos | mzRT MS2 | All | 100% |
| PC O-32:1 | GP | Phosphatidylcholine | pos | mzRT | All | 100% |
| PC O-33:0 | GP | Phosphatidylcholine | pos | mz MS2 | All | 46% |
| PC O-33:1 | GP | Phosphatidylcholine | pos | mz MS2 | All | 67% |
| PC O-34:0 | GP | Phosphatidylcholine | pos | mzRT MS2 | All | 100% |
| PC O-34:1 | GP | Phosphatidylcholine | neg | mzRT MS2 | All | 100% |
| PC O-34:2 | GP | Phosphatidylcholine | neg | mzRT MS2 | All | 100% |
| PC O-34:3 | GP | Phosphatidylcholine | neg | mzRT MS2 | All | 100% |
| PC O-35:5 | GP | Phosphatidylcholine | pos | mz MS2 | All | 86% |
| PC O-36:1 | GP | Phosphatidylcholine | pos | mz MS2 | All | 100% |
| PC O-36:2 A | GP | Phosphatidylcholine | pos | mzRT MS2 | All | 100% |
| PC O-36:3 | GP | Phosphatidylcholine | pos | mzRT MS2 | All | 100% |
| PC O-36:4 | GP | Phosphatidylcholine | neg | mzRT MS2 | All | 100% |
| PC O-36:5 | GP | Phosphatidylcholine | pos | mzRT MS2 | All | 100% |
| PC O-36:6 | GP | Phosphatidylcholine | pos | mzRT MS2 | All | 100% |
| PC O-37:5 | GP | Phosphatidylcholine | pos | mz MS2 | All | 100% |
| PC O-38:2 | GP | Phosphatidylcholine | pos | mz MS2 | All | 100% |
| PC O-38:3 | GP | Phosphatidylcholine | pos | mzRT MS2 | All | 100% |
| PC O-38:4 | GP | Phosphatidylcholine | pos | mzRT MS2 | All | 100% |
| PC O-38:5 | GP | Phosphatidylcholine | pos | mzRT MS2 | All | 100% |
| PC O-38:6 | GP | Phosphatidylcholine | pos | mzRT MS2 | All | 100% |
| PC O-38:7 | GP | Phosphatidylcholine | pos | mzRT MS2 | All | 100% |
| PC O-39:9 | GP | Phosphatidylcholine | pos | MS2 | All | 90% |
| PC O-40:3 | GP | Phosphatidylcholine | pos | mz MS2 | All | 100% |
| PC O-40:4 | GP | Phosphatidylcholine | pos | mzRT | All | 100% |
| PC O-40:5 | GP | Phosphatidylcholine | pos | mzRT MS2 | All | 100% |
| PC O-40:6 | GP | Phosphatidylcholine | pos | mzRT MS2 | All | 100% |
| PC O-40:7 | GP | Phosphatidylcholine | pos | mzRT MS2 | All | 100% |
| PC O-40:8 | GP | Phosphatidylcholine | pos | mzRT MS2 | All | 100% |
| PC O-42:4 | GP | Phosphatidylcholine | pos | mzRT MS2 | All | 100% |
| PC O-42:5 | GP | Phosphatidylcholine | pos | mzRT MS2 | All | 100% |
| PC O-42:6 | GP | Phosphatidylcholine | pos | mzRT MS2 | All | 100% |
| PC O-42:7 | GP | Phosphatidylcholine | pos | mz MS2 | All | 94% |
| PC O-42:8 | GP | Phosphatidylcholine | pos | mz MS2 | All | 78% |
| PC O-44:4 | GP | Phosphatidylcholine | pos | mz MS2 | All | 91% |
| PC O-44:5 | GP | Phosphatidylcholine | pos | mzRT MS2 | All | 100% |
| PC O-44:6 | GP | Phosphatidylcholine | pos | mz MS2 | All | 100% |
| PC O-44:8 | GP | Phosphatidylcholine | pos | mz MS2 | All | 78% |
| PC O-46:7 | GP | Phosphatidylcholine | pos | mz MS2 | All | 100% |
| PC O-46:8 | GP | Phosphatidylcholine | pos | mz MS2 | All | 93% |
| PE 32:1 | GP | Phosphatidylethanolamine | neg | mz MS2 | All | 41% |
| PE 34:0 | GP | Phosphatidylethanolamine | neg | mz MS2 | All | 44% |
| PE 34:1 | GP | Phosphatidylethanolamine | neg | mzRT MS2 | All | 100% |
| PE 34:2 | GP | Phosphatidylethanolamine | neg | mzRT MS2 | All | 100% |
| PE 36:1 | GP | Phosphatidylethanolamine | neg | mz MS2 | All | 100% |
| PE 36:2 | GP | Phosphatidylethanolamine | neg | mz MS2 | All | 100% |
| PE 36:3 | GP | Phosphatidylethanolamine | neg | mzRT MS2 | All | 100% |
| PE 36:4 | GP | Phosphatidylethanolamine | pos | mzRT MS2 | All | 100% |
| PE 36:5 | GP | Phosphatidylethanolamine | neg | mz MS2 | All | 63% |
| PE 37:4 | GP | Phosphatidylethanolamine | neg | mz MS2 | All | 63% |
| PE 38:3 | GP | Phosphatidylethanolamine | neg | mz MS2 | All | 93% |
| PE 38:4 | GP | Phosphatidylethanolamine | pos | mzRT MS2 | All | 100% |
| PE 38:5 | GP | Phosphatidylethanolamine | neg | mz MS2 | All | 100% |
| PE 38:6 | GP | Phosphatidylethanolamine | pos | mzRT MS2 | All | 100% |

| | | | | | | |
|---|---|---|---|---|---|---|
| PE 40:4 | GP | Phosphatidylethanolamine | neg | mz MS2 | All | 89% |
| PE 40:5 | GP | Phosphatidylethanolamine | neg | mz MS2 | All | 88% |
| PE 40:6 | GP | Phosphatidylethanolamine | neg | mz MS2 | All | 100% |
| PE O-34:1 | GP | Phosphatidylethanolamine | neg | mz MS2 | All | 81% |
| PE O-34:2 | GP | Phosphatidylethanolamine | neg | mzRT MS2 | All | 100% |
| PE O-34:3 | GP | Phosphatidylethanolamine | neg | mzRT MS2 | All | 100% |
| PE O-36:2 | GP | Phosphatidylethanolamine | neg | mzRT MS2 | All | 100% |
| PE O-36:3 | GP | Phosphatidylethanolamine | neg | mzRT MS2 | All | 100% |
| PE O-36:4 | GP | Phosphatidylethanolamine | neg | mz MS2 | All | 100% |
| PE O-36:5 | GP | Phosphatidylethanolamine | neg | mzRT MS2 | All | 100% |
| PE O-36:6 | GP | Phosphatidylethanolamine | neg | mzRT MS2 | All | 91% |
| PE O-37:5 | GP | Phosphatidylethanolamine | neg | mz MS2 | All | 95% |
| PE O-38:2 | GP | Phosphatidylethanolamine | neg | mz MS2 | All | 69% |
| PE O-38:3 | GP | Phosphatidylethanolamine | neg | mzRT MS2 | All | 91% |
| PE O-38:4 | GP | Phosphatidylethanolamine | neg | mzRT MS2 | All | 100% |
| PE O-38:5 | GP | Phosphatidylethanolamine | neg | mzRT MS2 | All | 100% |
| PE O-38:6 | GP | Phosphatidylethanolamine | neg | mzRT MS2 | All | 100% |
| PE O-38:7 | GP | Phosphatidylethanolamine | neg | mzRT MS2 | All | 100% |
| PE O-40:5 | GP | Phosphatidylethanolamine | neg | mzRT MS2 | All | 99% |
| PE O-40:6 | GP | Phosphatidylethanolamine | neg | mzRT MS2 | All | 100% |
| PE O-40:7 | GP | Phosphatidylethanolamine | neg | mzRT MS2 | All | 100% |
| PE O-40:8 | GP | Phosphatidylethanolamine | neg | mzRT MS2 | All | 100% |
| PE O-42:6 | GP | Phosphatidylethanolamine | neg | mz MS2 | All | 69% |
| PE O-42:7 | GP | Phosphatidylethanolamine | neg | mz MS2 | All | 92% |
| PE P-34:1 | GP | Phosphatidylethanolamine | pos | mzRT MS2 | All | 70% |
| PE P-36:1 | GP | Phosphatidylethanolamine | pos | mzRT MS2 | All | 100% |
| PE P-36:2 | GP | Phosphatidylethanolamine | pos | mzRT MS2 | All | 100% |
| PE P-36:4 | GP | Phosphatidylethanolamine | pos | mzRT MS2 | All | 100% |
| PE P-36:5 | GP | Phosphatidylethanolamine | pos | mz MS2 | All | 69% |
| PE P-37:4 | GP | Phosphatidylethanolamine | pos | mz MS2 | All | 64% |
| PE P-38:3 | GP | Phosphatidylethanolamine | pos | mz MS2 | All | 67% |
| PE P-38:5 | GP | Phosphatidylethanolamine | pos | mzRT MS2 | All | 100% |
| PE P-38:6 | GP | Phosphatidylethanolamine | pos | mz MS2 | All | 100% |
| PE P-40:4 | GP | Phosphatidylethanolamine | pos | mzRT MS2 | All | 96% |
| PE P-40:5 | GP | Phosphatidylethanolamine | pos | mzRT | All | 94% |
| PE P-40:6 | GP | Phosphatidylethanolamine | pos | mz MS2 | All | 100% |
| PE P-40:7 | GP | Phosphatidylethanolamine | pos | mz MS2 | All | 100% |
| PG 34:1\|PG 16:0_18:1 | GP | Phosphatidylglycerol | neg | mz MS2 | All | 59% |
| PI 32:0\|PI 16:0_16:0 | GP | Phosphatidylinositol | neg | mz MS2 | All | 93% |
| PI 32:1 | GP | Phosphatidylinositol | neg | mzRT MS2 | All | 99% |
| PI 34:0\|PI 16:0_18:0 | GP | Phosphatidylinositol | neg | mz MS2 | All | 75% |
| PI 34:1\|16:0_18:1 | GP | Phosphatidylinositol | neg | mzRT MS2 | All | 100% |
| PI 34:2\|16:0_18:2 | GP | Phosphatidylinositol | neg | mzRT MS2 | All | 100% |
| PI 36:1\|18:0_18:1 | GP | Phosphatidylinositol | neg | mzRT MS2 | All | 100% |
| PI 36:2\|18:0_18:2 | GP | Phosphatidylinositol | neg | mzRT MS2 | All | 100% |
| PI 36:3\|18:1_18:2 | GP | Phosphatidylinositol | neg | mzRT MS2 | All | 100% |
| PI 36:4\|16:0_20:4 | GP | Phosphatidylinositol | neg | mzRT MS2 | All | 100% |
| PI 37:4\|PI 17:0_20:4 | GP | Phosphatidylinositol | neg | mz MS2 | All | 99% |
| PI 38:3\|18:0_20:3 | GP | Phosphatidylinositol | neg | mzRT MS2 | All | 100% |
| PI 38:4\|18:0_20:4 | GP | Phosphatidylinositol | neg | mzRT MS2 | All | 100% |
| PI 38:5 | GP | Phosphatidylinositol | neg | mzRT MS2 | All | 100% |
| PI 38:6\|PI 16:0_22:6 | GP | Phosphatidylinositol | neg | mz MS2 | All | 100% |
| PI 40:4\|PI 18:0_22:4 | GP | Phosphatidylinositol | neg | mz MS2 | All | 91% |
| PI 40:5\|PI 18:0_22:5 | GP | Phosphatidylinositol | neg | mz MS2 | All | 99% |
| PI 40:6\|18:0_22:6 | GP | Phosphatidylinositol | neg | mzRT MS2 | All | 100% |
| PS 36:1\|PS 18:0_18:1 | GP | Phosphatidylserine | neg | mz MS2 | All | 80% |
| PS 36:2\|PS 18:0_18:2 | GP | Phosphatidylserine | neg | mz MS2 | All | 70% |
| PS 38:4\|PS 18:0_20:4 | GP | Phosphatidylserine | neg | mz MS2 | All | 100% |
| PS 40:5\|PS 18:0_22:5 | GP | Phosphatidylserine | neg | mz MS2 | All | 100% |
| PS 40:6\|PS 18:0_22:6 | GP | Phosphatidylserine | neg | mz MS2 | All | 100% |
| SHexCer 34:1 | SP | Sulfatide | neg | mz MS2 | All | 100% |
| SM d28:1 | SP | Sphingomyelin | pos | mz MS2 | All | 62% |
| SM d30:1 | SP | Sphingomyelin | pos | mzRT MS2 | All | 100% |
| SM d30:2 | SP | Sphingomyelin | pos | mz MS2 | All | 54% |
| SM d31:1 | SP | Sphingomyelin | neg | mz MS2 | All | 53% |

| | | | | | | |
|---|---|---|---|---|---|---|
| SM d32:0 | SP | Sphingomyelin | pos | mzRT MS2 | All | 100% |
| SM d32:1 | SP | Sphingomyelin | pos | mzRT MS2 | All | 100% |
| SM d32:2 | SP | Sphingomyelin | pos | mzRT MS2 | All | 100% |
| SM d33:1 | SP | Sphingomyelin | pos | mzRT MS2 | All | 100% |
| SM d34:0 | SP | Sphingomyelin | pos | mzRT | All | 100% |
| SM d34:1 | SP | Sphingomyelin | pos | mzRT MS2 | All | 100% |
| SM d34:2 | SP | Sphingomyelin | pos | mzRT MS2 | All | 100% |
| SM d35:1 | SP | Sphingomyelin | pos | mz MS2 | All | 100% |
| SM d35:2 | SP | Sphingomyelin | pos | mz MS2 | All | 100% |
| SM d36:0 | SP | Sphingomyelin | pos | mzRT MS2 | All | 100% |
| SM d36:1 | SP | Sphingomyelin | pos | mzRT MS2 | All | 100% |
| SM d36:2 | SP | Sphingomyelin | pos | mzRT MS2 | All | 100% |
| SM d36:3 | SP | Sphingomyelin | pos | mzRT MS2 | All | 100% |
| SM d37:1 | SP | Sphingomyelin | pos | mzRT MS2 | All | 100% |
| SM d38:0 | SP | Sphingomyelin | pos | mzRT | All | 100% |
| SM d38:1 | SP | Sphingomyelin | pos | mzRT MS2 | All | 100% |
| SM d38:2 | SP | Sphingomyelin | pos | mzRT MS2 | All | 100% |
| SM d39:1 | SP | Sphingomyelin | pos | mzRT MS2 | All | 100% |
| SM d39:2 | SP | Sphingomyelin | pos | mzRT | All | 99% |
| SM d40:0 | SP | Sphingomyelin | pos | mzRT MS2 | All | 100% |
| SM d40:1 | SP | Sphingomyelin | pos | mzRT MS2 | All | 100% |
| SM d40:2 | SP | Sphingomyelin | pos | mzRT MS2 | All | 100% |
| SM d40:3 | SP | Sphingomyelin | neg | mzRT MS2 | All | 100% |
| SM d41:1 | SP | Sphingomyelin | pos | mzRT MS2 | All | 100% |
| SM d41:2 | SP | Sphingomyelin | pos | mzRT MS2 | All | 100% |
| SM d41:3 | SP | Sphingomyelin | neg | mz MS2 | All | 91% |
| SM d42:0 | SP | Sphingomyelin | pos | mzRT MS2 | All | 83% |
| SM d42:1 | SP | Sphingomyelin | pos | mzRT MS2 | All | 100% |
| SM d42:2 | SP | Sphingomyelin | pos | mzRT MS2 | All | 100% |
| SM d42:3 | SP | Sphingomyelin | pos | mzRT MS2 | All | 100% |
| SM d42:4 | SP | Sphingomyelin | neg | mz MS2 | All | 100% |
| SM d43:1 | SP | Sphingomyelin | pos | mzRT MS2 | All | 100% |
| SM d43:2 | SP | Sphingomyelin | pos | mzRT MS2 | All | 100% |
| SM d44:1 | SP | Sphingomyelin | pos | mz MS2 | All | 84% |
| SM d44:2 | SP | Sphingomyelin | pos | mzRT MS2 | All | 100% |
| SM d44:3 | SP | Sphingomyelin | pos | mz MS2 | All | 100% |
| SM d44:5 | SP | Sphingomyelin | pos | MS2 | All | 74% |
| ST 27:1;O | ST | Sterol Lipid | pos | mz MS2 | All | 100% |
| ST 27:2;O | ST | Sterol Lipid | pos | mz MS2 | All | 100% |
| ST 28:1;O;S | ST | Sterol Lipid | neg | mz MS2 | All | 100% |
| ST 29:1;O;S | ST | Sterol Lipid | neg | mz MS2 | All | 94% |
| | | | | | | |
| TG 46:0 | GL | Triglyceride | pos | mzRT MS2 | All | 100% |
| TG 46:1 | GL | Triglyceride | pos | mzRT MS2 | All | 100% |
| TG 46:2 | GL | Triglyceride | pos | mzRT MS2 | All | 91% |
| TG 48:0 | GL | Triglyceride | pos | mzRT MS2 | All | 100% |
| TG 48:1 | GL | Triglyceride | pos | mzRT MS2 | All | 100% |
| TG 48:2 | GL | Triglyceride | pos | mzRT MS2 | All | 100% |
| TG 48:3 | GL | Triglyceride | pos | mzRT MS2 | All | 99% |
| TG 50:0 | GL | Triglyceride | pos | mzRT MS2 | All | 100% |
| TG 50:1 | GL | Triglyceride | pos | mzRT MS2 | All | 100% |
| TG 50:2 | GL | Triglyceride | pos | mzRT MS2 | All | 100% |
| TG 50:3 | GL | Triglyceride | pos | mzRT MS2 | All | 100% |
| TG 50:4 | GL | Triglyceride | pos | mzRT MS2 | All | 100% |
| TG 51:2 | GL | Triglyceride | pos | mzRT MS2 | All | 100% |
| TG 51:3 | GL | Triglyceride | pos | mzRT MS2 | All | 100% |
| TG 51:4 | GL | Triglyceride | pos | mzRT MS2 | All | 100% |
| TG 52:1 | GL | Triglyceride | pos | mzRT MS2 | All | 100% |
| TG 52:2 | GL | Triglyceride | pos | mzRT MS2 | All | 100% |
| TG 52:3 | GL | Triglyceride | pos | mzRT | All | 100% |
| TG 52:4 | GL | Triglyceride | pos | mzRT MS2 | All | 100% |
| TG 53:2 | GL | Triglyceride | pos | mzRT MS2 | All | 100% |
| TG 53:3 | GL | Triglyceride | pos | mzRT MS2 | All | 100% |
| TG 54:1 | GL | Triglyceride | pos | mzRT MS2 | All | 100% |
| TG 54:2 | GL | Triglyceride | pos | mzRT MS2 | All | 100% |

| | | | | | | |
|---|---|---|---|---|---|---|
| TG 54:3 | GL | Triglyceride | pos | mzRT MS2 | All | 100% |
| TG 54:4 | GL | Triglyceride | pos | mzRT MS2 | All | 100% |
| TG 54:5 | GL | Triglyceride | pos | mzRT MS2 | All | 100% |
| TG 54:6 | GL | Triglyceride | pos | mzRT MS2 | All | 100% |
| TG 55:3 | GL | Triglyceride | pos | mzRT MS2 | All | 99% |
| TG 56:2 | GL | Triglyceride | pos | mzRT MS2 | All | 100% |
| TG 56:3 | GL | Triglyceride | pos | mzRT MS2 | All | 100% |
| TG 56:4 | GL | Triglyceride | pos | mzRT MS2 | All | 100% |
| TG 56:5 | GL | Triglyceride | pos | mzRT MS2 | All | 100% |
| TG 56:6 | GL | Triglyceride | pos | mzRT MS2 | All | 100% |
| TG 56:7 | GL | Triglyceride | pos | mzRT MS2 | All | 100% |
| TG 56:8 | GL | Triglyceride | pos | mzRT MS2 | All | 100% |
| TG 58:8 | GL | Triglyceride | pos | mzRT MS2 | All | 100% |
| TG 58:9 | GL | Triglyceride | pos | mzRT MS2 | All | 100% |
| TG 58:10 | GL | Triglyceride | pos | mzRT MS2 | All | 94% |
| TG 58:11 | GL | Triglyceride | pos | mz MS2 | All | 92% |
| TG 60:10 | GL | Triglyceride | pos | mz MS2 | All | 90% |
| TG 60:11 | GL | Triglyceride | pos | mzRT MS2 | All | 94% |
| TG 60:12 | GL | Triglyceride | pos | mz MS2 | All | 78% |
| TG O-42:5 | GL | Triglyceride | pos | mz MS2 | All | 100% |
| TG O-50:1 | GL | Triglyceride | pos | mz MS2 | All | 100% |
| TG O-52:2 | GL | Triglyceride | pos | mz MS2 | All | 100% |
| DG 42:8 | GL | Diglyceride | pos | MS2 | DBS/PSC only | 64% |
| LPE-N (FA)38:5 | GP | Lysophosphatidylethanolamine | neg | mz MS2 | DBS/PSC only | 60% |
| O1_PC 34:3 | GP | Phosphatidylcholine (Ox) | neg | mz MS2 | DBS/PSC only | 68% |
| CAR 17:0 | FA | Acyl Carnitine | pos | mz MS2 | DBS only | 26% |
| Cer d36:2 | SP | Ceramide | neg | mz MS2 | DBS only | 85% |
| Cer d40:3 | SP | Ceramide | pos | mz MS2 | DBS only | 26% |
| Cer d42:4 | SP | Ceramide | neg | mz MS2 | DBS only | 26% |
| Cer d44:2 | SP | Ceramide | pos | mz MS2 | DBS only | 26% |
| Cer d44:3 | SP | Ceramide | pos | mz MS2 | DBS only | 26% |
| FA 18:0 (2OH) | FA | Free Fatty Acid | neg | mz MS2 | DBS only | 100% |
| FA 20:0 (2OH) | FA | Free Fatty Acid | neg | mz MS2 | DBS only | 70% |
| FA 21:0 (2OH) | FA | Free Fatty Acid | neg | mz MS2 | DBS only | 70% |
| FA 22:0 (2OH) | FA | Free Fatty Acid | neg | mz MS2 | DBS only | 86% |
| FA 22:0 (behenic acid) | FA | Free Fatty Acid | neg | mzRT MS2 | DBS only | 100% |
| FA 23:0 (2OH) | FA | Free Fatty Acid | neg | mz MS2 | DBS only | 78% |
| FA 26:0 (2OH) | FA | Free Fatty Acid | neg | mz MS2 | DBS only | 100% |
| FA 27:0 (2OH) | FA | Free Fatty Acid | neg | mz MS2 | DBS only | 70% |
| FA 28:0 (2OH) | FA | Free Fatty Acid | neg | mz MS2 | DBS only | 70% |
| FA 28:0 (montanic acid) | FA | Free Fatty Acid | neg | mzRT MS2 | DBS only | 100% |
| FA 30:0 | FA | Free Fatty Acid | neg | mz MS2 | DBS only | 100% |
| FA 32:0 | FA | Free Fatty Acid | neg | mz MS2 | DBS only | 100% |
| FAHFA 38:0\|FAHFA 16:0/22:0;O | FA | Fatty Acyl Esters of Hydroxy Fatty Acid | neg | mz MS2 | DBS only | 70% |
| FAHFA 40:0\|FAHFA 18:0/22:0;O | FA | Fatty Acyl Esters of Hydroxy Fatty Acid | neg | mz MS2 | DBS only | 70% |
| Hex2Cer 42:3;2O | SP | Hexosylceramide | pos | mz MS2 | DBS only | 26% |
| LPE 22:5 | GP | Lysophosphatidylethanolamine | pos | mz MS2 | DBS only | 29% |
| O1_Cer d42:3 | SP | Ceramide (Ox) | pos | MS2 | DBS only | 27% |
| O1_FA 18:3 | FA | Free Fatty Acid (Ox) | neg | mz MS2 | DBS only | 64% |
| O1_FA 21:0 | FA | Free Fatty Acid (Ox) | neg | mz MS2 | DBS only | 70% |
| O1_PC 24:0 | GP | Phosphatidylcholine (Ox) | neg | mz MS2 | DBS only | 26% |
| O1_PC 36:3 | GP | Phosphatidylcholine (Ox) | neg | mz MS2 | DBS only | 28% |
| O1_SM d32:1 | SP | Sphingomyelin (Ox) | pos | mz MS2 | DBS only | 26% |
| O2_FA 22:0 | FA | Free Fatty Acid (Ox) | neg | mz MS2 | DBS only | 70% |
| PA 34:1\|PA 16:0_18:1 | GP | Phosphatidic Acid | neg | mz MS2 | DBS only | 26% |
| PA 34:2\|PA 16:0_18:2 | GP | Phosphatidic Acid | neg | mz MS2 | DBS only | 26% |
| PA 36:2\|PA 18:0_18:2 | GP | Phosphatidic Acid | neg | mz MS2 | DBS only | 26% |
| PA 36:3\|PA 18:1_18:2 | GP | Phosphatidic Acid | neg | mz MS2 | DBS only | 26% |
| PA 36:4\|PA 16:0_20:4 | GP | Phosphatidic Acid | neg | mz MS2 | DBS only | 26% |
| PA 38:4\|PA 18:0_20:4 | GP | Phosphatidic Acid | neg | mz MS2 | DBS only | 30% |
| PA 38:5\|PA 18:1_20:4 | GP | Phosphatidic Acid | neg | mz MS2 | DBS only | 26% |
| PC 24:0 | GP | Phosphatidylcholine | pos | mz MS2 | DBS only | 26% |
| PC O-38:0 | GP | Phosphatidylcholine | pos | mz MS2 | DBS only | 26% |
| PE 32:0\|PE 16:0_16:0 | GP | Phosphatidylethanolamine | neg | mz MS2 | DBS only | 28% |

| | | | | | | |
|---|---|---|---|---|---|---|
| PE 34:3\|PE 16:0_18:3 | GP | Phosphatidylethanolamine | neg | mz MS2 | DBS only | 28% |
| PE 35:1 | GP | Phosphatidylethanolamine | pos | mz MS2 | DBS only | 26% |
| PE O-37:7 | GP | Phosphatidylethanolamine | neg | mz MS2 | DBS only | 28% |
| PE O-39:5 | GP | Phosphatidylethanolamine | neg | mz MS2 | DBS only | 30% |
| PE O-40:4 | GP | Phosphatidylethanolamine | neg | mz MS2 | DBS only | 26% |
| PEtOH 34:1 | GP | Phosphatidylethanol | neg | mz MS2 | DBS only | 34% |
| PEtOH 34:2 | GP | Phosphatidylethanol | neg | mz MS2 | DBS only | 21% |
| PS 34:1\|PS 16:0_18:1 | GP | Phosphatidylserine | neg | mz MS2 | DBS only | 30% |
| PS 34:2\|PS 16:0_18:2 | GP | Phosphatidylserine | neg | mz MS2 | DBS only | 26% |
| PS 36:3\|PS 18:1_18:2 | GP | Phosphatidylserine | neg | mz MS2 | DBS only | 26% |
| PS 36:4\|PS 16:0_20:4 | GP | Phosphatidylserine | neg | mz MS2 | DBS only | 30% |
| PS 38:6\|PS 16:0_22:6 | GP | Phosphatidylserine | neg | mz MS2 | DBS only | 26% |
| PS 40:4\|PS 18:0_22:4 | GP | Phosphatidylserine | pos | MS2 | DBS only | 30% |
| PS 40:8\|PS 20:4_20:4 | GP | Phosphatidylserine | neg | mz MS2 | DBS only | 26% |
| PS 42:10\|PS 20:4_22:6 | GP | Phosphatidylserine | neg | mz MS2 | DBS only | 26% |
| CAR 14:2 | FA | Acyl Carnitine | pos | mzRT | PI & DBS only | 57% |
| LPC 17:1 | GP | Lysophosphatidylcholine | pos | mzRT | PI & DBS only | 88% |
| LPE 22:4 | GP | Lysophosphatidylethanolamine | neg | mz MS2 | PI & DBS only | 51% |
| O1_FA 25:0 | FA | Free Fatty Acid (Ox) | neg | mz MS2 | PI & DBS only | 99% |
| PC O-36:0 | GP | Phosphatidylcholine | pos | mz MS2 | PI & DBS only | 44% |
| PS 38:3\|PS 18:0_20:3 | GP | Phosphatidylserine | neg | mz MS2 | PI & DBS only | 55% |
| Cer d42:3 | SP | Ceramide | pos | mz MS2 | Plasma only | 100% |
| FA 20:0 (arachidic acid) | FA | Free Fatty Acid | neg | mz MS2 | Plasma only | 100% |
| O2_FA 18:0 | FA | Free Fatty Acid (Ox) | neg | mz MS2 | Plasma only | 98% |
| TG 51:1 | GL | Triglyceride | pos | mzRT MS2 | Plasma only | 100% |
| FA 13:0 | FA | Free Fatty Acid | neg | mz MS2 | PSC only | 43% |
| FA 20:5 | FA | Free Fatty Acid | neg | mz MS2 | PSC only | 100% |
| DG 23:1 | GL | Diglyceride | pos | MS2 | Card contam. | 100% |
| DG 25:1 | GL | Diglyceride | pos | MS2 | Card contam. | 100% |
| DG 31:0 | GL | Diglyceride | pos | MS2 | Card contam. | 52% |
| FA 15:4 | FA | Free Fatty Acid | neg | mz MS2 | Card contam. | 100% |
| FA 36:0 | FA | Free Fatty Acid | neg | mz MS2 | Card contam. | 100% |
| NAE 9:0 | FA | N-acyl Ethanolamine | pos | MS2 | Card contam. | 100% |
| NAE 15:4 | FA | N-acyl Ethanolamine | pos | MS2 | Card contam. | 87% |
| O1_FA 22:0 | FA | Free Fatty Acid (Ox) | neg | mz MS2 | Card contam. | 99% |
| O1_FA 20:0 | FA | Free Fatty Acid (Ox) | neg | mz MS2 | Card contam. | 70% |
| O2_FA 21:1 | FA | Free Fatty Acid (Ox) | neg | mz MS2 | Card contam. | 59% |
| ST 29:2;O | ST | Sterol Lipid | pos | mz MS2 | DBS contam. | 26% |
| DG 25:0 | GL | Diglyceride | pos | MS2 | PSC contam. | 43% |
| DG 28:4 | GL | Diglyceride | pos | MS2 | PSC contam. | 43% |
| FA 15:0 | FA | Free Fatty Acid | neg | mz MS2 | PSC contam. | 43% |
| FA 17:0 | FA | Free Fatty Acid | neg | mz MS2 | PSC contam. | 43% |
| FAHFA 40:1 | FA | Fatty Acyl Esters of Hydroxy Fatty Acid | neg | mz MS2 | PSC contam. | 55% |
| NAE 18:0 | FA | N-acyl Ethanolamine | pos | MS2 | PSC contam. | 50% |
| NAE 20:0 | FA | N-acyl Ethanolamine | pos | MS2 | PSC contam. | 43% |
| NAE 20:1 | FA | N-acyl Ethanolamine | pos | MS2 | PSC contam. | 43% |
| NAE 20:2 | FA | N-acyl Ethanolamine | pos | MS2 | PSC contam. | 43% |
| ST 24:1;O5 | ST | Sterol Lipid | neg | mz MS2 | PSC contam. | 43% |

*Annotation level indicates method used to annotate the lipids. Mz = accurate mass; RT = retention time; MS2 = reference spectra match.

**Sample type designation indicates in which of the 3 sample types the corresponding lipid annotation can be found.

*** Sample fill is the percentage of samples the corresponding lipid is found in. There are 42 plasma, 54 PSC, and 48 DBS samples.

# Chapter 2: Improving Quantitative Accuracy in Nontargeted Lipidomics by Evaluating Adduct Formation

*Reproduced from "Improving Quantitative Accuracy in Nontargeted Lipidomics by Evaluating Adduct Formation" by Lauren M. Bishop, Tong Shen, and Oliver Fiehn, in Analytical Chemistry (2023).*

## 2.1 Abstract

For large-scale lipidomic analyses, accurate and reproducible quantification of endogenous lipids is crucial for comparing results within and across studies. Many lipids present in liquid chromatography–electrospray ionization–mass spectrometry form various adducts with buffer components. The mechanisms and conditions that dictate adduct formation are still poorly understood. In a positive mode, neutral lipids like mono-, di-, and triacylglycerides and cholesteryl esters typically generate [M + NH4]+ adduct ions, although [M + Na]+, [M + K]+, and other (more complex) species can also be significantly abundant in MS1 precursor ion spectra. Variations in the ratios of these adducts (within and between matrices) can lead to dramatic inaccuracies during quantification. Here, we examine 48 unique diacylglycerol (DAG) species across 2366 mouse samples for eight matrix-specific data sets of plasma, liver, kidney, brain, heart muscle, gastrocnemius muscle, gonadal, and inguinal fat. Typically, no single adduct ion species accounted for more than 60% of the total observed abundance across each data set. Even within a single matrix, DAGs showed a high variability of adduct ratios. The ratio of [M + NH4]+ adduct ions was increased for longer-chain DAGs and for polyunsaturated DAGs, at the expense of reduced ratios of [M + Na]+ adducts. When using three deuterated internal DAG standards, we found that absolute concentrations were estimated with up to 70% error when only one adduct ion was used instead of all adducts combined. Importantly, when combining [M + NH4]+ and [M + Na]+ adduct ions, quantification results were within 5% accuracy compared to all adduct ions combined. Additional variance can be caused by other factors, such as instrument conditions or matrix effects.

## 2.2 Introduction

The ability to identify hundreds of endogenous lipids using nontargeted workflows has made lipidomic analysis an important tool for biological discoveries. As methods for comprehensive lipid profiling have become more robust by liquid chromatography–high-resolution tandem mass spectrometry (LC–HRMS/MS), the complexity and scale of these analyses have continued to increase. In response to the upsurge of large-scale analyses, recent studies have explored the reliability of these methods through assessment of batch effects, differences in LC–MS platforms, and interlab performances. (1–3) Despite continuous advancements in LC–MS, nontargeted workflows remain challenged by issues of repeatability, data transferability, and quantitative accuracy. (4,5)

For both targeted and nontargeted analyses, it is most common to use the most abundant adduct form to represent an entire lipid subclass. Yet, LC–MS1 data are composed of thousands of m/z-retention time features that include natural isotopes, in-source fragments, and adducts. While these features are typically low abundant and often removed from analysis, adduct ions are regularly utilized for reporting the (semi)quantitative abundances of lipids. (6,7) In nontargeted lipidomic analyses by positive mode electrospray ionization (+ESI), polar lipid species will often yield protonated ion types [M + H]+, whereas neutral lipids will primarily form ammoniated [M + NH4]+ and sodiated [M + Na]+ adducts. (8) However, many lipid subclasses can also form abundant adduct species with alkali metals or experience in-source neutral losses, such as [M + H – H2O]+. (9,10) This variability in adduct formation is caused by both technical and biological factors. LC mobile phase additives, system contaminants, and matrix components are known to alter adduct ratios. (11,12) Previous studies have proposed methods to reduce or enhance specific adducts, (13,14) but such alterations may not be suitable to measure hundreds of lipids across many

lipid classes. Even data interpretation may be altered when different adduct forms are selected. (15) Strangely, links between adduct selection and quantitative accuracy have not been thoroughly investigated yet, although tools such as MS-FLO, CAMERA, RAMClustR, and Binner currently assist in identifying and joining adduct species. (16–19)

Hence, we explore the extent of variability in adduct formation in nontargeted lipidomic analyses and its impact on the quantitative accuracy. To evaluate adduct trends, eight data sets of different tissue matrices acquired between two instruments were analyzed for ESI positive mode adduct forms. For this analysis, diacylglycerol (DAG) species were utilized to demonstrate trends in adduct formation, given their proclivity for forming multiple significantly abundant adducts. Potential contributing factors to adduct ratio variability were investigated such as peak intensity, acyl group length, degree of unsaturation, and the biological matrix. Additionally, we compare the use of single adducts to joining adducts on the impacts of both relative quantification and absolute quantification via the estimation of molar concentrations. Resulting from this work, guidelines for proper adduct selection are proposed.

## 2.3 Experimental Section

### 2.3.1 Materials

UltimateSPLASH ONE lipidomics standards and supplemental standards of oleic acid-D9, arachidonic acid-D11, cholesterol-D7, and C17-sphingosine were purchased from Avanti Polar Lipids. Additional supplement standards of decanoyl-l-carnitine-D3, dodecanoyl-l-carnitine-D3, and octadecanoyl-l-carnitine-D3 were purchased from Cambridge Isotope Laboratories, and palmitic acid-D3 was purchased from CDN Isotopes. All reagents used were of LC–MS grade. Biological samples were provided as part of the mouse longevity project of the NIH Longevity Consortium. Mice were procured and maintained as previously described. (20) Tissue samples of

gonadal fat, inguinal fat, gastrocnemius muscle (gastroc), liver, kidney, heart, brain, and blood plasma were harvested and stored at −80 °C until analysis.

### 2.3.2 Sample Preparation

Gastrocnemius muscle, liver, kidney, heart, and brain samples were lyophilized for 24 h and homogenized using a SPEX SamplePrep 2010 GenoGrinder prior to extraction. The gonadal fat and inguinal fat samples were homogenized using a SPEX SamplePrep 2010 GenoGrinder concomitant with extractions. Twenty μL of plasma, 5 mg of gonadal and inguinal fat, 2 mg of lyophilized gastrocnemius muscle, and 1 mg of lyophilized liver, kidney, heart, and brain tissue samples were extracted by suspending in 225 μL of −20 °C cold methanol treated with the UltimateSPLASH ONE and supplemental standards. 750 μL of −20 °C cold methyl-tert-butyl ether (MTBE) containing a cholesteryl ester 22:1 standard was added to each sample and then vortexed for 10 min. Next, 188 μL of LC–MS grade water was added and vortexed for 5 min to induce the phase separation. Samples were centrifuged for 2 min at 14,000g before 350 μL of the upper nonpolar layer was collected and dried. 175 μL of the nonpolar phase was dried for the gonadal fat and inguinal fat samples due to the high lipid content of the matrix type. The remaining fractions of matrix-containing samples were combined to form pooled quality control (QC) samples. Samples were resuspended using 100 μL of methanol/toluene (9:1, v/v) with 50 ng/mL of 12-[(cyclohexylamine) carbonyl]amino]-dodecanoic acid (CUDA) and stored at −20 °C until analysis.

### 2.3.3 LC-MS/MS Data Acquisition

For nontargeted lipidomics analysis, 1 μL (gonadal and inguinal fat), 2 μL (gastroc), and 3 μL (plasma, liver, kidney, heart, and brain) of the resuspended nonpolar phase was injected into two ThermoFisher Scientific Vanquish UHPLC + liquid chromatography systems coupled to Q-Exactive HF orbital ion trap mass spectrometers. The LC system was equipped with a Waters

Acquity UPLC CSH C18 column (100 × 2.1 mm; 1.7 μm) and a Waters Acquity VanGuard CSH C18 precolumn (5 × 2.1 mm; 1.7 μm). The column compartment and mobile phase preheater were set at 65 °C, and the mobile phase flow rate was 0.6 mL/min. Mobile phase A was acetonitrile/water (60/40, v/v) with 0.1% formic acid and 10 mM ammonium formate as modifiers, and mobile phase B consisted of isopropanol/acetonitrile (90:10, v/v) with 0.1% formic acid and 10 mM ammonium formate. The LC gradient started with mobile phase B at 15%, increasing to 30% between 0 and 2 min. B was brought from 30 to 48% between 2 and 2.5 min, 48 to 82% between 2.5 and 11 min, and 82 to 99% from 11 to 11.5 min 99% B was maintained between 11.5 and 12 min and then brought back to 15% between 12 and 12.1 min and held there between 12.1 and 14.2 min for re-equilibration. The injection needle was washed 10 s after each injection with isopropanol.

Positive mode electrospray ionization (ESI+) used a spray voltage of 3.6 kV, capillary temperature of 300C, sheath gas flow rate of 60 units nitrogen, and auxiliary gas flow rate of 25 units nitrogen. Data were collected from 0 to 13 min of the LC gradient in the scan range of 120–1700 m/z using data-dependent acquisition (DDA) with the top four ions from each MS1 scan being selected for MS/MS fragmentation. DDA MS/MS was acquired with a stepped normalized collision energy of 20, 30, and 40%. MS1 spectra were collected with a resolving power setting of 60,000 measured at 200 m/z, and MS/MS spectra were collected at a resolving power setting of 15,000. To increase the total number of MS/MS spectra, five consecutive runs were made using the R package “IE-Omics” (21) for each matrix type under positive electrospray conditions. All spectra were stored in centroid, “.raw” format.

### 2.3.4 Data Analysis and Adduct Selection

The data were converted from ".raw" format into ".abf" format using the Analysis Base File converter. Deconvolution, peak picking, alignment, and compound identification were completed through open source software MS-DIAL v4.48. (22) Compounds were annotated using an internally curated mzRT library where lipids were matched by accurate mass and retention time, as well as matching accurate precursor masses and MS/MS fragmentation patterns against the LipidBlast library. (23) Annotated DAG species were isolated from each completed data set and reprocessed through MS-FLO to identify ion adducts, duplicate peaks, and isotopic features. (16) [M + NH4]+, [M + Na]+, [M + K]+, [M + H – H2O]+, [M + H]+, and dimerized adduct forms were considered. All adduct ions were verified by accurate mass, retention time, and correlations of peak intensity between adduct types of the same DAG compound. Peak height was used as the spectral intensity for all data analysis. Samples were normalized by Systematic Error Removal by Random Forest (SERRF) (24) to correct for instrument signal drifts. Protonated and dimerized DAG species were detected when the lipid was highly abundant but were consistently measured at 1–2% of the total abundance. These adduct forms were never consistently measured above 5% for the eight matrices analyzed; therefore, they were omitted from analysis. Three deuterated, monounsaturated DAG standards of known concentrations were included in the acquisition and utilized for estimations of absolute molar concentrations.

## 2.4 Results and Discussion

### 2.4.1 Overview

We identified 48 unique DAG species across eight mouse matrices: blood plasma (Pl), gonadal fat (GF), inguinal fat (IF), gastrocnemius muscle (gastroc, Gs), liver (Lv), kidney (Kd), heart (Ht), and brain (Br). All deuterated DAG internal standards were measured in all samples. Through evaluation of all matrices, four adduct species were found to be the most common; [M + Na]+, [M + NH4]+, [M + K]+, and [M + H – H2O]+. Protonated and dimerized adduct forms were consistently absent or low abundant in the data sets and omitted from this analysis. Adduct response ratios for each DAG molecule were calculated from the summed intensities of the four adducts measured in this analysis.

### 2.4.2 Evaluation of Adduct Ratios

To explore the impact of adduct formation on large-scale lipidomics studies, we analyzed the differences in adduct ratios from three perspectives: across individual biological samples, between different DAG species, and between data sets of different tissue matrices. Utilizing results from more than 240 unique biological samples analyzed for each tissue, we first evaluated the variability of adduct ratios on a sample-to-sample basis. The consistency of these adduct ratios was assessed using the median of the relative standard deviation (% RSD) values of all annotated DAG species across all samples per tissue type. In a few cases, a large variance was found for adduct ratios, as exemplified for MS1 spectra of plasma DAG 36:4 with [M + NH4]+ at 634.54 m/z, [M + Na]+ at 639.50 m/z, and [M + K]+ at 655.47 m/z (Figure 1). These examples represent the potential for significant variation as impacted by changes in instrument conditions over time or by variations in endogenous concentrations. Yet, the median% RSD of adduct ratios across biological samples was consistently <15% RSD for the two major adduct forms (Table 1). Conversely, liver and brain

samples showed higher variability for [M + NH4]+ adducts, which were consistently measured with less than 20% of the total ion abundance (Tables 1 and S1). This trend was also observed for other low-abundance adducts such as potassiated adducts and water loss ion species (Table 1). There were negligible trends observed when the samples were organized by run order (Figure S1).

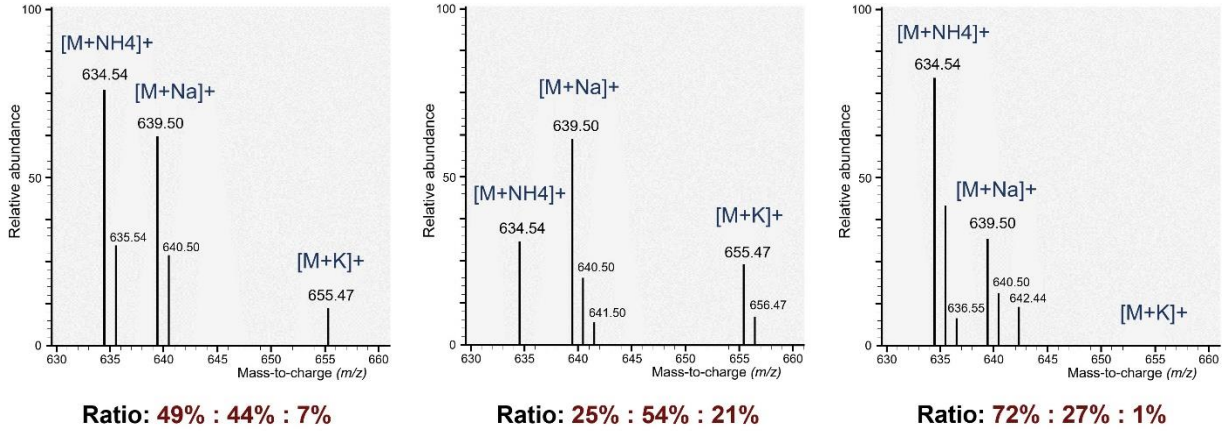


**Figure 2.1:** Examples of measurement variance in ratios of [M + NH4]+, [M + Na]+, and [M + K]+ ion types for an endogenous diacylglyceride, DAG (36:4), between three individual mouse plasma samples across one batch of lipidomics LC–HRMS analyses.

**Table 2.1:** Overall Measurement Variance (Median % RSD) of the Ratio of Adduct Forms in Diacylglycerides across Biological Samples

| matrix type | number of samples | $[M + Na]^+$ | $[M + NH_4]^+$ | $[M + K]^+$ | $[M + H\text{-}H_2O]^+$ |
|---|---|---|---|---|---|
| plasma | 279 | 6.9 % | 17.7 % | 19.1 % | - |
| gonadal fat | 277 | 9.4 % | 6.3 % | 19.3 % | - |
| inguinal fat | 279 | 7.5 % | 7.8 % | 13.5 % | - |
| gastroc | 245 | 7.4 % | 10.1 % | 17.3 % | 51.4 % |
| liver | 275 | 5.6 % | 25.0 % | 22.7 % | 37.4 % |
| kidney | 265 | 5.9 % | 15.2 % | 21.5 % | 14.8 % |
| heart | 268 | 3.5 % | 18.0 % | 22.1 % | 18.0 % |
| brain | 278 | 13.4 % | 20.2 % | 31.6 % | 23.3 % |

While each DAG was robustly measured at <15% RSD for the dominant [M + NH4]+ and [M + Na]+ adducts across samples for each matrix type, we found profound differences in the total adduct ratios between the DAG species observed within these matrices. For example, on average [M + NH4]+ ions made up 32% of the total intensity of all of the adducts across the 15 DAG species in plasma (Table 2). Yet, some DAGs showed 13% abundance for [M + NH4]+, while other DAGs were present at 77% abundance (Figure 2, Table S1). Hence, the variance of ion ratios across the different DAG species was markedly higher than the measurement variance across samples. We found considerably lower variance of adduct ratios for DAG species in gonadal and inguinal fat compared to other matrix types.

**Table 2.2:** Average Adduct Ion Ratios (±SD) across All Measured DAG Species for Each Matrix Type

| matrix type | number of DAG species | $[M + Na]^+$ (%) | $[M + NH_4]^+$ (%) | $[M + K]^+$ (%) | $[M + H\text{-}H_2O]^+$ (%) |
|---|---|---|---|---|---|
| plasma | 15 | 57 ± 12 | 32 ± 11 | 15 ± 4 | |
| gonadal fat | 20 | 38 ± 6 | 57 ± 9 | | |
| inguinal fat | 34 | 43 ± 6 | 44 ± 9 | 14 ± 4 | |
| gastroc | 34 | 40 ± 14 | 51 ± 17 | 8 ± 2 | |
| liver | 13 | 69 ± 9 | 12 ± 4 | 16 ± 4 | 8 ± 3 |
| kidney | 18 | 49 ± 16 | 31 ± 20 | 11 ± 4 | 17 ± 4 |
| heart | 18 | 57 ± 14 | 22 ± 15 | 13 ± 4 | 13 ± 3 |
| brain | 10 | 53 ± 9 | 19 ± 10 | 14 ± 5 | 21 ± 7 |

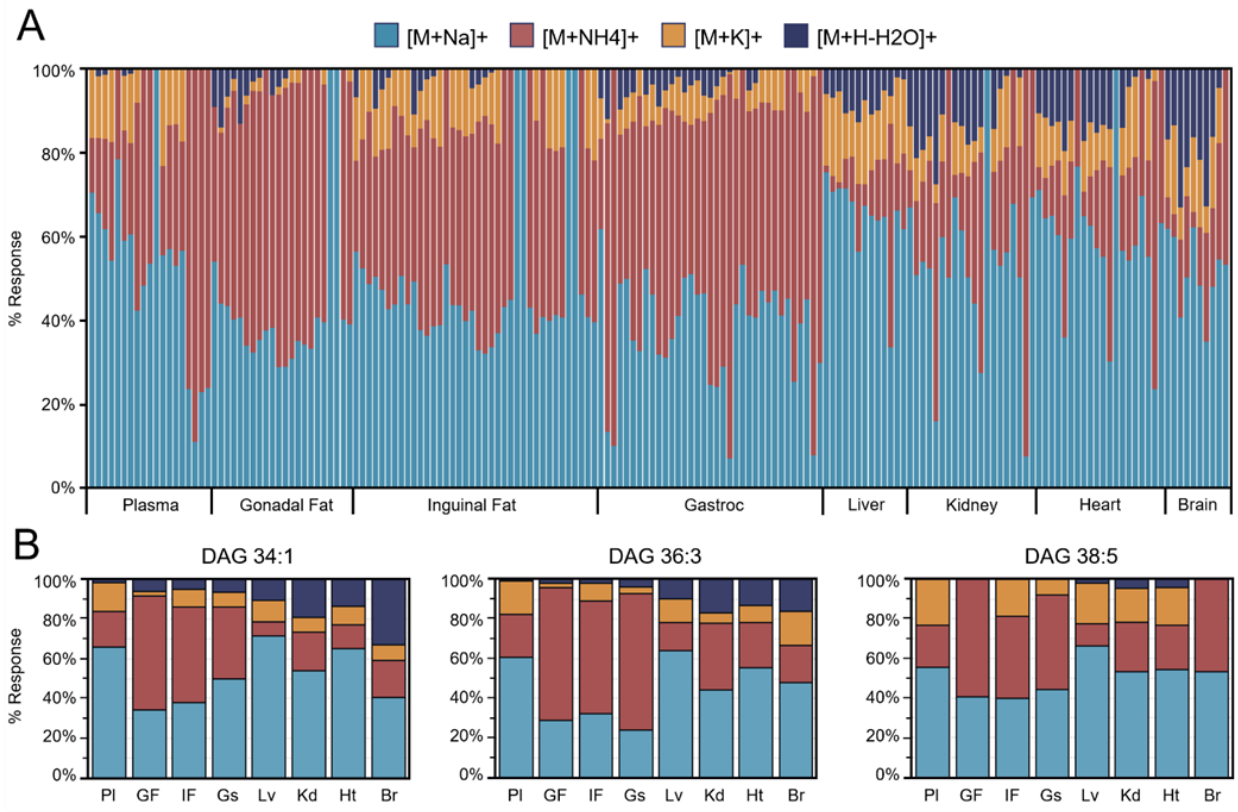


**Figure 2.2:** (A) Graphical representation of response ratios of all annotated endogenous DAG species for [M + Na]+, [M + NH4]+, [M + K]+, and [M + H – H2O]+ adducts in pooled QC samples across the eight mouse matrices analyzed. (B) Average adduct ratios for each matrix type between three commonly found DAG species.

However, significant changes in these ratios were still observed between specific annotations within fat tissues. For example, DAG 30:0 was detected with 62% abundance for the [M + Na]+ adduct and 23% for the [M + NH4]+ adduct in inguinal fat. Conversely, DAG 36:3 was present at a 35% relative ratio for the [M + Na]+ adduct and 55% for the [M + NH4]+ adduct. Therefore, even among the lesser variability of adipose tissue, we found up to 30% difference in adduct ratios between DAG species. This finding contradicts the notion that a single ion adduct might suffice to universally quantify lipids across an entire lipid subclass in any specific matrix type.

Variance of adduct ratios was even greater between matrix types (Figure 2A, Tables 2 and S1). Overall, sodiated adducts were detected at consistently high ratios across all matrices. For low

abundant DAG species, sometimes the sodiated adducts were the only detectable ion species, whereas for other DAG species, the sodiated adducts could form less than 10% of the total ion abundance (Figure 2A, Table S1). Similarly, the abundance of ammoniated adducts ranged from 90% to less than 5% for different DAG species across all matrices. Again, this finding reinforces the idea that a single adduct ion is not as reliable in the application of relative quantification methods or estimations of total lipid concentrations in classes that form multiple abundant adducts, such as DAGs. In some tissues, potassiated and neutral loss ion species reached up to 20% of the overall DAG ratio for individual DAG lipids (Figure 2A, Table S1). For example, the water neutral loss ion for DAG 34:1 reached 33% abundance in brain tissues, while DAG 38:5 was detected at 23% abundance for the [M + K]+ adduct in plasma (Figure 2B). DAG 36:3 showed up to 70% ion ratios for ammoniated adducts for fat and muscle tissues but considerably lower abundance in other matrices with only 15% abundance in liver (Figure 2B, Table S1). Overall [M + H – H2O]+ adduct ratios were noticeably higher in liver, kidney, heart, and brain (Figure 2a), specifically for DAG 34:1 and DAG 36:3 but nearly absent in other matrices while water loss adduct ions in DAG 38:5 were consistently low abundant even in liver, kidney, heart, and brain (Figure 2b). Hence, ion ratios were found to be impacted by both the matrix-specific batches and the ionization patterns of individual DAG species.

### 2.4.3 Factors Contributing to Variance in Adduct Ratios

The observed variance between compounds in adduct formation for DAG lipids led us to examine DAG-specific properties that might impact the variation of adduct ratios. Here, we focused on three possible factors influencing adduct ratios: (a) carbon chain lengths, (b) degree of fatty acyl unsaturation, and (c) the absolute peak intensity of DAG species (Figure 3). We saw a remarkably consistent trend in decreasing abundance for [M + Na]+ ions in plasma with increasing

carbon chain lengths from 32 to 40 total carbons (Figure 3A, right panel). This decrease was balanced by an increase in the formation of ammoniated adduct ions, while the ratio of potassiated adducts remained stable with increasing acyl chain lengths (Figure 3). We summarized these observations for all DAG species and across all eight matrices in a heat map, showing that ammoniated adducts were consistently increased in abundance with an increasing number of carbons across all tissues (Figure 3A, left panel). However, sodiated and ammoniated trends were not always opposite. For example, brain DAG species represented the largest trend differences for [M + NH4]+ ions with a 30% ratio increase from 32 to 40 total carbons. Yet, sodiated DAG species in brain tissues remained fairly stable, while potassiated and water loss ion ratios both showed a consistent decrease with increased carbon chain lengths. In kidney, decreases in water loss ion ratios were also found with larger carbon chain lengths, whereas other matrix types showed only modest or no trends in adduct ratios, with the exception of ammoniated ions.

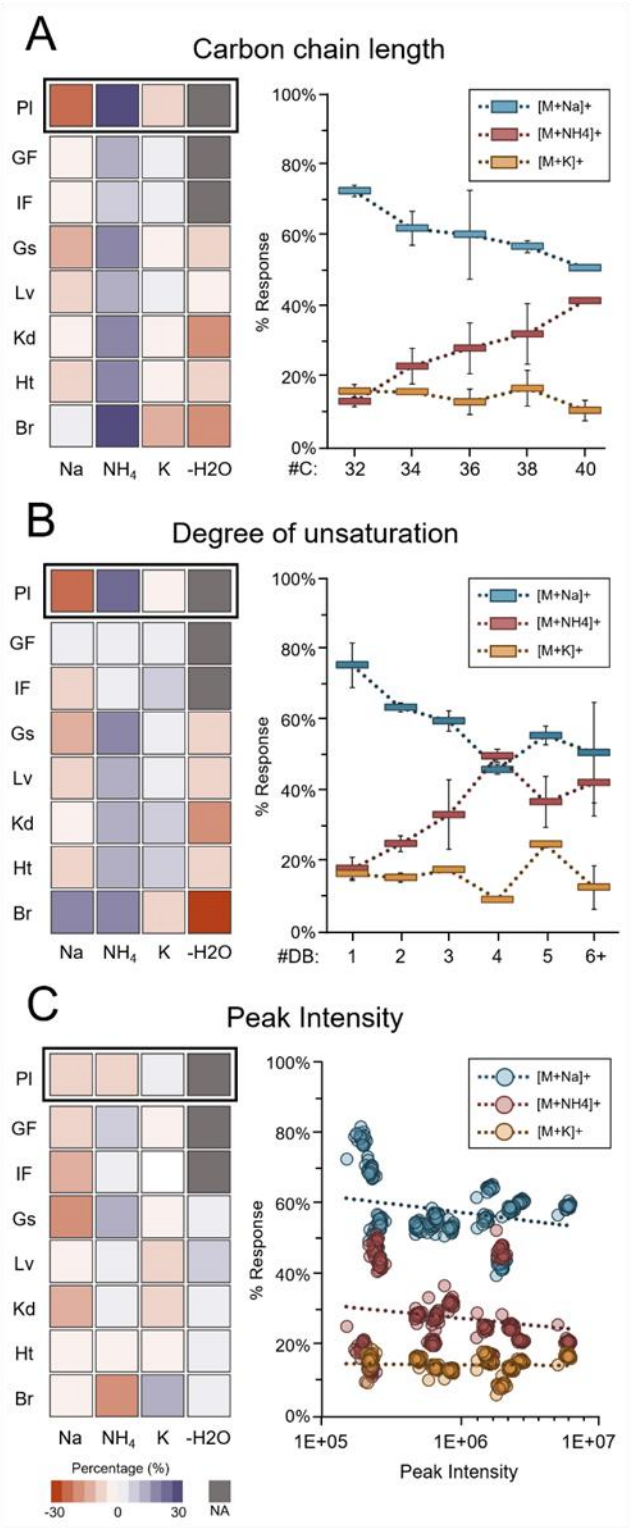


**Figure 2.3:** Changes in average adduct ratios across pooled QC samples. Left panels: heat maps per organ (blue: highest, red: lowest; gray: sporadic or no detection) Pl, plasma; GF, gonadal fat; IF, inguinal fat; Gs, gastrocnemius muscle; Lv, liver; Kd, kidney; Ht, heart, and Br, brain. Right panels: trend graphs averaging all organs. (A) Relative abundance per number of carbons. (B) Relative abundance per number of double bonds. (C) Relative abundance per average peak intensity across pooled QC samples.

Overall, very similar trend patterns were found for an increasing number of double bonds (Figure 3B). Again, the largest differences were found for plasma, specifically for the sodiated and ammoniated adducts (Figure 3B). Potassiated adducts showed minimal changes across all tissues, while water loss ion ratios consistently decreased with higher levels of unsaturation for all matrix types for which these ions were detectable. Interestingly, a 15% increase in the adduct ratio for sodiated adducts was observed in brain tissue. Taken together, these observations detail strong structural influences on adduct formation in DAG species that is correlated to both carbon chain length and degree of unsaturation, especially for primary adduct forms. (25) To address a potential bias in the analysis due to the correlation of carbon chain lengths and degree of unsaturation, we repeated the analyses across increasing numbers of double bonds in C34 and C36 DAGs, as well as across monounsaturated and diunsaturated species of increasing carbon chain length (Figure S2). The same overall trends were observed as before, indicating that both parameters contributed to differences in ion ratios.

Last, we assessed absolute peak intensity as an independent factor. The few DAG species measured with 100% [M + Na]+ across the different data sets were relatively low abundant, suggesting a connection between the biological concentration and adduct formation. Overall, only very modest trends were observed with high variance across intensity values and adduct species. For example, in plasma only very slight decreases were found for sodiated and ammoniated adducts (Figure 3C, right panel) and even absent trends in other tissues such as heart muscle. Nonetheless, sodiated adducts decreased with increased peak intensity in inguinal fat, gastrocnemius muscle, and kidney tissues at −10% levels. Other matrices showed less than 10% change in either direction, except for brain tissues, which showed a 19% decrease in [M + NH4]+ and a 16% increase in [M + K]+ in correspondence to increased peak intensities. Overall, therefore,

trends in adduct formation was mostly impacted by carbon chain lengths and degree of unsaturation but not by total peak intensities. Yet, the complexity of these processes inhibits accurate predictions regarding adduct formation in different matrix types or instrument conditions.

Other factors that we did not systematically evaluate were variance between instruments, reproducibility of buffer compositions across batches, or the stability of instrument conditions over time. Indeed, instrument conditions greatly affect the mechanisms of adduct formation (11,26) as well as in-source fragmentation. (27) In the present study, two LC-Orbitrap HF mass spectrometers were used during acquisition and led to distinct shifts in the relative adduct ratios, particularly with respect to water loss ion species. The prevalence of these water losses is likely due to different ion source conditions because other parameters such as solvents, flow rates, and buffers were kept identical. (27) Biological influences also serve as potential instigators of matrix-specific changes in adduct formation. Similar to the trends observed for peak intensities of individual lipid species, total lipid content is also known to slightly influence instrument response and could help explain the comparable adduct trends in the lipid-rich adipose and gastrocnemius tissues. (28) Additionally, the formation of alkali metal adducts has often been linked to in vivo concentrations and may be strongly impacted by matrix effects. (29) This idea is supported by the notable differences in potassium adduct ion abundance between gonadal and inguinal fat samples. Similarly, the primary adduct for most DAGs, [M + Na]+, presents average shifts of 10–15% between the different data sets acquired on the same LC–MS system, again indicating potential influence of endogenous sodium levels. It is therefore reasonable to assume that the variation observed between data sets is caused by a combination of technical and biological factors. We therefore set out to determine a more robust choice in the use of internal standards to address both types of variance.

### 2.4.4 Adduct Selection for Accurate Quantification

While relative quantitation has remained the primary approach for nontargeted analyses, there have been increasing efforts to incorporate more robust methods for absolute quantification into these workflows. (30,31) Although detailing true absolute concentrations is unrealistic for thousands of nontargeted analytes, standardized comparisons of lipidomic analyses across batches, instruments, and laboratories must transit from reporting arbitrary peak intensities to estimates of molar concentration. (32) Current methods use single-point calibration or surrogate calibrants with appropriate correction factors to account for changes in ionization efficiencies within lipid subclasses. (33) In addition, the nonlinearity of signal responses should be considered. (34) In estimating molar concentrations using these procedures, the impact of adduct formation has been underexplored, possibly due to the assumption that isotopically labeled internal standards will behave nearly identical to their corresponding endogenous compound. While this is likely true for each identical pair of endogenous lipid species and its exact isotope-labeled counterpart, we here see that such comparisons do not hold true across all species in a lipid subclass like DAGs, even among similarly structured species. Therefore, we investigated the influence of joining adduct intensities on the accuracy of absolute quantification in comparison with utilizing a single representative adduct form.

First, to ensure that there were no unintended effects of combining adducts on data interpretation, we evaluated the median precision of absolute peak intensity measurements across 25 QC samples (Table S2). All annotated DAG species across the eight matrix types exhibited an equal or improved precision for combined adducts in comparison to measuring only a single adduct form. Thus, we infer that data quality either improves or stays the same when adducts are joined. We then evaluated quantitative accuracy for monounsaturated DAG species using different

adducts and combinations of adducts. Specifically, we studied peak intensities of sodiated and ammoniated adducts in isolation, in combination between these two dominant ions, and in combination of all four adduct forms. For this evaluation, we employed three deuterated monounsaturated DAG internal standards with DAG 31:1-d5 at 25 μg/mL extraction solvent, DAG 33:1-d5 at 50 μg/mL, and DAG 35:1-d5 at 75 μg/mL. The concentrations of DAG species were adjusted to the extraction solvent volume for the different matrices and plotted against the total peak intensity for each adduct combination (Figure 4A). The three concentrations of DAG internal standards were fitted with a linear regression and the resulting slope was used for absolute quantification. All adduct combinations displayed a R2 value greater than 0.94.

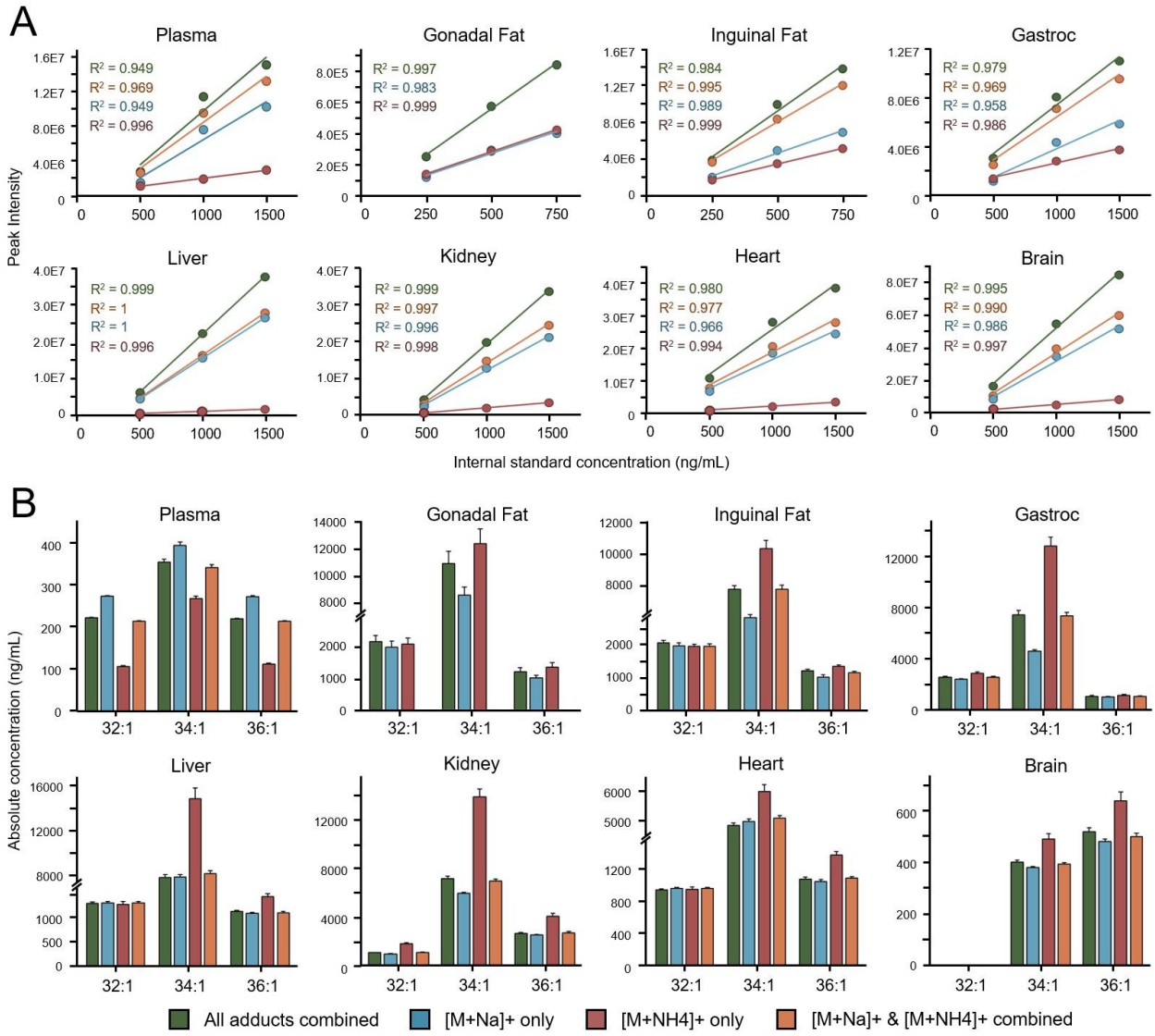


**Figure 2.4:** (A) Linearity of three deuterated, monounsaturated DAG internal standards through different combinations of adduct ions. (B) Estimated molar concentrations of DAG 32:1, DAG 34:1, and DAG 36:1 were calculated from the slopes of the deuterated standard peak intensities. The same combinations of adducts were used between the standards and endogenous DAG compounds.

We theorized that joining all four adduct forms provided the most accurate concentrations because it encompassed all available data for the specific compound. Yet, even this estimate of quantitative concentrations may still include unrecognized systematic errors. We then compared calculated endogenous DAG concentrations for [M + Na]+, [M + NH4]+, and {[M + Na]+ and [M + NH4]+} against the combination of all four adducts (Figure 4B). When solely relying on [M +

Na]+ ions for quantification, differences of up to 25% in absolute concentrations were found compared to the use of all four adducts across the eight data sets, as exemplified in measuring DAG 34:1 in gastroc tissues. Overall, however, most DAG species quantified by [M + Na]+ showed a difference in estimated molar concentrations of less than 10% in the different tissues. Conversely, when only [M + NH4]+ ions were used for quantifications, most DAG species showed more than 20% quantification errors (Figure 4B). Importantly, the combination of sodiated and ammoniated adduct intensities, {[M + Na]+ and [M + NH4]+}, proved to be the most reliable way to measure DAG concentrations with only a maximum of 5% difference to the calculated concentrations from using all adducts (including potassiated and water loss ion species). We therefore strongly recommend using the most dominant ion species in lipid quantifications, especially for DAGs, to correct adduct formation differences among matrix types. Interestingly, we found that the presumed accuracy of quantifying endogenous DAG lipid using a single adduct was correlated to the respective adduct ratios between the internal standard and the endogenous lipid species. Figure 5 demonstrates that when the response ratio of a single adduct varied by >20% between the endogenous species and the corresponding internal standard, the absolute concentration would also vary by >20% with respect to our control of using all four adduct forms.

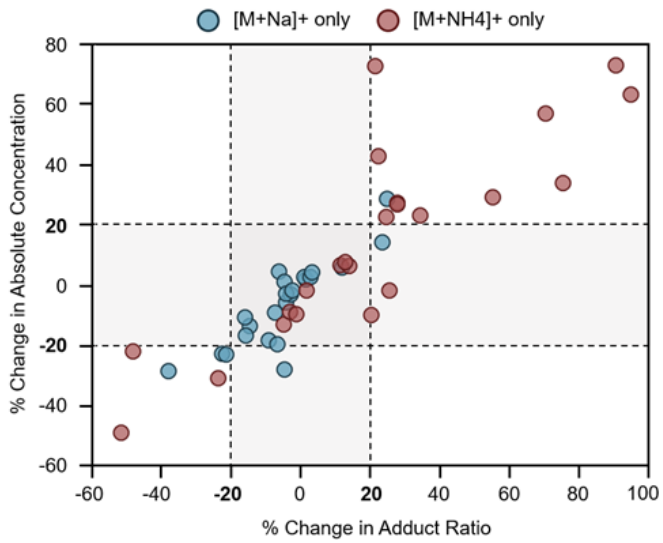


**Figure 2.5:** Correlation of the percent change in absolute concentrations and percent change in adduct ratios between endogenous DAGs and the corresponding deuterated DAG standards.

## 2.5 Conclusions

From these observations, we suggest that the relative ratio of adducts is the most important variable to consider for quantitative accuracy. To avoid significant inaccuracies in the relative and absolute ends of quantification, at least 80% of the total abundance should be contained within the adducts selected for analysis. Nontargeted lipidomic studies performed across multiple batches, different LC–MS systems, or separate laboratories should prioritize the proper adduct selection to ensure sufficient data transferability for quantitative analyses.

## 2.6 References


(1) Olshansky, G.; Giles, C.; Salim, A.; Meikle, P.J. Challenges and opportunities for prevention and removal of unwanted variation in lipidomic studies. Prog. Lipid Res. 2022, 87, 101177.

(2) Ghorasaini, M.; Mohammed, Y.; Adamski, J.; Bettcher, L.; Bowden, J. A.; Cabruja, M.; Contrepois, K.; Ellenberger, M.; Gajera, B.; Haid, M.; Hornburg, D.; Hunter, C.; Jones, C. M.; Klein, T.; Mayboroda, O.; Mirzaian, M.; Moaddel, R.; Ferrucci, L.; Lovett, J.; Nazir, K.; Pearson, M.; Ubhi, B. K.; Raftery, D.; Riols, F.; Sayers, R.; Sijbrands, E. J. G.; Snyder, M. P.; Su, B.; Velagapudi, V.; Wil-liams, K. J.; de Rijke, Y. B.; Giera, M. Cross-Laboratory Standardization of Preclinical Lipidomics Using Differential Mobility Spectrometry and Multiple Reaction Monitoring. Anal. Chem. 2021, 93, 16369– 16378.

(3) Triebl, A.; Burla, B.; Selvalatchmanan, J.; Oh, J.; Tan, S.H.; Chan, M.Y.; Mellet, N.A.; Meikle, P.J.; Torta, F.; Wenk, M.R. Shared reference materials harmonize lipidomics across MS-based detection platforms and laboratories. J. Lipid Res. 2020, 61, 105-115.

(4) Ulmer, C.Z.; Koelmel, J.P.; Jones, C.M.; Garrett, T.J.; Aristizabal-Henao, J.J.; Vesper, H.W.; Bowden, J.A. A Review of Efforts to Improve Lipid Stability during Sample Preparation and Standardization Efforts to Ensure Accuracy in the Reporting of Lipid Measurements. Lipids. 2021, 56, 3-16.

(5) Cajka, T; Fiehn, O. Toward Merging Untargeted and Targeted Methods in Mass Spectrometry-Based Metabolomics and Lipidomics. Anal. Chem. 2016, 88, 524-545.

(6) Khan, M.J.; Codreanu, S.G.; Goyal, S.; Wages, P.A.; Gorti, S.K.K.; Pearson, M.J.; Uribe, I.; Sherrod, S.D.; McLean, J.A.; Porter, N.A.; Robinson, R.A.S. Evaluating a targeted

multiple reaction monitoring approach to global untargeted lipidomic analyses of human plasma. Rapid Commun. Mass Spectrom. 2020, 34, e8911.

(7) Mortier, K.A.; Zhang, G.; Van Peteghem, C.H.; Lambert, W.E. Adduct formation in quantitative bioanalysis: Effect of ionization conditions on paclitaxel. J. Am. Soc. Mass Spectrom. 2004, 15, 585-592.

(8) Murphy, R.C. Challenges in mass spectrometry-based lipidomics of neutral lipids. TrAC, Trends Anal. Chem. 2018, 107, 91-98.

(9) Kruve, A.; Kaupmees, K. Adduct Formation in ESI/MS by Mobile Phase Additives. J. Am. Soc. Mass Spectrom. 2017, 28, 887-894.

(10) Knittelfelder, O.L.; Weberhofer, B.P.; Eichmann, T.O.; Kohlwein, S.D.; Rechberger, G.N. A versatile ultra-high performance LC-MS method for lipid profiling. J. Chromatogr. B. 2014, 951-952, 119-128.

(11) Alechaga, E.; Moyano, E.; Galceran, M.T. Ion-molecule ad-duct formation in tandem mass spectrometry. Bioanal. Anal. Chem. 2016, 408, 1269-1277.

(12) Dziadosz, M. Multiple analyte adduct formation in liquid chromatography-tandem mass spectrometry - Advantages and limitations in the analysis of biologically-related samples. J. Chromatogr. B. 2018, 1084, 1-3.

(13) Yang, X.J.; Qu, Y.; Yuan, Q.; Wan, P.; Du, Z.; Chen, D.; Wong, C. Effect of ammonium on liquid- and gas-phase protonation and deprotonation in electrospray ionization mass spectrometry. Analyst. 2012, 138, 659-665.

(14) Gonzalez-Riano, C.; Gradillas, A.; Barbas, C. Exploiting the formation of adducts in mobile phases with ammonium fluoride for the enhancement of annotation in liquid

chromatography-high resolution mass spectrometry based lipidomics. J. Chromatogr. Open. 2021, 1, 100018.

(15) Abbassi-Ghadi, N.; Jones, E.A.; Gomez-Romero, M.; Golf, O.; Kumar, S.; Huang, J.; Kudo, H.; Goldin, R.D.; Hanna, G.B.; Takats, Z. A Comparison of DESI-MS and LC-MS for the Lipidomic Profiling of Human Cancer Tissue. J. Am. Soc. Mass. Spectrom. 2016, 27, 255-264.

(16) DeFelice, B.C.; Mehta, S.S.; Samra, S.; Cajka, T.; Wancewicz, B.; Fahrmann, J.F.; Fiehn, O. Mass Spectral Feature List Optimizer (MS-FLO): A Tool to Minimize False Positive Peak Reports in Untargeted Liquid Chromatography–Mass Spectroscopy (LC-MS) Data Processing. Anal. Chem. 2017, 89,3250-3255.

(17) Kuhl, C.; Tautenhahn, R.; Böttcher, C.; Larson, T. R.; Neumann, S. CAMERA: An Integrated Strategy for Compound Spectra Extraction and Annotation of Liquid Chromatography/Mass Spectrometry Data Sets. Anal. Chem. 2012, 84, 283-289.

(18) Broeckling, C.D.; Afsar, F.A.; Neumann, S.; Ben-Hur, A.; Prenni, J.E. RAMClust: A Novel Feature Clustering Method Enables Spectral-Matching-Based Annotation for Metabolomics Data. Anal. Chem. 2014, 86, 14, 6812-6817.

(19) Kachman, M.; Habra, H.; Duren, W.; Wigginton, J.; Sajjakulnukit, P.; Michailidis, G.; Burant, C.; Karnovsky, A. Deep annotation of untargeted LC-MS metabolomics data with Binner. Bioinformatics. 2020, 36, 1801-1806.

(20) Miller, R.A.; Harrison, D.E.; Astle, C.M.; Fernandez, E.; Flurkey, K.; Han, M.; Javors, M.A.; Li, X.; Nadon, N.L.; Nelson, J.F.; Pletcher, S.; Salmon, A.B.; Sharp, Z.B.; Van Roekel, S.; Winkleman, L.; Strong, R. Rapamycin-mediated lifespan increase in mice is

dose and sex dependent and metabolically distinct from dietary restriction. Aging Cell, 2014, 13, 468-477.

(21) Koelmel, J.P.; Kroeger, N.M.; Gill, E.L.; Ulmer, C.Z.; Bowd-en, J.A.; Patterson, R.E.; Yost, R.A.; Garrett, T.J. Expanding Lipidome Coverage Using LC-MS/MS Data-Dependent Acquisition with Automated Exclusion List Generation. J. Am. Soc. Mass. Spectrom. 2017, 28, 908-917.

(22) Tsugawa, H.; Cajka, T.; Kind, T.; Ma, Y.; Higgins, B.; Ikeda, K.; Kanazawa, M.; VanderGheynst, J.; Fiehn, O.; Arita, M. MS-DIAL: data-independent MS/MS deconvolution for comprehensive metabolome analysis. Nat. Methods. 2015, 12, 523-526.

(23) Kind, T.; Liu, K.; Lee, D.Y.; DeFelice, B.; Meissen, J.K.; Fiehn, O. LipidBlast in silico tandem mass spectrometry database for lipid identification. Nat. Methods. 2013, 10, 755-758.

(24) Fan, S.; Kind, T.; Cajka, T.; Hazen, S.L.; Tang, W.H.W.; Kaddurah-Daouk, R.; Irvin, M.R.; Arnett, D.K.; Barupal, D.K.; Fiehn, O. Systematic Error Removal Using Random Forest for Normalizing Large-Scale Untargeted Lipidomics Data. Anal. Chem. 2019, 91, 3590-3596.

(25) Broeckling, C.D; Ganna, A.; Layer, M.; Brown, K.; Sutton, B.; Ingelsson, E.; Peers, G.; Prenni, J.E. Enabling Efficient and Confident Annotation of LC−MS Metabolomics Data through MS1 Spectrum and Time Prediction. Anal. Chem. 2016, 88, 18, 9226-9234.

(26) Li, X.; Ma, M.; Scherban, K.; Tam, Y.K. Liquid chromatography-electrospray mass spectrometric studies of ginkgolides and bilobalide using simultaneous monitoring of proton, ammonium and sodium adducts. Analyst. 2002,127, 641-646.

(27) Criscuolo, A.; Zeller, M.; Fedorova, M. Evaluation of Lipid In-Source Fragmentation on Different Orbitrap-based Mass Spectrometers. J. Am. Soc. Mass Spectrom. 2020, 31, 463-466.

(28) Erngren, I.; Haglof, J.; Engskog, M.K.R.; Nestor, M.; Hedeland, M; Arvidsson, T.; Pettersson, C. Adduct formation in electrospray ionisation-mass spectrometry with hydrophilic interaction liquid chromatography is strongly affected by the inorganic ion concentration of the samples. J. Chromatogr. A. 2019, 1600, 174-182.

(29) Wang, M.; Wang, C.; Han, X. Selection of internal standards for accurate quantification of complex lipid species in biological extracts by electrospray ionization mass spectrometry—What, how and why? Mass Spectrom. Rev. 2017, 36, 693-714.

(30) Rakusanova, S.; Fiehn, O.; Cajka, T. Toward building mass spectrometry-based metabolomics and lipidomics atlases for biological and clinical research. TrAC. Trends Anal. Chem. 2023, 158, 116825.

(31) Lange, M.; Fedorova, M. Evaluation of lipid quantification accuracy using HILIC and RPLC MS on the example of NIST® SRM® 1950 metabolites in human plasma. Anal. Bioanal. Chem. 2020, 412, 3573-3584.

(32) Drotleff, B.; Illison, J.; Schlotterbeck, J.; Lukowski, R.; Lämmerhofer, M. Comprehensive lipidomics of mouse plasma using class-specific surrogate calibrants and SWATH acquisition for large-scale lipid quantification in untargeted analysis. Anal. Chim. Acta. 2019, 1086, 90-102.

(33) Yu, H.; Huan, T. Patterned Signal Ratio Biases in Mass Spectrometry-Based Quantitative Metabolomics. Anal. Chem. 2021, 93, 4, 2254-2262.

## 2.7 Supplemental Information

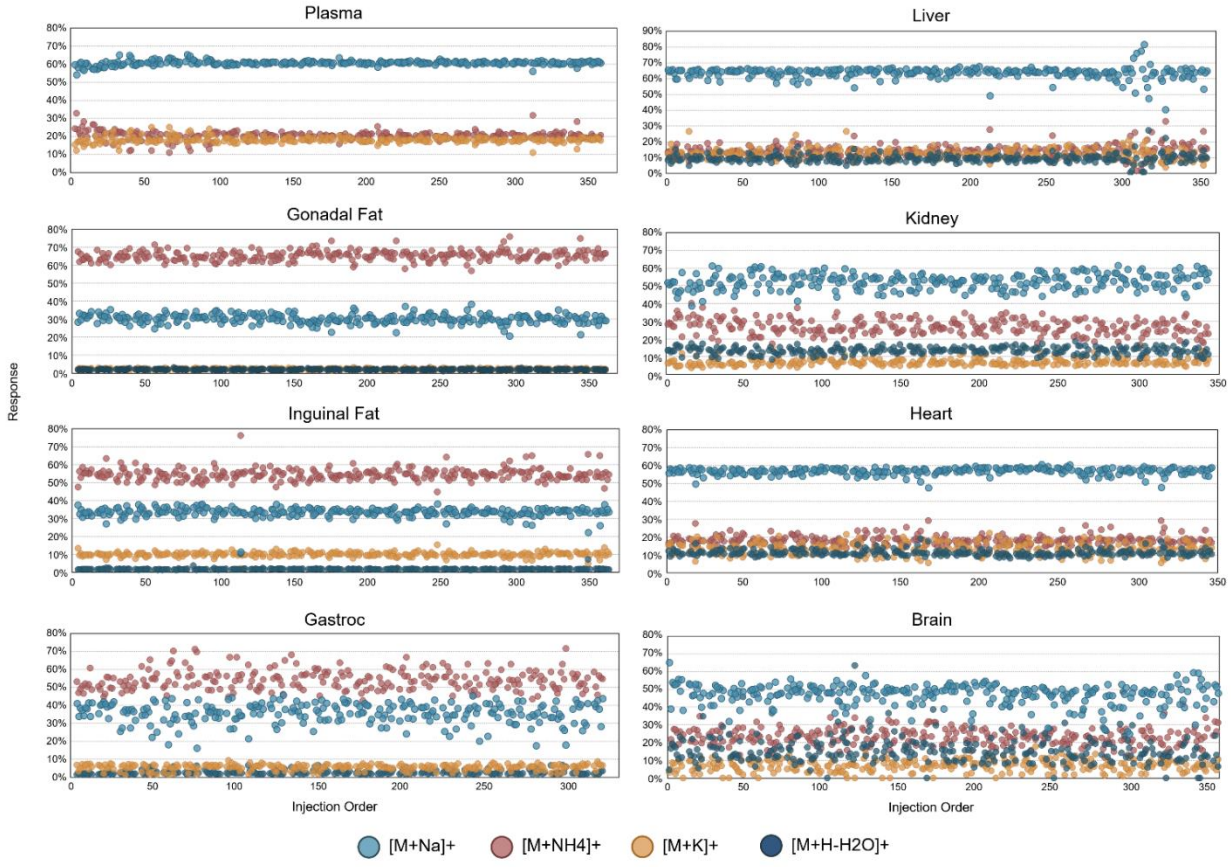


**Figure S1:** The adduct ratios for DAG 36:3 measured in each biological sample relative to injection order.

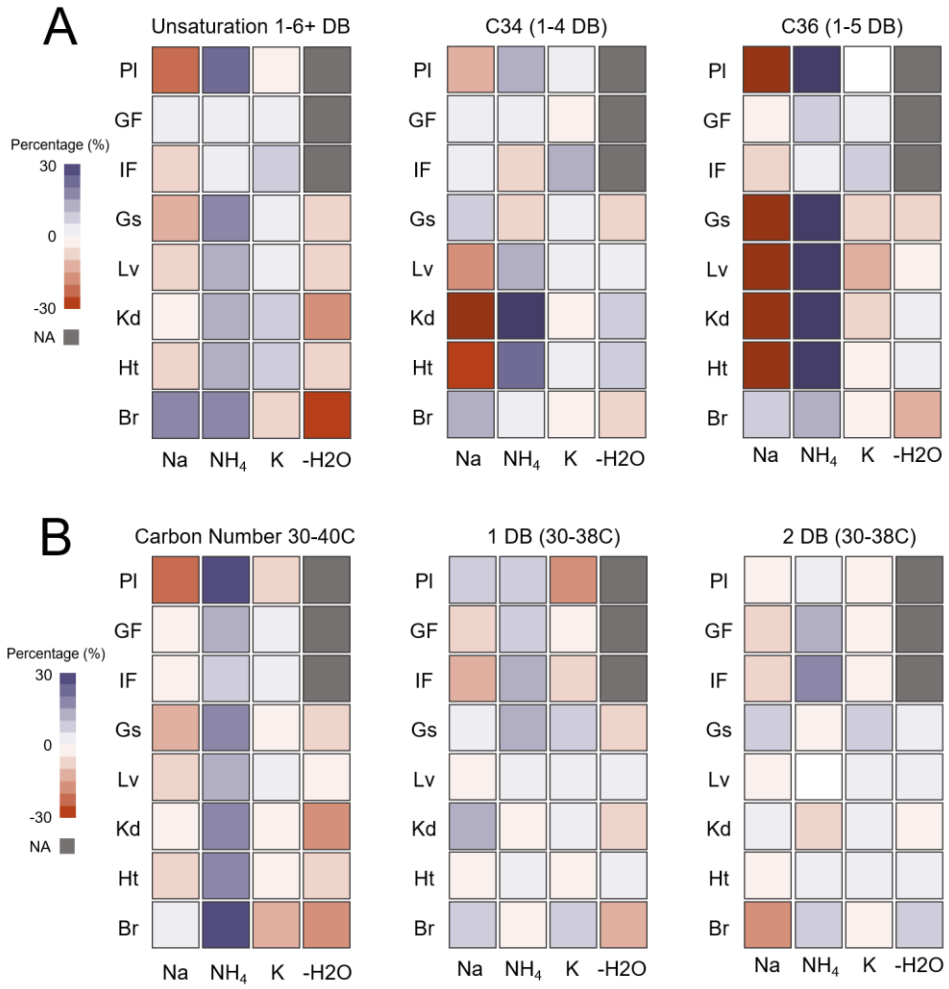


**Figure S2:** (A) The change in average ratio for each adduct ion based on the degree of unsaturation. The left-most panel highlights the trends in adduct ratios between the number of double bonds, regardless of carbon chain length. The middle and right-most charts show adduct ratio changes across an increasing degree of unsaturation with a constant number of carbons. Blue indicates an increase in relative ratio of the adduct ion and red indicates a decrease. (B) The change in average ratio for each adduct ion based on the number of carbons. The left-most panel shows the average change in adduct ratio relative to increasing carbon chain length with any number of double bonds. The middle and right-most charts show the same analysis with a constant degree of unsaturation, respectively.

**Table S1:** Average ratio of adduct forms for each annotated lipid across all matrices.

| Matrix | Lipid Name | [M+Na]+ | [M+NH4]+ | [M+K]+ | [M+H-H2O]+ |
|---|---|---|---|---|---|
| Plasma | DAG 32:1 | 0.707 | 0.131 | 0.163 | - |
| | DAG 34:1 | 0.659 | 0.180 | 0.148 | 0.015 |
| | DAG 34:2 | 0.619 | 0.216 | 0.154 | 0.012 |
| | DAG 34:3 | 0.542 | 0.282 | 0.173 | - |
| | DAG 36:1 | 0.786 | 0.214 | - | - |
| | DAG 36:2 | 0.590 | 0.263 | 0.130 | 0.015 |
| | DAG 36:3 | 0.604 | 0.218 | 0.166 | 0.009 |
| | DAG 36:4 | 0.423 | 0.496 | 0.079 | - |
| | DAG 36:5 | 0.484 | 0.516 | - | - |
| | DAG 38:3 | 0.536 | 0.464 | - | - |
| | DAG 38:4 | 1 | - | - | - |
| | DAG 38:5 | 0.555 | 0.214 | 0.230 | - |
| | DAG 38:6 | 0.570 | 0.294 | 0.133 | - |
| | DAG 38:7 | 0.533 | 0.340 | 0.131 | - |
| | DAG 40:7 | 0.568 | 0.261 | 0.172 | - |
| | DAG 40:8 | 0.236 | 0.764 | - | - |
| | DAG 50:0 | 0.110 | 0.890 | - | - |
| | DAG 50:1 | 0.229 | 0.771 | - | - |
| | DAG 50:2 | 0.239 | 0.761 | - | - |
| Gonadal Fat | DAG 30:0 | 0.530 | 0.363 | - | 0.087 |
| | DAG 32:0 | 0.440 | 0.407 | 0.012 | 0.138 |
| | DAG 32:1 | 0.438 | 0.477 | 0.026 | 0.065 |
| | DAG 32:2 | 0.402 | 0.548 | 0.029 | 0.022 |
| | DAG 34:0 | 0.412 | 0.468 | - | 0.131 |
| | DAG 34:1 | 0.341 | 0.578 | 0.021 | 0.063 |
| | DAG 34:2 | 0.324 | 0.624 | 0.023 | 0.028 |
| | DAG 34:3 | 0.354 | 0.592 | 0.032 | 0.020 |
| | DAG 34:4 | 0.377 | 0.623 | - | - |
| | DAG 36:1 | 0.383 | 0.555 | - | 0.061 |
| | DAG 36:2 | 0.289 | 0.653 | 0.020 | 0.040 |
| | DAG 36:3 | 0.291 | 0.667 | 0.023 | 0.021 |
| | DAG 36:4 | 0.309 | 0.661 | 0.030 | - |
| | DAG 36:5 | 0.351 | 0.615 | 0.032 | - |
| | DAG 38:2 | 0.342 | 0.658 | - | - |
| | DAG 38:3 | 0.333 | 0.667 | - | - |
| | DAG 38:5 | 0.408 | 0.592 | - | - |
| | DAG 38:6 | 0.394 | 0.565 | 0.036 | - |
| | DAG 39:7 | 1 | - | - | - |
| | DAG 39:8 | 1 | - | - | - |
| | DAG 40:7 | 0.402 | 0.598 | - | - |
| | DAG 40:8 | 0.395 | 0.587 | 0.028 | - |
| Inguinal Fat | DAG 30:0 | 0.563 | 0.217 | 0.152 | 0.066 |
| | DAG 30:1 | 0.525 | 0.309 | 0.167 | - |
| | DAG 30:2 | 0.486 | 0.412 | 0.100 | - |
| | DAG 32:0 | 0.504 | 0.288 | 0.115 | 0.093 |
| | DAG 32:1 | 0.474 | 0.334 | 0.144 | 0.048 |
| | DAG 32:2 | 0.426 | 0.383 | 0.169 | 0.019 |
| | DAG 32:3 | 0.435 | 0.471 | 0.086 | - |
| | DAG 33:1 | 0.505 | 0.381 | 0.110 | - |
| | DAG 33:2 | 0.436 | 0.401 | 0.156 | - |
| | DAG 34:0 | 0.489 | 0.317 | 0.077 | 0.106 |
| | DAG 34:1 | 0.377 | 0.480 | 0.090 | 0.051 |
| | DAG 34:2 | 0.363 | 0.515 | 0.097 | 0.024 |
| | DAG 34:3 | 0.387 | 0.449 | 0.148 | 0.016 |
| | DAG 34:4 | 0.387 | 0.425 | 0.184 | - |
| | DAG 35:1 | 0.534 | 0.466 | - | - |
| | DAG 35:2 A | 0.437 | 0.422 | 0.138 | - |
| | DAG 35:2 B | 0.435 | 0.419 | 0.144 | - |
| | DAG 35:3 | 0.397 | 0.440 | 0.159 | - |

| | | | | | |
|---|---|---|---|---|---|
| | DAG 36:1 | 0.424 | 0.424 | 0.109 | 0.044 |
| | DAG 36:2 | 0.329 | 0.547 | 0.088 | 0.036 |
| | DAG 36:3 | 0.322 | 0.568 | 0.092 | 0.019 |
| | DAG 36:4 | 0.336 | 0.532 | 0.124 | 0.007 |
| | DAG 36:5 | 0.370 | 0.452 | 0.177 | - |
| | DAG 37:2 | 0.432 | 0.568 | - | - |
| | DAG 37:3 | 0.450 | 0.550 | - | - |
| | DAG 37:7 | 1 | - | - | - |
| | DAG 37:8 | 1 | - | - | - |
| | DAG 38:2 | 0.432 | 0.568 | - | - |
| | DAG 38:3 | 0.370 | 0.511 | 0.123 | - |
| | DAG 38:4 | 0.409 | 0.591 | - | - |
| | DAG 38:5 | 0.400 | 0.412 | 0.189 | - |
| | DAG 38:6 | 0.413 | 0.392 | 0.194 | - |
| | DAG 38:7 | 0.410 | 0.410 | 0.188 | - |
| | DAG 39:7 | 1 | - | - | - |
| | DAG 39:9 | 1 | - | - | - |
| | DAG 40:6 | 0.463 | 0.537 | - | - |
| | DAG 40:7 | 0.410 | 0.405 | 0.189 | - |
| | DAG 40:8 | 0.396 | 0.387 | 0.216 | - |
| **Gastroc** | DAG 30:0 | 0.619 | 0.216 | 0.098 | 0.069 |
| | DAG 30:1 | 0.134 | 0.731 | 0.009 | 0.118 |
| | DAG 30:2 | 0.101 | 0.899 | - | - |
| | DAG 32:0 | 0.489 | 0.355 | 0.060 | 0.096 |
| | DAG 32:1 | 0.500 | 0.360 | 0.074 | 0.066 |
| | DAG 32:2 | 0.353 | 0.522 | 0.069 | 0.054 |
| | DAG 32:3 | 0.328 | 0.610 | 0.064 | - |
| | DAG 33:1 | 0.524 | 0.341 | 0.076 | 0.059 |
| | DAG 33:2 | 0.462 | 0.415 | 0.087 | 0.036 |
| | DAG 34:1 | 0.319 | 0.550 | 0.045 | 0.088 |
| | DAG 34:2 | 0.312 | 0.596 | 0.042 | 0.050 |
| | DAG 34:3 | 0.356 | 0.545 | 0.063 | 0.035 |
| | DAG 34:4 | 0.412 | 0.479 | 0.092 | 0.017 |
| | DAG 35:1 | 0.503 | 0.374 | 0.070 | 0.055 |
| | DAG 35:2 A | 0.510 | 0.356 | 0.095 | 0.037 |
| | DAG 35:3 | 0.462 | 0.420 | 0.091 | 0.026 |
| | DAG 36:1 | 0.464 | 0.411 | 0.061 | 0.062 |
| | DAG 36:2 | 0.247 | 0.650 | 0.036 | 0.067 |
| | DAG 36:3 | 0.242 | 0.686 | 0.032 | 0.039 |
| | DAG 36:4 | 0.290 | 0.648 | 0.043 | 0.018 |
| | DAG 36:5 | 0.071 | 0.916 | 0.006 | 0.006 |
| | DAG 37:3 | 0.437 | 0.489 | 0.070 | - |
| | DAG 38:1 | 0.534 | 0.466 | - | - |
| | DAG 38:2 | 0.411 | 0.486 | 0.050 | 0.049 |
| | DAG 38:3 | 0.407 | 0.499 | 0.061 | 0.032 |
| | DAG 38:4 | 0.470 | 0.448 | 0.078 | - |
| | DAG 38:5 | 0.445 | 0.478 | 0.079 | - |
| | DAG 38:6 | 0.473 | 0.431 | 0.097 | - |
| | DAG 38:7 | 0.413 | 0.492 | 0.097 | - |
| | DAG 40:3 | 0.453 | 0.547 | - | - |
| | DAG 40:5 | 0.255 | 0.745 | - | - |
| | DAG 40:6 | 0.392 | 0.550 | 0.055 | - |
| | DAG 40:7 | 0.451 | 0.447 | 0.100 | - |
| | DAG 40:8 | 0.078 | 0.907 | 0.015 | - |
| | DAG 40:9 | 0.298 | 0.702 | - | - |
| **Liver** | DAG 32:0 | 0.754 | 0.016 | 0.172 | 0.058 |
| | DAG 32:1 | 0.707 | 0.037 | 0.188 | 0.067 |
| | DAG 34:0 | 0.714 | 0.015 | 0.216 | 0.052 |
| | DAG 34:1 | 0.717 | 0.070 | 0.109 | 0.105 |
| | DAG 34:2 | 0.686 | 0.108 | 0.110 | 0.098 |
| | DAG 34:3 | 0.566 | 0.163 | 0.148 | 0.126 |
| | DAG 36:1 | 0.673 | 0.051 | 0.201 | 0.073 |
| | DAG 36:2 | 0.652 | 0.108 | 0.133 | 0.107 |
| | DAG 36:3 | 0.640 | 0.145 | 0.119 | 0.097 |

| | | | | | |
|---|---|---|---|---|---|
| | DAG 36:4 | 0.648 | 0.138 | 0.164 | 0.050 |
| | DAG 36:5 | 0.334 | 0.531 | 0.066 | 0.063 |
| | DAG 38:5 | 0.663 | 0.112 | 0.207 | 0.018 |
| | DAG 38:6 | 0.618 | 0.181 | 0.177 | 0.024 |
| **Kidney** | DAG 32:0 | 0.670 | 0.090 | 0.104 | 0.136 |
| | DAG 32:1 | 0.512 | 0.178 | 0.104 | 0.213 |
| | DAG 34:1 | 0.540 | 0.191 | 0.076 | 0.191 |
| | DAG 34:2 | 0.524 | 0.256 | 0.059 | 0.159 |
| | DAG 34:3 | 0.159 | 0.522 | 0.046 | 0.274 |
| | DAG 35:2 A | 0.601 | 0.182 | 0.112 | 0.108 |
| | DAG 35:3 | 0.502 | 0.498 | - | - |
| | DAG 36:0 | 0.691 | 0.053 | 0.126 | 0.125 |
| | DAG 36:1 | 0.621 | 0.139 | 0.113 | 0.135 |
| | DAG 36:2 | 0.503 | 0.241 | 0.076 | 0.179 |
| | DAG 36:3 | 0.441 | 0.338 | 0.050 | 0.170 |
| | DAG 36:4 | 0.275 | 0.528 | 0.061 | 0.137 |
| | DAG 37:7 | 1 | - | - | - |
| | DAG 38:2 | 0.573 | 0.186 | 0.104 | 0.142 |
| | DAG 38:5 | 0.540 | 0.255 | 0.175 | 0.047 |
| | DAG 38:6 | 0.577 | 0.256 | 0.175 | 0.015 |
| | DAG 40:5 | 0.665 | 0.314 | - | - |
| | DAG 40:7 | 0.503 | 0.314 | 0.165 | 0.018 |
| | DAG 40:8 | 0.076 | 0.924 | - | - |
| | DAG 42:7 | 0.694 | 0.306 | - | - |
| **Heart** | DAG 32:0 | 0.710 | 0.054 | 0.128 | 0.104 |
| | DAG 32:1 | 0.644 | 0.096 | 0.144 | 0.115 |
| | DAG 34:1 | 0.650 | 0.120 | 0.095 | 0.134 |
| | DAG 34:2 | 0.604 | 0.179 | 0.093 | 0.124 |
| | DAG 34:3 | 0.361 | 0.340 | 0.107 | 0.194 |
| | DAG 35:2 A | 0.593 | 0.185 | 0.096 | 0.122 |
| | DAG 35:3 | 0.768 | 0.232 | - | - |
| | DAG 36:0 | 0.652 | 0.058 | 0.121 | 0.171 |
| | DAG 36:1 | 0.626 | 0.117 | 0.130 | 0.126 |
| | DAG 36:2 | 0.575 | 0.186 | 0.090 | 0.152 |
| | DAG 36:3 | 0.552 | 0.230 | 0.085 | 0.132 |
| | DAG 36:4 | 0.303 | 0.464 | 0.091 | 0.142 |
| | DAG 37:7 | 1 | - | - | - |
| | DAG 38:2 | 0.569 | 0.181 | 0.113 | 0.140 |
| | DAG 38:5 | 0.545 | 0.223 | 0.193 | 0.042 |
| | DAG 38:6 | 0.579 | 0.210 | 0.191 | 0.017 |
| | DAG 40:5 | 0.687 | 0.297 | - | - |
| | DAG 40:7 | 0.554 | 0.231 | 0.195 | 0.022 |
| | DAG 40:8 | 0.235 | 0.732 | 0.027 | - |
| | DAG 42:7 | 0.634 | 0.366 | - | - |
| **Brain** | DAG 32:0 | 0.615 | 0.074 | 0.137 | 0.165 |
| | DAG 34:0 | 0.599 | 0.053 | 0.211 | 0.133 |
| | DAG 34:1 | 0.406 | 0.186 | 0.077 | 0.329 |
| | DAG 34:2 | 0.509 | 0.197 | 0.070 | 0.235 |
| | DAG 36:0 | 0.621 | 0.036 | 0.178 | 0.161 |
| | DAG 36:1 | 0.482 | 0.139 | 0.161 | 0.215 |
| | DAG 36:2 | 0.346 | 0.257 | 0.064 | 0.323 |
| | DAG 36:3 | 0.486 | 0.190 | 0.173 | 0.162 |
| | DAG 36:4 | 0.551 | 0.281 | 0.133 | 0.043 |
| | DAG 38:5 | 0.533 | 0.467 | - | - |

**Table S2:** Adduct dependent measurement variance (median %RSD) of absolute peak intensity across 25 QC samples.

| Matrix | Lipid Name | [M+Na]+ | [M+NH4]+ | [M+K]+ | [M+H-H2O]+ |
|---|---|---|---|---|---|
| Plasma | DAG 32:1 | 3.2% | 11.8% | 12.6% | 3.3% |
| | DAG 34:1 | 5.4% | 3.3% | 6.7% | 4.7% |
| | DAG 34:2 | 5.1% | 2.4% | 6.8% | 4.2% |
| | DAG 34:3 | 3.4% | 4.6% | 5.4% | 3.6% |
| | DAG 36:1 | 6.7% | 8.5% | - | 6.1% |
| | DAG 36:2 | 4.4% | 3.5% | 6.0% | 3.9% |
| | DAG 36:3 | 4.8% | 3.1% | 5.9% | 3.6% |
| | DAG 36:4 | 5.2% | 4.4% | 9.9% | 4.5% |
| | DAG 36:5 | 4.1% | 5.5% | - | 3.0% |
| | DAG 38:3 | 5.9% | 4.3% | - | 4.6% |
| | DAG 38:5 | 3.9% | 5.3% | 2.7% | 3.2% |
| | DAG 38:6 | 4.1% | 5.8% | 7.3% | 3.8% |
| | DAG 38:7 | 4.1% | 4.3% | 6.6% | 3.4% |
| | DAG 40:7 | 4.3% | 3.3% | 5.0% | 3.4% |
| | DAG 40:8 | 4.3% | 3.5% | 47.5% | 2.9% |
| Gonadal Fat | DAG 30:0 | 10.3% | 8.6% | - | 9.9% |
| | DAG 32:0 | 8.7% | 6.5% | 21.7% | 6.2% |
| | DAG 32:1 | 8.8% | 8.2% | 13.9% | 8.2% |
| | DAG 32:2 | 9.2% | 9.0% | 15.7% | 8.9% |
| | DAG 34:0 | 9.1% | 10.8% | - | 9.8% |
| | DAG 34:1 | 7.1% | 8.4% | 7.3% | 7.7% |
| | DAG 34:2 | 8.0% | 8.9% | 7.3% | 8.6% |
| | DAG 34:3 | 8.1% | 8.0% | 9.4% | 8.1% |
| | DAG 34:4 | 10.5% | 7.8% | - | 8.6% |
| | DAG 36:1 | 8.5% | 10.1% | - | 9.5% |
| | DAG 36:2 | 7.0% | 9.3% | 7.3% | 8.7% |
| | DAG 36:3 | 7.2% | 8.8% | 6.0% | 8.2% |
| | DAG 36:4 | 8.1% | 8.1% | 8.1% | 8.1% |
| | DAG 36:5 | 9.3% | 7.7% | 19.2% | 8.3% |
| | DAG 38:2 | 10.5% | 11.0% | - | 10.5% |
| | DAG 38:3 | 6.1% | 6.7% | - | 6.2% |
| | DAG 38:5 | 9.3% | 8.9% | - | 8.7% |
| | DAG 38:6 | 8.6% | 7.9% | 17.4% | 8.2% |
| | DAG 40:7 | 9.0% | 8.0% | - | 8.5% |
| | DAG 40:8 | 8.3% | 7.0% | 16.9% | 7.1% |
| Inguinal Fat | DAG 30:0 | 5.2% | 4.7% | 8.2% | 4.8% |
| | DAG 30:1 | 5.6% | 3.9% | 8.0% | 4.2% |
| | DAG 30:2 | 7.7% | 5.7% | 33.6% | 5.8% |
| | DAG 32:0 | 2.9% | 4.0% | 4.7% | 2.9% |
| | DAG 32:1 | 4.6% | 3.2% | 4.1% | 3.6% |
| | DAG 32:2 | 3.7% | 3.4% | 4.4% | 3.3% |
| | DAG 32:3 | 9.9% | 6.7% | 28.3% | 8.0% |
| | DAG 33:1 | 4.2% | 4.8% | 13.9% | 3.9% |
| | DAG 33:2 | 4.9% | 3.7% | 9.9% | 4.0% |
| | DAG 34:0 | 5.8% | 5.5% | 20.1% | 4.7% |
| | DAG 34:1 | 3.1% | 4.7% | 3.4% | 3.1% |
| | DAG 34:2 | 3.1% | 4.5% | 2.9% | 3.6% |
| | DAG 34:3 | 5.0% | 3.5% | 4.6% | 4.1% |
| | DAG 34:4 | 4.2% | 4.1% | 5.1% | 3.5% |
| | DAG 35:1 | 6.0% | 4.7% | - | 5.3% |
| | DAG 35:2 | 4.5% | 5.2% | 5.5% | 3.3% |
| | DAG 35:3 | 4.8% | 4.0% | 9.6% | 3.7% |
| | DAG 36:1 | 6.0% | 4.6% | 7.8% | 4.2% |
| | DAG 36:2 | 4.2% | 3.3% | 5.1% | 3.7% |
| | DAG 36:3 | 3.4% | 3.3% | 3.2% | 3.0% |
| | DAG 36:4 | 4.0% | 3.6% | 3.2% | 3.2% |
| | DAG 36:5 | 3.7% | 3.5% | 4.1% | 3.4% |
| | DAG 37:2 | 5.4% | 8.4% | - | 5.4% |
| | DAG 37:3 | 7.1% | 5.0% | - | 5.0% |

| | | | | | |
|---|---|---|---|---|---|
| | DAG 38:2 | 6.0% | 5.6% | - | 3.6% |
| | DAG 38:3 | 4.6% | 4.0% | 5.5% | 3.9% |
| | DAG 38:4 | 3.1% | 4.8% | - | 3.4% |
| | DAG 38:5 | 3.8% | 3.4% | 3.7% | 2.5% |
| | DAG 38:6 | 5.2% | 3.7% | 4.3% | 4.3% |
| | DAG 38:7 | 5.1% | 5.8% | 7.7% | 4.6% |
| | DAG 40:6 | 8.3% | 5.7% | - | 6.2% |
| | DAG 40:7 | 3.8% | 3.7% | 4.2% | 2.8% |
| | DAG 40:8 | 4.0% | 3.5% | 4.7% | 3.6% |
| **Gastroc** | DAG 30:0 | 3.0% | 5.2% | 3.3% | 3.3% |
| | DAG 30:1 | 6.6% | 5.4% | 24.2% | 4.2% |
| | DAG 30:2 | 13.0% | 5.2% | - | 5.3% |
| | DAG 32:0 | 2.4% | 5.6% | 3.8% | 3.6% |
| | DAG 32:1 | 2.7% | 4.2% | 3.0% | 3.1% |
| | DAG 32:2 | 2.5% | 4.0% | 3.3% | 3.0% |
| | DAG 32:3 | 2.9% | 4.7% | 4.7% | 3.1% |
| | DAG 33:1 | 3.0% | 4.5% | 3.1% | 3.4% |
| | DAG 33:2 | 3.1% | 4.4% | 3.4% | 3.4% |
| | DAG 34:1 | 2.5% | 5.8% | 2.2% | 5.0% |
| | DAG 34:2 | 3.9% | 5.1% | 4.6% | 4.7% |
| | DAG 34:3 | 2.4% | 4.9% | 2.3% | 3.8% |
| | DAG 34:4 | 3.7% | 4.8% | 3.5% | 3.9% |
| | DAG 35:1 | 4.8% | 6.3% | 6.8% | 5.9% |
| | DAG 35:2 | 5.1% | 5.1% | 3.8% | 4.8% |
| | DAG 35:3 | 3.1% | 4.7% | 4.6% | 3.5% |
| | DAG 36:1 | 4.9% | 6.1% | 6.0% | 5.4% |
| | DAG 36:2 | 3.9% | 6.8% | 5.4% | 5.4% |
| | DAG 36:3 | 3.1% | 6.9% | 3.0% | 5.9% |
| | DAG 36:4 | 4.3% | 5.5% | 4.4% | 4.8% |
| | DAG 36:5 | 5.6% | 4.6% | 24.1% | 4.4% |
| | DAG 37:3 | 3.5% | 5.3% | 5.5% | 4.6% |
| | DAG 38:1 | 5.3% | 5.8% | - | 4.7% |
| | DAG 38:2 | 3.9% | 6.2% | 3.9% | 5.2% |
| | DAG 38:3 | 4.4% | 5.9% | 3.6% | 4.6% |
| | DAG 38:4 | 3.7% | 4.8% | 3.4% | 3.9% |
| | DAG 38:5 | 4.3% | 5.6% | 3.1% | 4.8% |
| | DAG 38:6 | 3.3% | 4.8% | 3.7% | 3.8% |
| | DAG 38:7 | 3.8% | 5.3% | 3.6% | 4.0% |
| | DAG 40:5 | 14.9% | 6.0% | - | 6.0% |
| | DAG 40:6 | 5.9% | 6.8% | 7.7% | 6.3% |
| | DAG 40:7 | 4.9% | 6.8% | 5.3% | 6.0% |
| | DAG 40:8 | 6.7% | 5.6% | 22.1% | 5.4% |
| | DAG 40:9 | 9.6% | 6.5% | - | 5.8% |
| **Liver** | DAG 32:0 | 3.3% | 5.9% | 2.5% | 3.2% |
| | DAG 32:1 | 3.1% | 6.3% | 2.4% | 3.2% |
| | DAG 34:0 | 2.9% | 5.7% | 2.5% | 2.6% |
| | DAG 34:1 | 2.9% | 6.4% | 2.0% | 3.4% |
| | DAG 34:2 | 2.1% | 4.2% | 1.3% | 2.2% |
| | DAG 34:3 | 2.5% | 4.5% | 3.2% | 3.4% |
| | DAG 36:1 | 3.1% | 5.5% | 2.4% | 2.9% |
| | DAG 36:2 | 2.5% | 5.3% | 2.5% | 2.9% |
| | DAG 36:3 | 2.5% | 4.1% | 1.6% | 2.6% |
| | DAG 36:4 | 3.0% | 4.7% | 2.2% | 3.1% |
| | DAG 36:5 | 6.9% | 5.6% | 29.2% | 4.2% |
| | DAG 38:5 | 3.3% | 4.1% | 2.7% | 3.1% |
| | DAG 38:6 | 3.0% | 4.8% | 2.8% | 3.1% |
| **Kidney** | DAG 32:0 | 2.0% | 4.6% | 3.8% | 2.2% |
| | DAG 32:1 | 3.6% | 4.2% | 5.9% | 2.2% |
| | DAG 34:1 | 1.5% | 4.8% | 1.5% | 2.6% |
| | DAG 34:2 | 1.7% | 4.0% | 1.6% | 2.3% |
| | DAG 34:3 | 3.4% | 2.6% | 6.9% | 2.0% |
| | DAG 35:2 | 3.5% | 4.2% | 4.5% | 3.1% |
| | DAG 35:3 | 2.9% | 4.3% | - | 2.2% |

| | | | | | |
|---|---|---|---|---|---|
| | DAG 36:0 | 2.6% | 5.5% | 5.9% | 2.2% |
| | DAG 36:1 | 3.0% | 6.7% | 2.7% | 3.6% |
| | DAG 36:2 | 1.8% | 4.0% | 1.7% | 2.0% |
| | DAG 36:3 | 1.4% | 3.7% | 1.6% | 2.2% |
| | DAG 36:4 | 2.3% | 2.6% | 2.6% | 1.6% |
| | DAG 38:2 | 2.4% | 5.6% | 2.6% | 2.9% |
| | DAG 38:5 | 2.6% | 4.1% | 2.0% | 2.0% |
| | DAG 38:6 | 2.1% | 4.9% | 2.1% | 2.5% |
| | DAG 40:5 | 9.5% | 26.1% | 360.0% | 7.0% |
| | DAG 40:7 | 2.2% | 4.6% | 2.1% | 2.0% |
| | DAG 40:8 | 10.0% | 3.0% | - | 3.1% |
| **Heart** | DAG 32:0 | 1.9% | 5.3% | 3.1% | 2.1% |
| | DAG 32:1 | 1.6% | 3.2% | 2.2% | 1.5% |
| | DAG 34:1 | 1.7% | 4.0% | 1.3% | 1.9% |
| | DAG 34:2 | 2.0% | 2.9% | 1.5% | 2.2% |
| | DAG 34:3 | 2.1% | 2.4% | 2.9% | 1.5% |
| | DAG 35:2 | 2.3% | 3.7% | 11.7% | 1.9% |
| | DAG 35:3 | 2.2% | 4.1% | - | 2.0% |
| | DAG 36:0 | 1.9% | 4.4% | 3.3% | 2.0% |
| | DAG 36:1 | 2.0% | 3.3% | 2.2% | 2.0% |
| | DAG 36:2 | 2.2% | 3.1% | 2.8% | 2.4% |
| | DAG 36:3 | 1.8% | 3.0% | 1.7% | 2.1% |
| | DAG 36:4 | 1.5% | 2.5% | 2.1% | 1.6% |
| | DAG 38:2 | 2.1% | 3.8% | 2.8% | 2.2% |
| | DAG 38:5 | 2.0% | 3.1% | 4.0% | 2.3% |
| | DAG 38:6 | 1.8% | 3.7% | 1.4% | 2.1% |
| | DAG 40:5 | 2.3% | 4.4% | 292.6% | 2.3% |
| | DAG 40:7 | 1.4% | 2.8% | 1.9% | 1.6% |
| | DAG 40:8 | 6.7% | 4.1% | - | 3.3% |
| **Brain** | DAG 32:0 | 5.1% | 12.6% | 5.1% | 5.7% |
| | DAG 34:0 | 5.1% | 10.6% | 6.4% | 5.8% |
| | DAG 34:1 | 5.4% | 9.0% | 5.3% | 6.4% |
| | DAG 34:2 | 6.6% | 18.8% | 41.7% | 5.7% |
| | DAG 36:0 | 4.5% | 9.6% | 5.6% | 5.2% |
| | DAG 36:1 | 5.6% | 9.1% | 5.0% | 6.2% |
| | DAG 36:2 | 4.4% | 13.9% | 14.9% | 5.3% |
| | DAG 36:3 | 3.9% | 9.0% | 9.0% | 5.1% |
| | DAG 36:4 | 3.9% | 8.4% | 8.1% | 4.6% |
| | DAG 38:5 | 13.3% | 16.9% | - | 8.5% |

# Chapter 3: Data-informed Selection of Internal Standards for Quantitative Nontargeted Lipidomics

*Reproduced from unpublished manuscript: "Data-informed Selection of Internal Standards for Quantitative Nontargeted Lipidomics" by Lauren M. Bishop, Uri Keshet, Tong Shen, and Oliver Fiehn. Ready for submission.*

## 3.1 Abstract

Nontargeted lipidomic LC-MS workflows enable discovery of novel lipid species while simultaneously detecting well-known lipids. Despite improvements to data quality and reliability, re-use of nontargeted lipidomics data across studies has been limited by inadequate approaches to quantification. Hence, reporting absolute molar concentrations will largely improve transferability of data and confidence in nontargeted data reports. Typical single-point calibrations are hindered by mismatched ionization effects between the internal standards and endogenous species, thus leading to quantitative inaccuracies when left uncorrected. Here, the impact of sample matrix effects and differences in chemical structures between endogenous lipids and internal standards must be taken into account, and methods must properly choose the best-matching internal standard for each lipid subclass. To this end, we propose using a dual approach of estimating matrix effects and evaluating response differences in lipid structures. First, serial dilution of the pooled quality controls yields retention time windows of matrix effects for each subclass of endogenous lipids. Second, the different concentrations and structures of representative internal standards in each lipid subclass in a fortified commercial kit to determine structure-based response factors. Taken together, optimal internal standards and correction factors are formulated for each subclass. We validated the quantitative accuracy of nontargeted lipidomics quantifications in two different ways, by benchmarking against consensus concentration data provided by NIST SRM1950 reference human plasma and by using classic exogenous standard additions. We further validated

quantifications by using different LC-conditions and by QTOF- and Orbitrap high resolution mass spectrometers. We applied this method to quantify lipid species in blood plasma, serum, brain tissue, and liver, covering 5 orders of dynamic range for 392 endogenous lipid species covering 10 subclasses (triacylglycerols, diacylglycerols, sphingomyelins, ceramides, phosphatidylcholines and –ethanolamines including their lyso-forms, phosphatidylinositols, and acylcarnitines). The proposed method can be readily applied to most nontargeted lipidomics workflows.

## 3.2 Introduction

Nontargeted lipidomics is an indispensable tool for biomarker discovery and exploring disease mechanisms across diverse biological systems. Yet, nontargeted lipidomics by liquid chromatography-high resolution tandem mass spectrometry (LC-HRMS/MS) remains challenged by the lack of standardization in data acquisition, quality control and data reporting [1,2]. Current workflows involve complex automated and manual curation processes to produce reliable data [3,4]. At best, nontargeted analyses are viewed as semi-quantitative, with limited opportunity for comparing data between studies, laboratories, or analytical instruments. Even when following well-established workflows, reporting batch-subjective peak intensities limits translation of results to further investigations – a current bottleneck for the future of lipidomics [5]. Therefore, reporting absolute quantities, or estimates of molar concentration, may improve data transferability and standardization.

Classically, absolute quantification of chemicals by mass spectrometry relied on employing stable isotope labeled standards for each analyte, using in-matrix dilution curves to remove any effect of co-eluting matrix components [6]. Although effective for targeted analyses, complete coverage for thousands of varying knowns and unknowns is unattainable. Typically, internal standards in nontargeted analyses have been primarily utilized for normalization schemes

with limited representation of different chemical classes [7]. Additionally, ongoing challenges in data reproducibility have raised concerns of viability for absolute quantification in nontargeted applications. However, over the past 10 years, implementation of more robust quality controls and a stronger understanding of pre-analytical factors have created far more reliable data and provided better measures of data quality in nontargeted datasets [8-10]. Furthermore, commercial providers now offer comprehensive, standardized internal standard kits with the capabilities of both qualitative and quantitative applications [11,12]. To date, many lipidomics platforms use a single-point calibration approach to quantification, with one representative internal standard per lipid subclass. Such single standard provides a qualitative and quantitative benchmark, implicitly assuming that ionization efficiency differences due to chemical structure and/or matrix effect are relatively uniform per subclass. While this assumption is sufficient for inter-subclass comparisons, nontargeted analyses present a vast diversity of lipid species, including significant variability of acyl chain structures and retention times within the same lipid class [13]. Several strategies have been proposed to improve upon the single-point quantitation approach, including matrix-matched calibration, determination of response factors, and assessment of matrix effects by post-column infusion [14-16]. However, these methods are not compatible with all nontargeted workflows and would require thorough validation to be implemented on a large, high throughput scale. The addition of commercially-available, comprehensive internal standard mixes is most feasible in an established nontargeted workflow, yet the efficacy of quantification has only been evaluated in global targeted assays and the quantitative biases are still mostly unknown [17].

Hence, we here explored the accuracy and reliability of absolute quantification in nontargeted lipidomics using a commercial internal standard mix and propose a high throughput-friendly workflow for optimal internal standard selection. We used a two-pronged approach: (a)

we performed an integrated multi-point calibration of multiple internals standards per lipid subclass to evaluate effects of structural differences such as number of double bonds and carbon numbers; (b) we used serial sample dilutions to estimate the extent of matrix effects for all endogenous lipids using a re-purposed signal response evaluation of the pooled quality control samples, originally presented by Overdahl et al. [18] Method blanks were employed to measure the average matrix factor of each internal standard and the relationships between standards of the same subclass were utilized to determine response factors. A primary validation was performed with human plasma K2EDTA and additional reference human plasma (NIST SRM 1950) samples and standard addition experiments were acquired to evaluate quantitative accuracy. As a secondary validation of the integrated, quantitative nontargeted method, different acquisition methods and biological matrices were used to test the robustness and application of the proposed workflow.

## 3.3 Materials and Methods

### 3.3.1 Materials

UltimateSPLASH ONE lipidomic standards were purchased from Avanti Polar Lipids. Additional supplement standards of decanoyl-L-carnitine-D3, dodecanoyl-L-carnitine-D3, and octadecanoyl-L-carnitine-D3 were purchased from Cambridge Isotope Laboratories, and 12-[(cyclo-hexylamino) carbonyl]amino]-dodecanoic acid (CUDA) was purchased from Cayman Chemical. An additional 28 unlabeled lipid standards were purchased from Cayman Chemical (**Table S1**). All reagents used were of LC-MS grade. Human plasma treated with K2EDTA, human serum, and CD-1 mouse brain and liver whole organs were purchased from BioIVT and stored at −20°C until analysis. Standard reference material (SRM) for human plasma (SRM 1950) was acquired from the National Institute of Standards and Technology (NIST) and stored at −80°C.

### 3.3.2 Sample Preparation

The mouse brain and liver tissue samples were lyophilized for 24 hours and homogenized using a SPEX SamplePrep 2010 GenoGrinder prior to extraction. Twenty μL of human plasma, human serum, and NIST SRM 1950, and 2 mg of lyophilized mouse brain and mouse liver were extracted as described previously [19]. Empty tubes were extracted to serve as method blanks. The remaining fractions of matrix-containing extracts were combined to form pooled quality control (QC) samples. Additional samples were prepared in replicate for "sample-only" dilutions and aliquoted accordingly before concentrating extracts to complete dryness. For triplicates, matrix extracts were dried down at decreased volumes corresponding to dilution factors of 0.5x, 1x, 2x, 4x, 10x, and 50x, respectively. All samples were resuspended using 100 μL of methanol/toluene (9:1, v/v) with UltimateSPLASH ONE standard mix, supplemental internal standards, and 50 ng/mL of CUDA.

To evaluate signal responses, a serial dilution series was prepared using six replicates from the final resuspended extracts. These samples were diluted to factors of 2x, 4x, 10x, 20x, and 50x with a solution of methanol/toluene (9:1) with 50 ng/mL of CUDA to maintain the same concentration of CUDA across all samples for normalization purposes. Standard additions of lipid standards were prepared to evaluate the accuracy of quantitation. A mix of the unlabeled standards were prepared at UltimateSPLASH-compatible concentrations in methanol and dried overnight. Control matrix-containing samples were extracted and resuspended per the method described above and transferred to the vials of dried standard mix. All samples were transferred to amber vials and stored at −20°C until analysis.

### 3.3.3 Data acquisition by LC-HRMS/MS

Control samples and samples of all dilution levels were randomized to eliminate biases in this validation. For real sample studies, it is recommended to inject the dilution series in reverse order to prevent potential carryover. For nontargeted lipidomics analysis, 3 μL of the resuspended non-polar phase was injected into a Thermo Fisher Scientific Vanquish UHPLC+ liquid chromatography system coupled to a Q-Exactive HF orbital ion trap mass spectrometer. The default method for this validation was a 5 minute, high flow reverse-phase separation with a Waters Acquity premier BEH C18 column (50 × 2.1 mm; 1.7 μm). The column compartment and mobile phase preheater were set at 65°C, and the mobile phase flow rate was 0.8 mL/min. The positive mobile phase A was acetonitrile/water (60/40, v/v) with 0.1% formic acid and 10 mM ammonium formate as modifiers and mobile phase B consisted of isopropanol/acetonitrile (90:10, v/v) with 0.1% formic acid and 10 mM ammonium formate. Mobile phase A for negative mode analysis was prepared using acetonitrile/water (60/40, v/v) with 10 mM ammonium acetate, while mobile phase B consisted of isopropanol/acetonitrile (90/10, v/v) with 10 mM ammonium acetate. Both modes shared the same gradient: 0 min, 15% B; 0.75 min, 30% B; 0.975 min, 48% B; 4 min, 82% B; 4.125 min, 99% B; 4.5 min, 99% B, 4.58 min, 15% B, 5.5 min, 15% B. The injection needle was washed for 10 s before and after each injection with isopropanol. Positive mode and negative mode electrospray ionization (ESI) used a spray voltage of 3.6 kV, capillary temperature of 380°C, sheath gas flow rate of 60 units nitrogen, and auxiliary gas flow rate of 25 units nitrogen. The distance of the ESI probe from the sweep cone was increased to accommodate the higher flow rate from the LC.

In addition to the method detailed above, other variations of the data acquisition were performed to demonstrate robustness of the proposed quantitation method. Specifically, sample

data was acquired in positive mode using both the Orbitrap instrumentation with a longer LC gradient, as well as the original method run on an Agilent 6546 Q-TOF system. There were a few minor changes to the MS parameters between the Q-TOF and Orbitrap acquisitions, including a lower source temperature of 320°C in positive mode and 360°C in negative mode, a spray voltage of 3.5kV, and a sheath gas flow rate of 11 L/min. For the longer separation method, the LC system was set with a 0.6 mL/min flow rate and equipped with a Waters Acquity UPLC CSH C18 column (100 × 2.1 mm; 1.7 μm) and Waters Acquity VanGuard CSH C18 precolumn (5 ×2.1 mm; 1.7 μm). Other specifications for the longer acquisition method were published previously [19]. The MS parameters were adjusted for the lower flow rate by decreasing the ESI probe temperature to 300°C and adjusting the distance of the probe from the sweep cone.

Overall, data were collected from 0 to 5 min (13 min for the long method) of the LC gradient in scan range 120–1700 m/z using data-dependent acquisition (DDA) with the top two ions from each MS1 scan being selected for MS/MS fragmentation. DDA MS/MS was acquired with a stepped normalized collision energy of 20%, 30%, and 40%. MS1 spectra were collected with a resolving power setting of 60,000, and MS/MS spectra were collected at a resolving power setting of 15,000. To increase the total number of MS/MS spectra, five consecutive runs were made using the R package "IE-Omics" [20] for both positive and negative electrospray conditions. All spectra were stored in centroid, ".raw" format.

### 3.3.4 Data processing

Deconvolution, peak picking, alignment, and compound identification were completed through open source software MS-DIAL v4.92. [21] Compounds were annotated using an internally curated mzRT library where lipids were matched by accurate mass and retention time, as well as matching accurate precursor masses and MS/MS fragmentation patterns against the

LipidBlast library [22]. The primary result data matrix was processed with MS-FLO software to help identify ion adducts, duplicate peaks, and isotopic features [23]. Peak height was used as spectral intensity for all data analysis; however, peak area information was also exported to confirm data quality. Sample data was not normalized in order to properly assess variability in internal standard responses. The intensity of CUDA was used to assess injection quality on a sample-to-sample basis.

### 3.3.5 Signal response evaluation and quantification

The data curation process described above successfully filters out most of the non-biological features from the final dataset. However, the process of signal response evaluation provides a quality check of features prior to quantification. Following the guidelines of Overdahl et.al. [18], we used a standard linear regression through zero with a cut-off of $R^2 = 0.85$ to flag potential contaminant features. Flagged features were then subject to manual evaluation for nonlinear trends over the dilution series. Lipid species with a combination of high abundance and significant observed matrix effects were most likely to be falsely flagged by the proposed parameters and were better assessed with a polynomial regression.

The final curated datasets were subject to an internal standard assessment before absolute quantification, following the workflow in **Figure 1**. Matrix factor was determined by the difference in signal response of the internal standards in matrix as compared to method blanks. Response factors were calculated from the difference in slopes between internal standards of the same lipid subclass acquired in neat solution. Internal standards were then best-matched to the endogenous lipids using class-specific parameters. Peak heights were used to estimate absolute molar concentrations from the known quantity of the respective internal standard.

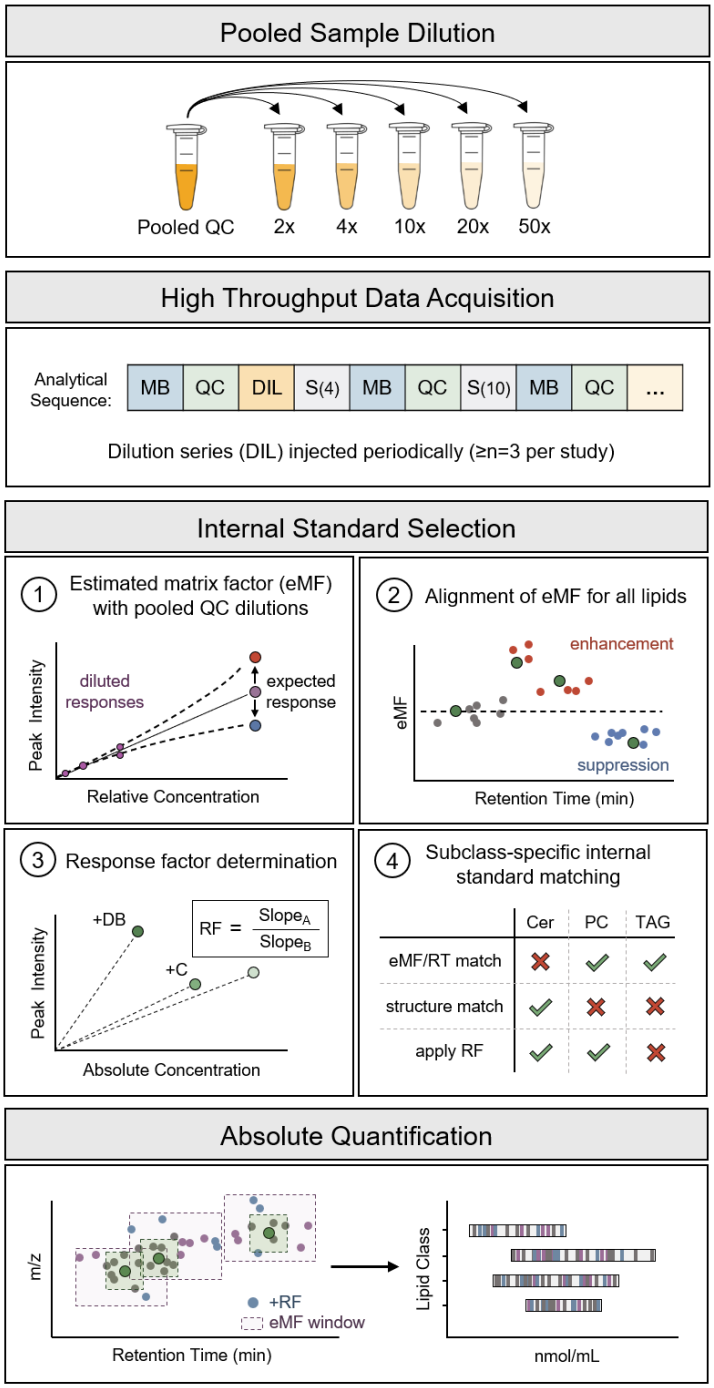


**Figure 3.1:** Proposed workflow for absolute quantification by class-specific internal standard selection. ***Top panel:*** Recommended pooled QC sample dilution scheme. ***Second panel:*** The dilution series integrated into a high throughput analytical sequence; MB = method blank, QC = pooled quality control, S = biological study samples. ***Third panel:*** Stepwise process for internal standard selection. (1) Utilization of diluted signal responses to evaluate matrix effects; (2) Determination of retention time windows for subclass-specific matrix effects; (3) Calculations of response factors (RF) for additions of carbon chain length (+C) and double bonds (+DB) using internal standard responses in method blanks; (4) Inform subclass-specific approaches for absolute quantification using the observed influences of matrix ions and chemical structure. ***Bottom panel:*** Endogenous lipids are matched to the corresponding internal standard (green) according to the recommended approach and quantified to provide estimates of molar concentration.

## 3.4 Results

### 3.4.1 Internal standard coverage and reliability

The initial validation of the proposed quantitative method was performed on the nontargeted analysis of lipids in human plasma. To summarize the final curated dataset used for this validation, 48 deuterated internal standards (ISTD) were measured in positive mode, representing 10 lipid subclasses that are robustly measured in human plasma: acylcarnitines (CAR), ceramides (Cer), diacylglycerols (DAG), lysophosphatidylcholines (LPC), lysophosphatidylethanolamines (LPE), phosphatidylcholines (PC), phosphatidylethanolamines (PE), phosphatidylinositols (PI), sphingomyelins (SM), and triacylglycerols (TAG). **Figure 2A** shows the extracted chromatograms of all internal standards in neat solution, with intensities normalized to the most abundant standard per subclass. A total of 398 unique lipid species were identified with 312 lipids classified within the ISTD-represented subclasses. Ether-linked PC lipids were quantified with PC ISTDs for this study. In negative mode, 30 internal standards were measured across 7 subclasses to represent the respective plasma dataset. With considerable overlap between the two electrospray modes, 225 ion species were annotated in negative mode, of which 145 were considered quantifiable with the corresponding ISTDs.

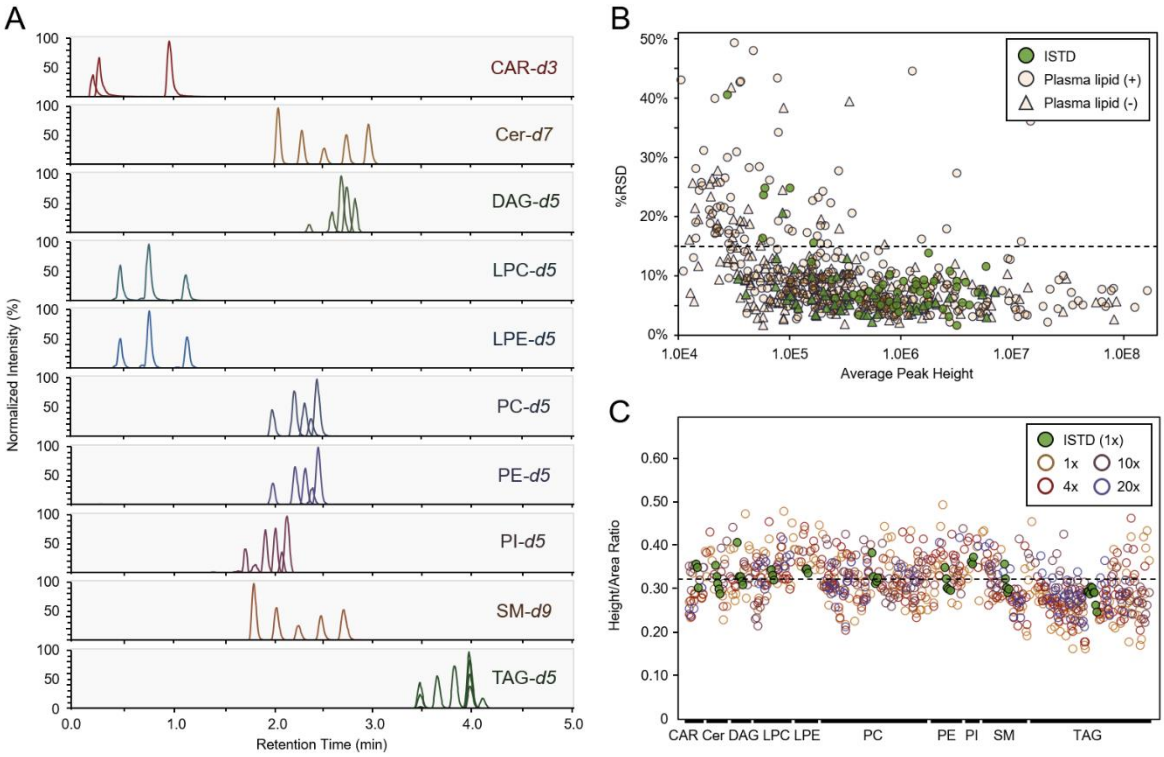


**Figure 3.2:** Performance of internal standards. (**A**) Relative intensity and retention time of all blood plasma-relevant deuterated internal standards in ESI positive mode. Subclass abbreviations are provided in the main text. (**B**) Percent relative standard deviation (%RSD) by average peak intensity of endogenous lipids and internal standards (ISTD) across pooled plasma replicates (n=6). (C) Changes in ratios of peak height to peak area across increasing dilution factors for all lipid subclasses.

Prior to quantitative assessment, repeatability and reliability of all known annotations were thoroughly evaluated. As recommended by our previous work, we first evaluated the ionization trends of all lipids to determine the most representative adduct species per subclass [19]. Only three subclasses lacked a consistent primary adduct form that represented more than 80% of the total peak intensity for the lipid species in each class: Cer (in both positive and negative mode), DAG (+ESI mode), and TAG (+ESI mode). These subclasses were represented by a combination of their top two adduct forms for this study, as displayed in **Figure S-1**, while for all other lipids, only the top-most abundant adduct species was used for quantification. Repeatability for all annotations was represented by the percent relative standard deviation (%RSD) of six technical

replicates (**Figure 2B**). Most compounds showed <15 %RSD technical error when detected at >50,000 raw intensity peak counts, or five-fold over the minimum peak identification threshold. Application of these parameters left 295 and 108 quantifiable lipids in positive and negative mode, respectively. Lipid species with <25% RSD and above the minimum peak height were quantified as part of the total estimated molar range but could not be properly assessed for quantitative accuracy.

In addition to the standard qualitative assessments, we examined the ratio of peak height to peak area across all of the final annotations. Peak area is typically considered best practice for quantification, although area integrations can be less reliable when representing partially resolved isomers. Peak area determinations may also be influenced by inconsistent integrations by automatic peak picking software, leading to larger errors than peak height determinations which show less dependencies to baseline estimates. We compared the height-to-area ratio of all lipids measured in positive mode across four dilution levels, as shown in **Figure 2C**, to confirm the suitability of using peak heights as a quantitative measure. Overall, there was less than a 12% difference in average ratio between the 20-fold diluted and undiluted peak shapes across all lipid subclasses. Internal standards were representative of their respective subclasses, with all labeled standards found within 6% of the mean peak ratio per subclass. Larger ratios could be attributed to not fully resolved peaks, specifically in higher density regions of the chromatogram (i.e. PC, PE, SM, TAG), and ultimately favored the use of peak height.

### 3.4.2 Selecting optimal internal standards for quantification

In essence, quantifications that use specific internal standards must choose from either the closest eluting internal standard or the most structurally similar reference compound. Hence, we explored the variability of ISTD and endogenous lipid responses within retention time windows to

define regions of comparable matrix effects, as well as explored the application of ISTD-generated response factors to accommodate the structural variations (carbon chain lengths, double bonds) in each lipid subclass. The influences of matrix effects and structural diversity on ionization efficiency were first investigated independently, and then used to inform a strategy for selecting the most optimal internal standards.

*(a) Estimating the impact of sample matrix*

To determine the effect of matrix components on lipid ionization, matrix factors (MF) were calculated from the ratio of peak response in presence of matrix ions to peak responses in neat solution [24]. As matrix-containing QC samples and method blanks were periodically acquired in our analysis, we determined an average matrix factor for each labeled standard, as illustrated in **Figure 3A**. In accordance with total ion density, the subclasses with the largest matrix factor differences were PC, SM, and TAG in positive mode, and PC, PE, and SM in negative mode. These regions demonstrated high variability in matrix effects between the individual standards, suggesting the use of narrow retention time windows for matching internal standards to endogenous lipids. However, regions of high matrix effects may extend beyond observed effects shown by the internal standards. Using the traditionally qualitative assessment of the signal response dilution series, the quantitative nontargeted lipidomics workflow then calculates an estimated matrix factor (eMF) for all endogenous lipids, as outlined in **Figure 3B**. For example, when examining the relationship between the three monounsaturated PC standards, samples needed to be diluted >20-fold in order to eliminate matrix effects completely (**Figure S-2**). Assuming the response at a 20-fold dilution is representative of minimal matrix effects, we calculated the expected matrix-free response by multiplying the peak intensity at this dilution level by the dilution factor (20). Individual matrix factors were then estimated for all lipids using the

actual undiluted signal intensities. All eMF values calculated for human plasma lipids are presented in **Table S-2**. When visualized as a function of retention time, matrix factors of the class-dependent ISTDs aligned well with the matrix factors of the endogenous lipids, for example, for PC lipids (**Figure 3C**). There are clear trends of ion enhancement and suppression across most of the lipid subclass in positive and negative mode, respectively. Most notably, the internal standard at RT = 1.923 min (PC 31:1-d5) has a MF of 4.01 in positive mode, nearly double the observed matrix effects compared to other PC standards. As it is the first labeled compound to elute for this subclass, it is assumed that this standard would be best matched to the lipids eluting earliest in the gradient. However, the data from **Figure 3C** indicates the window of presumed matrix effect is approximately 0.04 minutes and any lipid species outside of this RT window is therefore subject to other matrix influences – in this case significantly lesser effects. Additionally, this data proved the 20-fold dilution level to be most informative of the true matrix effect as compared to the other diluted responses, although many trends were already apparent at a 10-fold dilution factor.

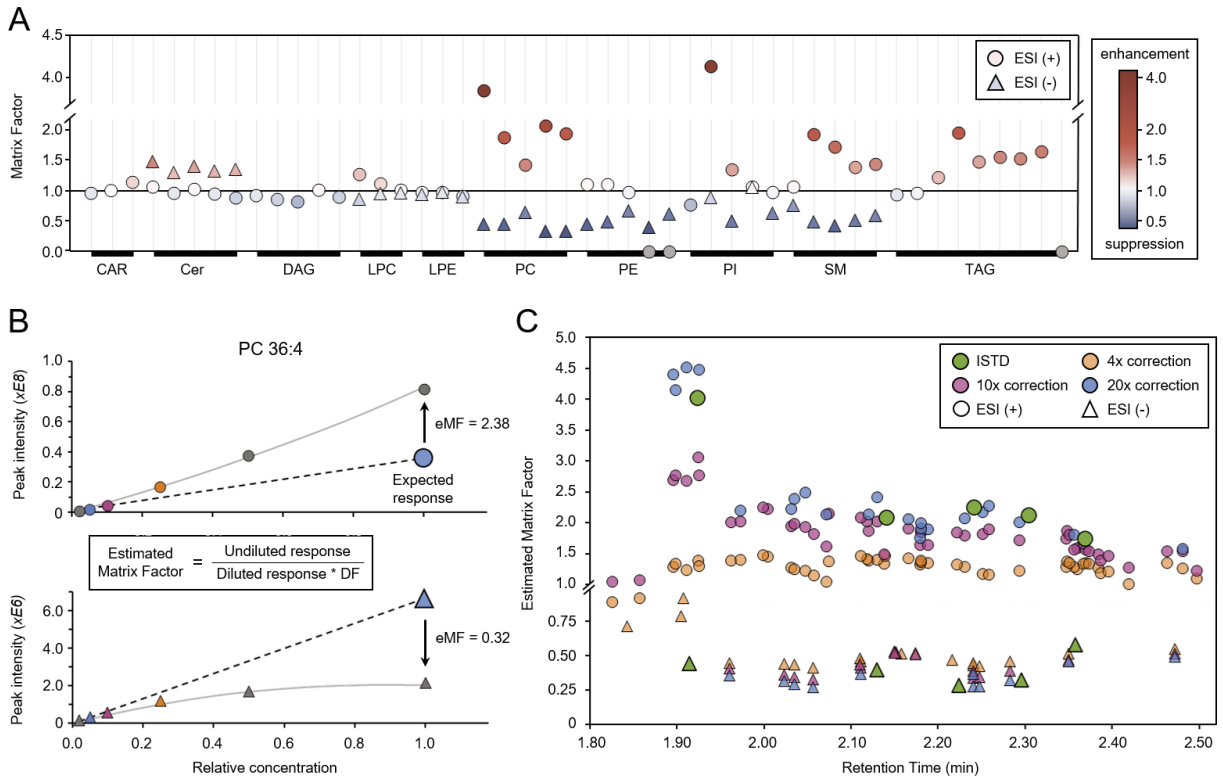


**Figure 3.3:** Estimations of matrix factor for all lipid species. (**A**) Calculated matrix factor for all internal standards. Matrix factors >1 indicate ion enhancement and matrix factors <1 indicate ion suppression. Internal standards are organized by increasing carbon number per lipid subclass. (**B**) Visualization of estimated matrix factor (eMF) calculations using 20x dilution responses for PC 36:4 in positive and negative mode, respectively. (**C**) Estimated matrix factors for all PC internal standards (green) and endogenous plasma PCs as a function of retention time. Endogenous PCs are shown at three levels of diluted response correction: 4x, 10x, 20x.

*(b) Determining and applying structural response factors.*

While the impact of matrix ions on ionization efficiency can be enumerated by estimated matrix factor, the effects of structural diversity on ionization are difficult to characterize without known concentrations. To determine the influence of acyl chain structures on quantitative accuracy, response factors were extrapolated from response differences between the subclass-specific internal standards in neat solution. Each lipid subclass was represented by 3-5 unique internal standard species, increasing incrementally by two carbon lengths, and representing different degrees of unsaturation (**Figure 4)**. Assuming a linear slope through zero, average

response factors were calculated between internal standard species ($RF_{IS}$) per subclass, to yield correction factors for each increment of two carbon-chain length differences and 0-2 double bonds. Overall, the sum compositions were notably similar when comparing the endogenous lipids with their class-specific internal standards. 79% of the annotated compounds were found within ±2 carbons and ±2 double bonds of their nearest internal standard (**Figure S-3**). CAR and LPE subclasses showed negligible response differences between ISTD species (**Figure 4**) and therefore did not require response factor corrections based on the relationship of their representative standards. In contrary, both LPC and PC standards showed an observable difference in response with increasing carbon chain lengths in addition to a notably large range of structural diversity to cover in the endogenous species. When structural disparity is greater than what is represented by the internal standards, response factors can be applied exponentially as a factor of carbon number and/or number of double bonds – or $RF^n$ where n is equal to the difference in carbon chain length and/or unsaturation level. While sphingolipids (SL; Cer, SM) displayed a consistent decrease in response over increased carbon chain lengths, the overall structural diversity of endogenous SLs was lesser than other subclasses. Therefore, response factors for sphingolipids are only applied in high matrix effect regions where retention time-based matching takes precedence over structure-based matching of ISTDs. Diacylglycerols and their ISTDs showed the largest disparity in responses, specifically with the addition of double bonds. Alongside a smaller trend due to carbon number alone, the lipid response for DAG 37:3-d5 is nearly double the response of DAG 35:1-d5, with a response factor equal to 1.91 per the addition of one carbon and one double bond to the sum composition. The significant impact of the unsaturation level is reinforced when comparing the responses of monounsaturated standards DAG 33:1-d5 and DAG 35:1-d5 ($RF_{IS}$ = 1.18) and the responses of the polyunsaturated standards DAG 37:3-d5 and DAG 39:4-d5 ($RF_{IS}$ = 1.42).

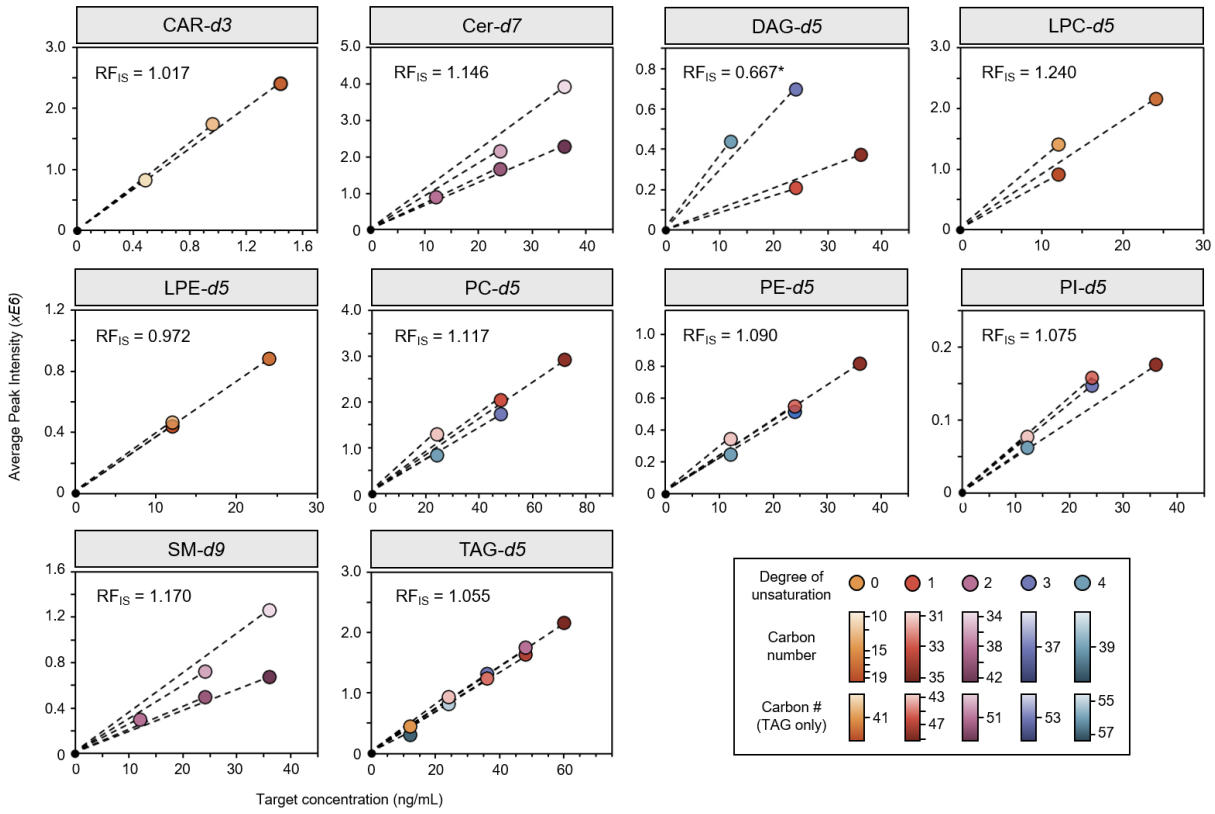


**Figure 3.4:** The relationships of internal standard responses in method blanks per lipid subclass. The average response factor between each internal standard increment (+ 2 carbon lengths, + 0-2 double bonds) is represented as RFIS. Internal standards are colored by sum composition. The number of double bonds is specified by color and carbon chain length is characterized by the respective color value scale. TAG species were given a separate value scale to maximize contrast.

Although many of the response factors are closely distributed around 1 when adjusted for the addition of a single carbon length or double bond, their application is crucial in cases of high structural disparity in order to preserve quantitative accuracy. Therefore, we confirmed the reliability of extrapolating response factors by exponential treatments. To this end, we used the NIST SRM1950 reference human plasma for which consensus concentrations have been established by a large international ring trial [25]. Using these reported concentrations of endogenous lipids in the NIST SRM1950 material, we estimated response factors for 78 lipid species in Cer, LPC, LPE, PC, PE, SM, and TAG subclasses that were quantified within 15% of

the consensus value with a classic single-point quantitation approach (**Table S-3)**. Each lipid was paired with the closest structural match as its reference response. For example, Cer d41:1 served as reference lipid for Cer d42:2 to determine the response factors in NIST plasma. These response factors were then compared to response factors generated by the internal standards. Additionally, a response factor was determined between the smallest and largest species per subclass and compared to the exponential extrapolation of the internal standard-generated value. Overall, response factors calculated from the NIST plasma correlated well with response factors obtained from ISTDs. For 88% of the test lipids, response factors varied within 0.2 units between the two calculation methods, and 70% of the test lipids varied even only by 0.1 units in response factors. Hence, this comparison validated using ISTDs to determine the extent by which double bonds or carbon chain lengths impact raw signal intensities for each lipid class in nontargeted LC-MS analyses.

*c) Designating class-specific approaches and evaluating quantitative accuracy*

Finally, the preferred method for selecting optimal ISTDs for quantification can be determined for each lipid subclass. First, we define if there is a retention-time based variability of estimated matrix factors, such as for PC lipids (**Figure 3A**). In this case, retention time-based matching of internal standards must be used. However, if all species of a lipid subclass have similar estimated matrix factors, independent of retention times (**Figure 3A**), then the structurally closest internal standard should be used. Subsequently, a response factor is used if the endogenous lipid shows structural differences to the internal standard. **Table 1** establishes the approaches used for each lipid subclass, using human plasma as an example. For subclasses with both uniform matrix effects and negligible response differences between internal standards, the slope of all viable internal standards, intercepted through the origin, can be used as a calibration curve. In this case,

using the slope of all the internal standards of a lipid subclass becomes similar to classic single point quantifications which uses a specific internal standard response to assume a linear trend through the origin. For human plasma, we found this practice to be effective for acylcarnitines and lysophosphatidylethanolamines where response factors varied less than 0.05 units from the ideal RF=1 slope. In other classes, however, we found larger deviations from RF=1 by structure-based differences. For example, PC, Cer, SM, and LPC lipids demonstrated deviations of $\Delta RF > 0.1$ units, while diacylglycerols showed the largest differences with deviations of $\Delta RF > 0.3$ units. Other compound classes exhibited lower variations, with $\Delta RF = 0.09$ units for PEs and only $\Delta RF < 0.06$ units for TAGs. Here, we recommend applying structure-based response factors at $\Delta RF > 0.06$, but such criterion should not be considered as a hard threshold because the difference in absolute concentrations would be small.

**Table 3.1:** Selecting internal standards (ISTD) via subclass-specific approaches for absolute quantification of lipids. Example for human plasma. eMF, estimated matrix factor. RT, retention time.

| Lipid Subclass | Acquisition mode | Number of viable ISTDs | ISTD match by eMF or RT | ISTD match by structure | Response Factor |
|---|---|---|---|---|---|
| CAR | ESI (+) | 3 | ISTD slope | | -- |
| Cer | ESI (+/-) | 5 | -- | ✓ | ✓ |
| DAG | ESI (+) | 4 | -- | ✓ | ✓ |
| LPC | ESI (+/-) | 3 | ✓ | -- | ✓ |
| LPE | ESI (+/-) | 3 | ISTD slope | | -- |
| PC | ESI (+/-) | 5 | ✓ | -- | ✓ |
| PE | ESI (+/-) | 3 | ✓ | -- | ✓ |
| PI | ESI (+/-) | 4 | ✓ | -- | ✓ |
| SM | ESI (+/-) | 5 | ✓ | -- | ✓ |
| TAG | ESI (+) | 7 | ✓ | -- | -- |

### 3.4.3 Evaluating the accuracy of data-informed lipid quantification

Using these methods, molar concentrations were calculated for all plasma lipids in both acquisition modes for which appropriate internal standards were included in the study (**Figure 5A)**. If more internal standards were included, additional lipid classed could be quantified in the same manner. The molar range of the endogenous lipids measured here spans five orders of magnitude in positive mode and four orders of magnitude in negative mode. Approximately 80% of the quantified lipids fell between 0.10 and 10 nmol/mL, which is consistent with previously reported ranges [17,26]. To further verify these ranges, NIST SRM1950 samples were acquired and compared to the published consensus values. In **Figure 5B**, these NIST SRM1950 consensus concentrations were normalized to 1.0, with the standard uncertainty of these consensus values normalized to the range of 0.8 to 1.2 for visualization purposes. A total of 249 unique lipid species were quantified in NIST SRM1950 with a corresponding reported concentration. Using the estimated matrix factors and response factors as explained before, we quantified 63% of the endogenous lipids within the consensus range between the two acquisition modes (**Figure 5B)**. 96% of all lipids were found within a 50% difference of the consensus range, indicating an overall good agreement with the consensus values for blood lipids in NIST SRM1950 human plasma.

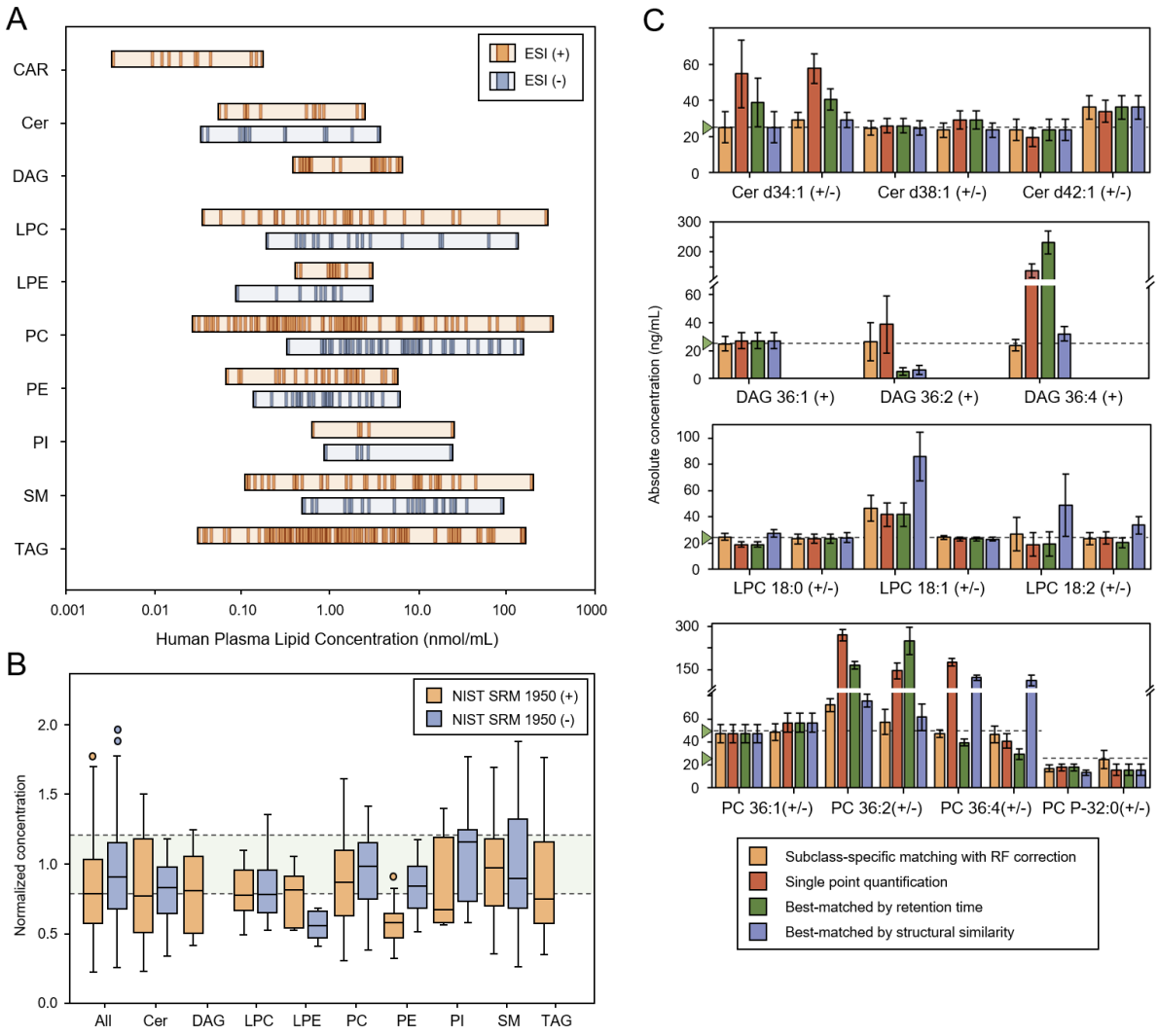


**Figure 3.5:** Quantification of endogenous lipids in human plasma. (**A**) Molar concentrations across all lipid subclasses. Each line (orange = ESI(+), blue = ESI(-)) represents a unique lipid species. (**B**) The range of estimated molar concentrations calculated from NIST SRM 1950 samples normalized to the reported consensus values and their standard uncertainty. (**C**) Testing the performance of three single-point quantitation approaches (red, green blue bars) via exogenous standard additions of plasma lipids in comparison to the proposed subclass-specific quantification (orange bars). The standard addition of unlabeled standards in human plasma was performed at 24 ng/mL for Cer, DAG, LPC, and ether-linked PC lipids, and 48 ng/mL for PC lipids.

The accuracy of quantification was further evaluated by using 24 and 48 ng/mL standard additions of unlabeled standards to human plasma extracts (**Figure 5C)**. Three single-point quantitative approaches were compared to our proposed method of subclass-specific ISTD matching by quantifying 28 endogenous lipid species across 8 subclasses: CAR, Cer, DAG, LPC,

PC, PE, SM, and TAG. The evaluated single-point quantification approaches included classic single-point calibration (selecting the best-matching ISTD by highest target concentration), selecting the best-matching ISTD by retention time, and selecting the best-matching ISTD by structure similarity. Overall, our method of data-informed selection of internal standards performed equally well or better than all other approaches for each of the 28 lipids examined here (**Figure 5C, Table S-4)**. While some of the compounds showed no difference between the four methods, others such as multiply unsaturated DAG species had high variability when the structure-based ionization efficiency was not accounted for or corrected. In PCs, where matrix effects are more variable, matching by structural similarity alone led to inconsistent results between the individual species.

### 3.4.4 Method robustness and additional applications

Nontargeted lipidomics acquisition methods vary between laboratories, including differences in separation techniques, gradient lengths, and MS instrumentation. To evaluate the robustness of the internal standards used here for absolute quantification, we acquired the same NIST SRM1950 samples using two alternate variations of the reversed phase lipid analysis. **Figure 6A** shows the comparison of estimated molar concentrations between a longer 13-minute LC gradient and a short 5-minute gradient, run on the same instrumentation. Overall, calculated concentrations correlated strongly with an $R^2 = 0.976$ and a median percent difference of 9.5% across all lipid classes. Next, we compared the performance of the data-informed selection of internal standards method using an LC-QTOF system to the reference Orbitrap MS system, as demonstrated in **Figure 6B**. The correlation of estimated molar concentrations was reliable between the two instrument platforms with a median percent difference of 20.6% across all lipid classes. The largest discrepancies in calculated concentrations were from DAG and LPE species,

where both the internal standards and endogenous lipids had notably lower peak intensities using the QTOF mass spectrometer than the Orbitrap MS system. Additionally, the %RSDs were consistently elevated across all lipids acquired by the QTOF, likely attributing to the quantitative inaccuracies.

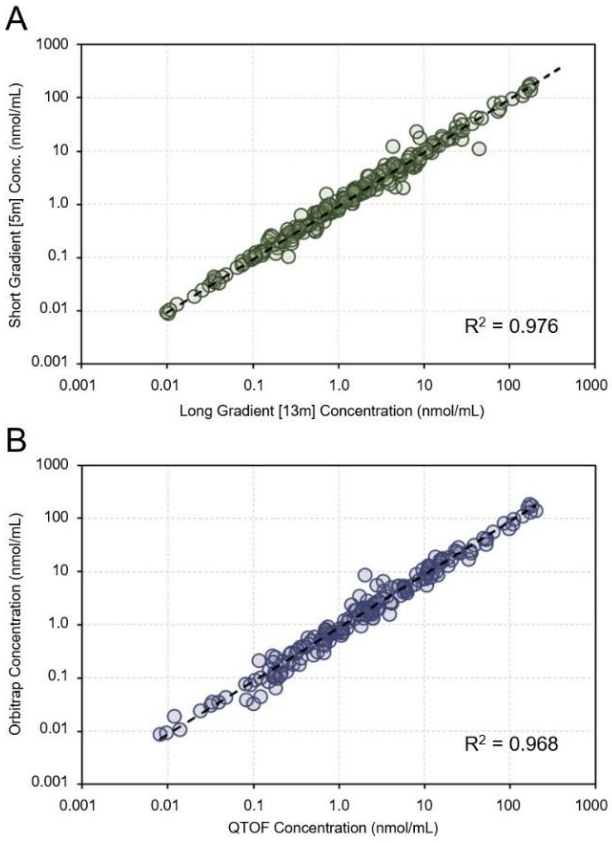


**Figure 3.6:** Comparison of data acquisition methods with NIST SRM 1950 in positive ionization mode. (**A**) Linear regression of molar concentrations (n=180) measured using a fast LC gradient (5 min) and a longer LC gradient (13 min). (**B**) Linear regression of molar concentrations (n=176) measured with two different high resolution LC-MS instruments.

Finally, we evaluated our proposed workflow for suitability in other biological matrices (i.e. human serum, mouse brain, and mouse liver). To assess the need for any method modifications, the matrix factor was measured for all internal standards in each matrix type (**Figure 7A**). Generally, the trends of ion suppression and enhancement between all four matrices were consistent for each lipid subclass. The mouse brain samples demonstrated the largest differences in matrix effects when compared to human plasma, especially for the DAG, PC, and SM standards where the total ion intensity of these regions was 4-fold higher on average. When using the estimated matrix factor approach for endogenous lipids, the PCs showed a distinct pattern of matrix effect in the brain samples versus in plasma. However, the high variability within the subclass still supports a retention time- and/or matrix factor-based approach to internal standard selection.

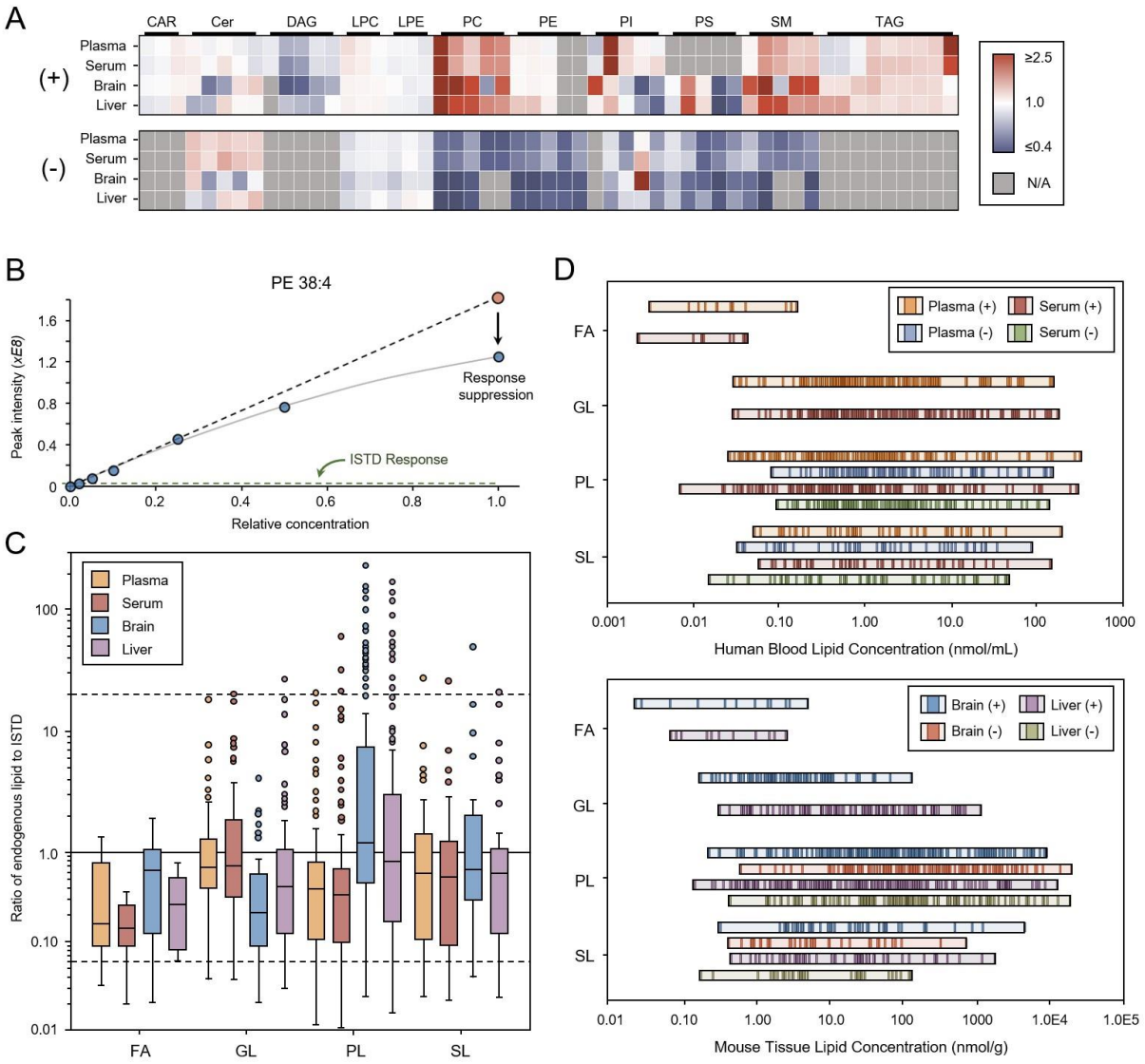


**Figure 3.7:** Quantification of lipids across different biological matrices. (**A**) Heatmaps comparing the measured matrix factor of all internal standards across 4 different matrices. (**B**) Visual representation of the response suppression of PE 38:4 in undiluted mouse brain tissue relative to the most abundant PE internal standard. (**C**) Peak intensity ratios of endogenous lipids to their respective internal standard organized by class: Fatty Acyls (FA), Glycerolipids (GL), Glycerophospholipids (PL), and Sphingolipids (SL). The dotted gridlines indicate a 20-fold difference from the internal standard. (**D**) Estimates of molar concentration for all lipids across human plasma, human serum, mouse brain, and mouse liver.

Perhaps the main concern with applying these internal standards for quantification of alternative matrices is a limited upper linear range when attempting to quantify highly abundant lipids. For example, many phospholipids are more abundant in brain and liver tissue than in serum. **Figure 7B** shows a nearly oversaturated phospholipid species in mouse brain, PE 38:4, that has a peak intensity approximately 100-fold higher than the most abundant internal standard. Similar to very low abundant lipids, the accuracy of quantitation may get compromised if there is a significantly greater ratio of responses between endogenous lipids and the respective internal standards. **Figure 7C** visualizes the distribution of annotated lipid responses relative to the matched internal standard in each biological matrix. Overall, the majority of compounds in each lipid class were within a 5-fold difference of their respective internal standard for all matrices. Using a ±20x difference in response ratio as a conservative threshold for quantitative accuracy, only 7% of endogenous lipids were outside the range for both blood matrices, and 13% were outside of the range for the tissue matrices. Consequently, estimates of molar concentration could be made with reasonable confidence for all tested matrices, as shown in **Figure 7D**. Ideally, lipid concentrations in kits of internal standards should closely match the expected concentrations in each matrix, demanding additional efforts by suppliers of isotope-labeled standards and analytical laboratories.

## 3.5 Discussion

Standardized quantification in nontargeted analyses has been proposed earlier, suggesting to adopt techniques from targeted methods into nontargeted workflows [27]. Most recently, this idea was reviewed as semi-quantitative analysis [28], to highlight the added uncertainties when quantifying analytes that show a noticeable structural difference to the internal standards used for quantification. Hence, a conservative view may imply that lipid quantifications can only be

reasonably used on the most abundant, classic mammalian lipids with 16-20 carbons in acyl chains, questioning the validity of reports of other lipidomic discoveries [29]. We here show that data-informed selection of internal standards enable quantification of a larger range of lipids, including longer, shorter or odd-numbered acyl-chains using calculated response factors from subclasses of lipids. Our proposed workflow for selecting internal standards selection provides more robust estimates of molar concentration than the classic single-point quantitation approach and can be readily applied to most nontargeted platforms. Yet, this workflow is necessarily limited to the number, type and concentration of internal standards and should best be altered to suit matrices other than blood.

The abundance of internal standards offers insights into trends of ionization efficiency for a given method. Adding more subclass-specific standards will provide more information to formally use such trends for improved quantification. Because the UltimateSPLASH ONE mix contains 3-5 labeled standards at different concentrations, we were able to use their relationships to better understand the impacts of matrix as well as determine which lipids are most influenced by chemical structure during ionization. It is well-established that acyl chain structure can have a notable effect on ionization, in addition to interacting with the solvent composition defined by the LC gradients [30,31]. While ionization response evaluations are typically performed in matrix, we argue that structure based efficiency differences are best compared in neat solution that only reflect differences in LC solvent compositions and ESI source parameters, not on the variable effects of matrices. The impact of matrix effects and chemical structure on ionization should best be assessed separately, as the latter is far more uniform in a given method. We acknowledge that the determination of response factors is limited by the number and diversity of labeled standards. However, our results were comparable when extrapolating ISTD-generated response factors by

$RF^n$ in neat solution, versus endogenous lipid-based RFs using published NIST SRM1950 consensus concentrations.

Matrix effects and systematic differences between ionization sources and acquisition parameters (like flow rates) are conceivably the largest threats to quantitative accuracy. Little is understood about the mechanisms of ionization enhancement and suppression, and the extent of the effects is usually unpredictable. Other methods have been proposed to help enumerate these effects, although regular integration into high throughput workflows is nonideal. Our addition of a periodic dilution series adds negligible costs to each acquisition and is the fastest way to establish windows of matrix effect on a study-specific level. We also theorize that once the extent of matrix effects has been established for a specific biological matrix on a validated LC-MS platform, these benchmarks do not need to be continually re-evaluated for said matrix. Essentially, reference profiles can be established for each matrix and each nontargeted method and then used in quantitative nontargeted data processing. We anticipate method limitations, such as when applied to matrices that have regions of large ion enhancements (or suppressions) where a specific ISTD can become incompatible with other ISTDs. For example, PC 33:1-d5 in mouse brain showed considerable matrix effects and was no longer interchangeable with the longer chain PC standards. Even though data-informed selection of internal standards is likely robust across different matrices, it is still highly recommended to evaluate the selection of internal standards as often as possible to guarantee quantitative accuracy.

When considering absolute quantification, true accuracy is unknowable. The NIST plasma reference material SRM1950 offers us the closest gauge for accuracy, although its finite availability and overall cost limits its reliability as a primary QC resource. Additionally, the consensus molar concentration values were published as an amalgamation of the quantitative

methods used by 31 different labs [25]. Nonetheless, these values continue to serve as an acceptable benchmark for quantitative methods in the greater field of targeted and nontargeted lipidomics [32,33]. Overall, our approach to quantification in nontargeted lipidomics fared well against the consensus values. LPEs measured in negative mode and PEs measured in positive mode appeared consistently lower than the consensus range. Other than a fault to the internal standard selection, previous work suggests these subclasses might be more susceptible to preanalytical instability [9,34]. Benchmarking quantitative accuracy by standard addition of known compounds may also fail, notably when the added concentration is at the limits of the linear range [35]. While higher variability of results was noted for the highly abundant SM d34:1, the experiment proved useful for comparing the efficacy of different single-point-based quantification approaches. These comparisons of quantitative accuracy supported the use of subclass-specific approaches, as each subclass ultimately requires a different treatment.

Finally, the data-informed selection of internal standards approach is ultimately limited by the availability of internal standards. The more representative an internal standard is of its endogenous target, the more reproducible the quantitation results become. We found that UltimateSPLASH ONE is sufficiently representative of human plasma and serum, though important lipid subclasses should be supplemented, such as acylcarnitines, free fatty acids, hexosylceramides, and ether-linked phospholipids. While cholesteryl esters are included in the SPLASH mix, ionization efficiency at high-flow conditions in the LC-MS ion sources used here prevented reliable quantification in plasma. The UltimateSPLASH ONE mix may be used for other biological matrices but is not optimized for highly abundant lipid species that are outside of the linear range. It also requires further evaluations to avoid isobaric overlaps of endogenous lipids that may co-elute with otherwise reliable ISTDs [36]. While data-informed selection of internal

standards should be agnostic to LC-MS methods, there are a number of factors that contribute to quantitative inaccuracies in data reporting. Therefore, we encourage the development of confidence levels when reporting absolute concentrations in lipidomics studies. Further work should be done to establish rules for data reporting and the building of repositories to promote data transferability across the entire field.

## 3.6 References


(1) Liebisch, G., Ahrends, R., Arita, M., Arita, M., Bowden, J. A., Ejsing, C. S., et al. (2019) Lipidomics needs more standardization. *Nat Metab* **1**, 745–747

(2) Lippa, K. A., Aristizabal-Henao, J.J., Beger, R. D., Bowden, J. A., Broeckling, C., Beecher, C., et al. (2022) Reference materials for MS-based untargeted metabolomics and lipidomics: a review by the metabolomics quality assurance and quality control consortium (mQACC). *Metabolomics* **18**, 24

(3) Ni, Z., Wölk, M., Jukes, G., Espinosa, K. M., Ahrends, R., Aimo, L., et al. (2022) Guiding the choice of informatics software and tools for lipidomics research applications. *Nat Methods* **20**, 193–204

(4) Guo, J., Yu, H., Xing, S., Huan, T. (2022) Addressing big data challenges in mass spectrometry-based metabolomics. *Chem Commun* **58**, 9979-9990

(5) Vvedenskaya, O., Holčapek, M., Vogeser, M., Ekroos, K., Meikle, P. J., Bendt, A.K. (2022) Clinical lipidomics – A community-driven roadmap to translate research into clinical applications. *J Mass Spectrom Adv Clin Lab* **24**, 1-4.

(6) Nilsson, L. B., Eklund, G. (2007) Direct quantification in bioanalytical LC–MS/MS using internal calibration via analyte/stable isotope ratio. *J Pharmaceut Biomed* **43**, 3, 1094-1099

(7) Drotleff, B., Lämmerhofer, M. (2019) Guidelines for Selection of Internal Standard-Based Normalization Strategies in Untargeted Lipidomic Profiling by LC-HR-MS/MS. *Anal Chem* **91**, 15, 9836–9843

(8) Lehmann, R. (2021) From bedside to bench—practical considerations to avoid pre-analytical pitfalls and assess sample quality for high-resolution metabolomics and lipidomics analyses of body fluids. *Anal Bioanal Chem* **413**, 5567–5585

(9) Wang, Q., Hoene, M., Hu, C., Fritsche, L., Ahrends, R., Liebisch, G., et al. (2023) Ex vivo instability of lipids in whole blood: preanalytical recommendations for clinical lipidomics studies. *J Lipid Res* **64**, 6, 100378

(10) Alves dos Santos, A. C., Vuckovic, D. (2024) Current status and advances in untargeted LC-MS tissue lipidomics studies in cardiovascular health. *TrAC, Trends Anal Chem* **170**, 117419

(11) Saigusa, D., Hishinuma, E., Matsukawa, N., Takahashi, M., Inoue, J., Tadaka, S., et al. (2021) Comparison of Kit-Based Metabolomics with Other Methodologies in a Large Cohort, towards Establishing Reference Values. *Metabolites* **11**, 10, 652

(12) Kuhring, M., Eisenberger, A., Schmidt, V., Kränkel, N., Leistner, D.M., Kirwan, J., et al. (2020) Concepts and Software Package for Efficient Quality Control in Targeted Metabolomics Studies: MeTaQuaC. *Anal Chem* **92**, 15, 10241–10245

(13) Yang, K., Han, X. (2011) Accurate Quantification of Lipid Species by Electrospray Ionization Mass Spectrometry – Meets a Key Challenge in Lipidomics. *Metabolites* **1**, 1, 21-40

(14) Drotleff, B., Illison, J., Schlotterbeck, J., Lukowski, R., Lämmerhofer, M. (2019) Comprehensive lipidomics of mouse plasma using class-specific surrogate calibrants and SWATH acquisition for large-scale lipid quantification in untargeted analysis. *Anal Chim*

*Acta* **1086**, 90-102

(15) Cífková, E., Holčapek, M., Lísa, M., Ovčačíková, M., Lyčka, A., Lynen, F., et al. (2012) Nontargeted Quantitation of Lipid Classes Using Hydrophilic Interaction Liquid Chromatography–Electrospray Ionization Mass Spectrometry with Single Internal Standard and Response Factor Approach. *Anal Chem* **84**, 22, 10064–10070

(16) Schoeny, H., Rampler, E., El Abiead, Y., Hildebrand, F., Zach, O., Hermann, G., et al. (2021) A combined flow injection/reversed-phase chromatography–high-resolution mass spectrometry workflow for accurate absolute lipid quantification with 13C internal standards. *Analyst* **146**, 2591-2599

(17) Medina, J., Borreggine, R., Teav, T., Gao, L., Ji, S., Carrard, J., et al. (2023) Omic-Scale High-Throughput Quantitative LC–MS/MS Approach for Circulatory Lipid Phenotyping in Clinical Research. *Anal Chem* **95**, 6, 3168–3179

(18) Overdahl, K. E., Collier, J. B., Jetten, A. M., Jarmusch, A. K. (2023) Signal Response Evaluation Applied to Untargeted Mass Spectrometry Data to Improve Data Interpretability. *J Am Soc Mass Spectrom* **34**, 9, 1941–1948

(19) Bishop, L. M., Shen, T., Fiehn, O. (2023) Improving Quantitative Accuracy in Nontargeted Lipidomics by Evaluating Adduct Formation. *Anal Chem* **95**, 12683-12690

(20) Koelmel, J. P., Kroeger, N. M., Gill, E. L., Ulmer, C. Z., Bowden, J. A,, Patterson, R. E., et al. (2017) Expanding lipidome coverage using LC–MS/MS data-dependent acquisition with automated exclusion list generation. *J Am Soc Mass Spectrom* **28**, 908-917

(21) Tsugawa, H., Cajka, T., Kind, T., Ma, Y., Higgins, B., Ikeda, K., et al. (2015) MS-DIAL: Data-independent MS/MS deconvolution for comprehensive metabolome analysis. *Nat Methods* **12**, 523-526

(22) Kind, T., Liu, K., Lee, D. Y., DeFelice, B., Meissen, J. K., Fiehn, O. (2013) LipidBlast in silico tandem mass spectrometry data-base for lipid identification. *Nat Methods* **10**, 755–758

(23) DeFelice, B. C., Mehta, S. S., Samra, S., Cajka, T., Wancewicz, B., Fahrmann, J.F., et al. (2017) Mass spectral feature list optimizer (MS-FLO): a tool to minimize false positive peak reports in untargeted liquid chromatography-mass spectroscopy (LC–MS) data processing. *Anal Chem* **89**, 3250-3255

(24) Modhave, Y. (2012) Matrix Effect in Bioanalysis: An Overview. *Int J Pharm Phytopharm Res* **1**, 6, 403-405

(25) Bowden, J. A., Heckert, A., Ulmer, C.Z., Yuan M., Zhao, X. H., Zhou, S., et al. (2017) Harmonizing lipidomics: NIST interlaboratory comparison exercise for lipidomics using SRM 1950–Metabolites in Frozen Human Plasma. *J Lipid Res* **58**, 12, 2275-2288

(26) Zhang, N. R., Hatcher, N. G., Kim Ekroos, K., Kedia, K., Kandebo, M., Marcus, J. N., et al. (2022) Validation of a multiplexed and targeted lipidomics assay for accurate quantification of lipidomes. *J Lipid Res* **63**, 6, 100218

(27) Cajka, T., Fiehn, O. (2016) Toward Merging Untargeted and Targeted Methods in Mass Spectrometry-Based Metabolomics and Lipidomics. *Anal Chem* **88**, 1, 524–545

(28) Beger, R. D., Goodacre, R., Jones, C. M., Lippa, K. A., Mayboroda, O. A., O'Neill, D., et al. (2024) Analysis types and quantification methods applied in UHPLC-MS metabolomics research: a tutorial. *Metabolomics* **20**, 95

(29) Köfeler, H. C., Eichmann, T. O., Ahrends, R., Bowden, J. A., Danne-Rasche, N., Dennis, E. A., et al. (2021) Quality control requirements for the correct annotation of lipidomics data. *Nature Commun* **12**, 4771

(30) Koivusalo M., Haimi, P., Heikinheimo, L., Kostiainen, R., Somerharju, P. (2001) Quantitative determination of phospholipid compositions by ESI-MS: effects of acyl chain length, unsaturation, and lipid concentration on instrument response. *J Lipid Res* **42**, 663–672.

(31) Cajka, T., Fiehn, O. (2016) Increasing lipidomic coverage by selecting optimal mobile-phase modifiers in LC–MS of blood plasma. *Metabolomics* **12**, 34

(32) Lange, M., Fedorova, M. (2020) Evaluation of lipid quantification accuracy using HILIC and RPLC MS on the example of NIST® SRM® 1950 metabolites in human plasma. *Anal Bioanal Chem* **412**, 15, 3573–3584

(33) Triebl, A., Burla, B., Selvalatchmanan, J., Oh, J., Tan, S. H., Chan, M. Y., et al. (2020) Shared reference materials harmonize lipidomics across MS-based detection platforms and laboratories. *J Lipid Res* **61**, 1, 105-115

(34) Reis, G. B., Rees, J. C., Ivanova, A. A., Kuklenyik, Z., Drew, N. M., Pirkle, J. L., et al. (2021) Stability of lipids in plasma and serum: Effects of temperature-related storage conditions on the human lipidome. *J Mass Spectrom Adv Clin Lab* **22**, 34-42

(35) Ellison, S. L. R., Thompson M. (2008) Standard additions: myth and reality. *Analyst* **133**, 992-997

(36) Höring, M., Ejsing, C. S., Krautbauer, S., Ertl, V. M., Burkhardt, R., Liebisch G. (2021) Accurate quantification of lipid species affected by isobaric overlap in Fourier-transform mass spectrometry. *J Lipid Res* **62**, 100050

## 3.7 Supplemental Information

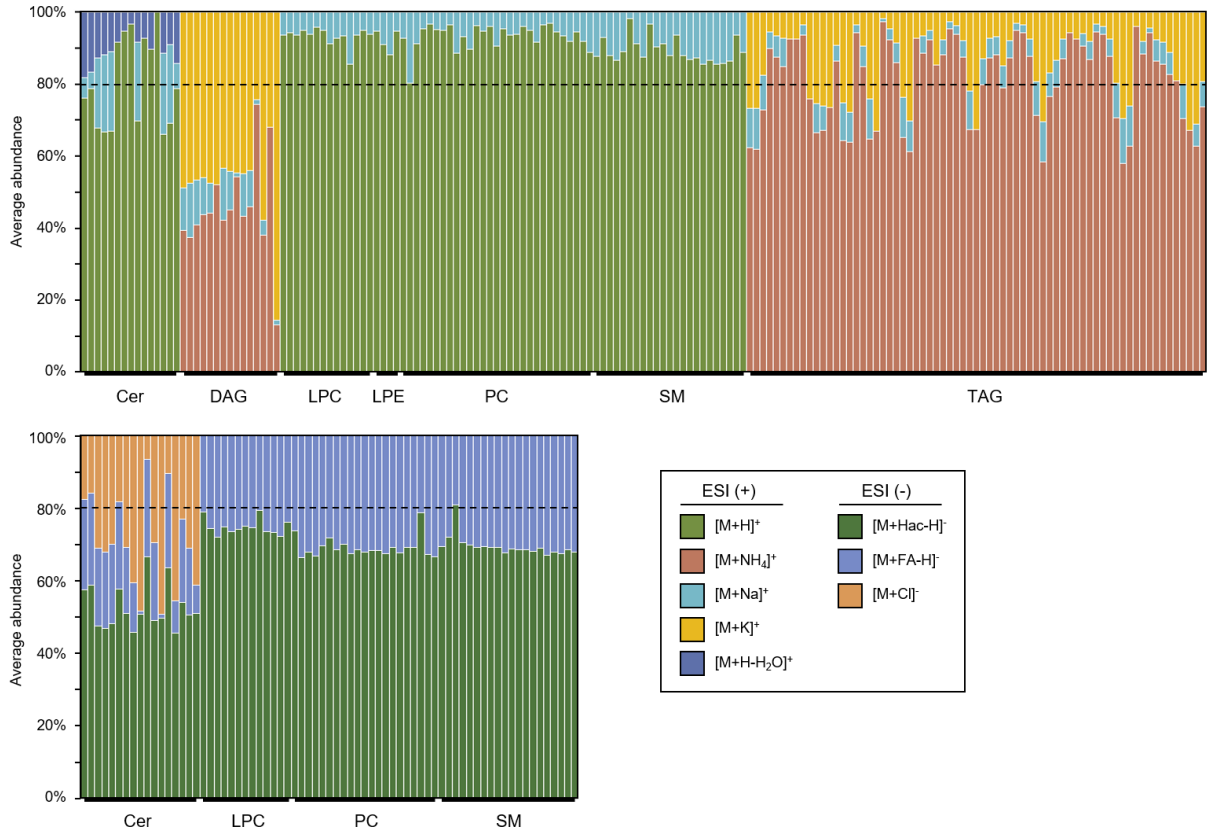


**Figure S-1**: Distribution of adduct species per lipid class in positive (top) and negative (bottom) ionization modes. The marker at 80% represents the threshold for adduct joining.

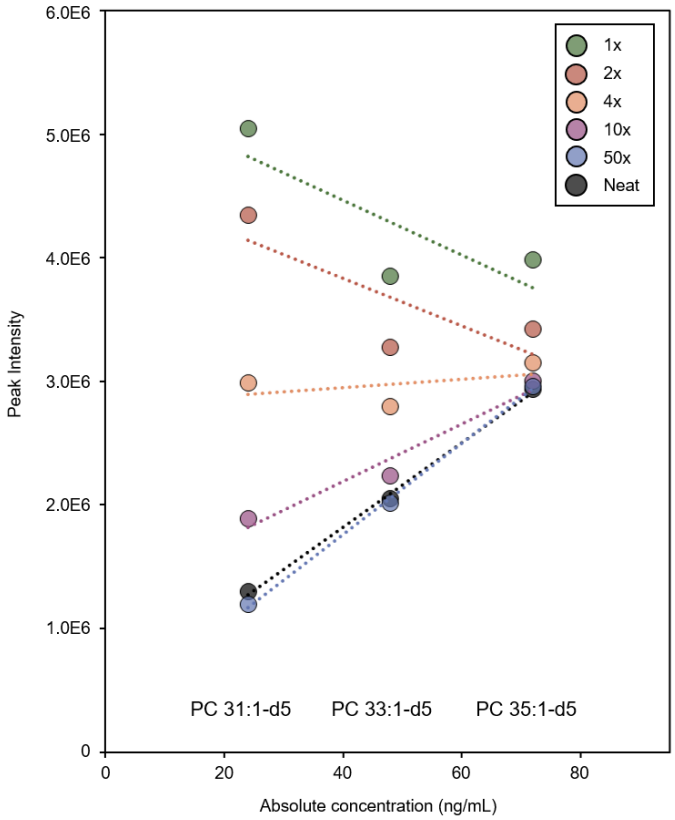


**Figure S-2**: The correction of matrix effects in monounsaturated PC internal standards over multiple dilution levels as compared to the response in method blanks.

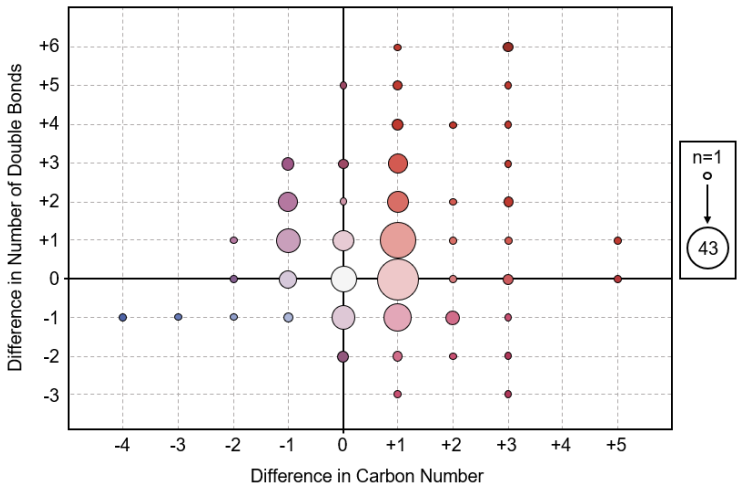


**Figure S-3:** The distribution of structural diversity in endogenous lipids (n=312) when compared to the most structurally-similar labeled internal standard. If the carbon chain length and/or the degree of unsaturation was equally between two standards, the smaller sum composition was used for comparison. Red indicates a larger carbon number and degree of unsaturation in the endogenous lipid and blue indicates a smaller structural composition. The color value is scaled to no structural difference (colorless).

**Table S-1:** List of unlabeled standards purchased from Cayman Chemical and Avanti Polar Lipids.

| Full Lipid Name | Sum Composition | Cayman Chemical ID# | Form |
|---|---|---|---|
| CAR(16:0) | CAR 16:0 | 26553 | Solid |
| Cer(d18:1/16:0) | Cer d34:1 | 10681 | Solid |
| Cer(d18:1/20:0) | Cer d38:1 | 10724 | Solid |
| Cer(d18:1/24:0) | Cer d42:1 | 62535 | Solid |
| DG(18:0/0:0/18:1) | DG 36:1 | 26876 | Solid |
| DG(18:1/0:0/18:1) | DG 36:2 | 26939 | Solid |
| DG(18:2/0:0/18:2) | DG 36:4 | 26983 | Solid |
| DG(18:3/0:0/18:3) | DG 36:6 | 26940 | Solid |
| LPC(18:0) | LPC 18:0 | 35308 | Solid |
| LPC(18:1) | LPC 18:1 | 20959 | Liquid in chloroform |
| LPC(18:2) | LPC 18:2 | 17153 | Liquid in chloroform |
| PC(18:0/18:0) | PC 36:0 | 15100 | Solid |
| PC(18:0/18:1) | PC 36:1 | 38152 | Solid |
| PC(18:1/18:1) | PC 36:2 | 15098 | Solid |
| PC(18:2/18:2) | PC 36:4 | 20954 | Liquid in chloroform |
| PC(P-16:0/16:0) | PC P-32:0 | 28348 | Solid |
| PC(P-18:0/22:6) | PC P-40:6 | 37134 | Liquid in ethanol |
| PC(16:0/9:0(CHO)) | PONPC | Avanti | Solid |
| PC(16:0/5:0(CHO)) | POVPC | Avanti | Solid |
| PE(16:0/20:4) | PE 36:4 | 25660 | Liquid in 30:70 chloroform:MeOH |
| PE(18:0/20:4) | PE 38:4 | 25871 | Liquid in 30:70 chloroform:MeOH |
| SM(d18:1/16:0) | SM d34:1 | 10007946 | Solid |
| TG(16:0/18:2/16:0) | TG 50:2 | 27072 | Solid |
| TG(18:1/16:0/18:1) | TG 52:2 | 26843 | Liquid in hexanes |
| TG(18:0/18:1/18:0) | TG 54:1 | 28864 | Solid |
| TG(18:0/18:2/18:0) | TG 54:2 | 26967 | Solid |
| TG(18:1/18:2/18:1) | TG 54:4 | 26972 | Solid |
| TG(18:1/18:1/20:0) | TG 56:2 | 29060 | Solid |

**Table S-2:** Estimations of matrix factor (eMF) for all lipid species in human plasma. Only compounds with an eMF value derived from a minimum 10x correction are presented.

| Lipid Name | Positive ESI mode | | | Negative ESI mode | | |
|---|---|---|---|---|---|---|
| | RT (min) | 10x eMF | 20x eMF | RT (min) | 10x eMF | 20x eMF |
| CAR 10:0-d3 | 0.224 | 1.00 | | | | |
| CAR 12:0-d3 | 0.282 | 1.00 | 1.05 | | | |
| CAR 18:0-d3 | 0.950 | 1.08 | 1.14 | | | |
| CAR 10:1 | 0.210 | 0.75 | | | | |
| CAR 16:0 | 0.630 | 1.00 | | | | |
| CAR 18:0 | 0.950 | 0.97 | | | | |
| CAR 18:1 | 0.691 | 1.16 | 1.12 | | | |
| CAR 18:2 | 0.515 | 1.12 | | | | |
| Cer d34:2-d7 | 2.039 | 1.19 | 1.31 | 2.028 | 1.17 | 1.47 |
| Cer d36:2-d7 | 2.272 | 1.09 | 1.28 | 2.261 | 1.07 | 1.30 |
| Cer d38:2-d7 | 2.491 | 1.13 | | 2.481 | 1.35 | 1.40 |
| Cer d40:2-d7 | 2.713 | 1.04 | | 2.703 | 1.34 | 1.36 |
| Cer d42:2-d7 | 2.933 | 0.98 | 1.11 | 2.924 | 1.22 | 1.35 |
| Cer d34:1 | 2.252 | 1.18 | | 2.241 | 0.86 | |
| Cer d36:1 | 2.485 | 1.07 | | 2.485 | | |
| Cer d38:1 | 2.725 | 1.01 | | 2.722 | | |
| Cer d40:1 | 2.956 | 1.09 | | 2.949 | 1.04 | |
| Cer d40:2 | 2.712 | 1.13 | | 2.733 | | |
| Cer d41:1 | 3.064 | 1.04 | | 3.055 | 1.01 | |
| Cer d41:2 | 2.842 | 0.98 | | 2.845 | | |
| Cer d42:1 | 3.172 | 0.99 | | 3.162 | 1.76 | 2.17 |
| Cer d42:2 | 2.945 | 1.10 | | 2.947 | 1.15 | |
| DAG 33:1-d5 | 2.572 | 0.86 | | | | |
| DAG 35:1-d5 | 2.800 | 0.76 | | | | |
| DAG 37:3-d5 | 2.661 | 0.88 | | | | |
| DAG 39:4-d5 | 2.720 | 0.92 | | | | |
| DAG 34:1 | 2.682 | 0.75 | | | | |
| DAG 34:2 | 2.495 | 0.77 | | | | |
| DAG 36:2 | 2.713 | 0.81 | | | | |
| DAG 36:3 | 2.517 | 0.83 | | | | |
| DAG 36:4 A | 2.329 | 0.75 | | | | |
| LPC 15:0-d5 | 0.473 | 1.30 | 1.47 | 0.456 | 0.80 | |
| LPC 17:0-d5 | 0.742 | 1.09 | 1.24 | 0.717 | 0.83 | |
| LPC 19:0-d5 | 1.104 | 1.03 | | 1.073 | 0.90 | |
| LPC 14:0 | 0.385 | 1.16 | | 0.367 | | |
| LPC 15:0 | 0.477 | 1.21 | | 0.457 | | |
| LPC 16:0 | 0.594 | 1.57 | 1.86 | 0.573 | 0.82 | 0.84 |
| LPC 16:1 | 0.429 | 1.10 | | 0.411 | | |
| LPC 17:0 | 0.748 | 1.06 | | | | |
| LPC 18:0 A | 0.837 | 1.20 | 1.17 | | | |
| LPC 18:0 B | 0.914 | 1.43 | 1.50 | 0.890 | 0.92 | 0.90 |
| LPC 18:1 | 0.653 | 1.22 | 1.40 | 0.636 | 1.01 | 1.04 |
| LPC 18:2 | 0.472 | 1.26 | 1.37 | 0.460 | 0.98 | 1.00 |
| LPC 20:1 | 0.972 | 1.11 | | 0.940 | | |
| LPC 20:2 | 0.727 | 1.32 | | 0.697 | | |
| LPC 20:3 | 0.554 | 1.12 | 1.31 | 0.534 | 0.82 | |
| LPC 20:4 | 0.454 | 1.22 | 1.32 | 0.439 | 0.94 | |
| LPC 20:5 | 0.356 | 1.40 | | | | |
| LPC 22:5 | 0.518 | 1.13 | | | | |
| LPC 22:6 | 0.430 | 1.10 | | 0.414 | | |
| LPC O-16:0 | 0.714 | 1.48 | 1.76 | 0.682 | 0.85 | |
| LPC O-16:1 | 0.689 | 1.27 | | 0.652 | 0.91 | |
| LPC O-18:0 | 1.076 | 1.27 | | 1.037 | | |

| | | | | | | |
|---|---|---|---|---|---|---|
| LPC O-18:1 | 0.772 | 1.10 | | 0.744 | | |
| LPE 15:0-d5 | 0.478 | 0.99 | | 0.461 | 0.93 | |
| LPE 17:0-d5 | 0.753 | 0.95 | | 0.728 | 0.98 | |
| LPE 19:0-d5 | 1.124 | 0.94 | | 1.091 | 0.90 | |
| LPE 16:0 | 0.601 | 0.92 | | 0.582 | 0.86 | |
| LPE 18:0 | 0.934 | 0.96 | | 0.902 | 1.14 | |
| LPE 18:1 | 0.664 | | | 0.634 | 0.90 | |
| LPE 18:2 | 0.472 | 1.04 | | 0.462 | 0.91 | |
| LPE O-16:1 | 0.695 | | | 0.671 | 0.89 | |
| LPE O-18:1 | 1.054 | 0.98 | | 1.025 | 0.89 | |
| PC 31:1-d5 | 1.923 | 2.89 | 4.01 | 1.914 | 0.45 | |
| PC 33:1-d5 | 2.140 | 1.86 | 2.07 | 2.130 | 0.44 | |
| PC 35:1-d5 | 2.368 | 1.43 | 1.74 | 2.358 | 0.64 | |
| PC 37:3-d5 | 2.241 | 1.87 | 2.24 | 2.224 | 0.33 | |
| PC 39:4-d5 | 2.304 | 1.81 | | 2.296 | 0.33 | |
| PC 32:0 | 2.231 | 1.77 | 2.06 | 2.216 | 0.47 | |
| PC 32:1 | 2.031 | 1.93 | 2.20 | 2.013 | | |
| PC 32:2 | 1.857 | 1.06 | | 1.839 | | |
| PC 33:1 | 2.138 | 1.48 | | 2.118 | | |
| PC 34:0 | 2.463 | 1.52 | | 2.457 | | |
| PC 34:1 | 2.251 | 1.80 | 2.15 | 2.240 | 0.34 | 0.28 |
| PC 34:2 | 2.072 | 1.60 | 2.11 | 2.056 | 0.32 | |
| PC 34:3 | 1.911 | 2.66 | 4.49 | 1.892 | | |
| PC 35:1 | 2.360 | 1.57 | | 2.354 | | |
| PC 35:2 | 2.179 | 1.63 | 1.74 | 2.158 | | |
| PC 35:4 | 1.924 | | | 1.907 | 0.92 | |
| PC 36:1 | 2.481 | 1.52 | 1.56 | 2.472 | 0.51 | 0.49 |
| PC 36:2 | 2.293 | 1.70 | 1.99 | 2.283 | 0.39 | 0.32 |
| PC 36:3 | 2.120 | 1.85 | 2.12 | 2.111 | 0.41 | 0.37 |
| PC 36:4 A | 1.925 | 2.75 | 4.46 | 1.905 | 0.79 | |
| PC 36:4 B | 2.035 | 1.97 | 2.37 | 2.023 | 0.36 | 0.32 |
| PC 36:5 A | 1.896 | 2.67 | 4.39 | 1.843 | 0.71 | |
| PC 37:4 | 2.139 | 2.06 | | | | |
| PC 38:2 | 2.497 | 1.20 | | 2.501 | | |
| PC 38:3 | 2.356 | 1.54 | 1.79 | 2.350 | 0.47 | 0.46 |
| PC 38:4 | 2.258 | 1.88 | 2.26 | 2.248 | 0.34 | 0.28 |
| PC 38:5 | 2.047 | 1.92 | 2.47 | 2.035 | 0.35 | 0.29 |
| PC 38:6 A | 1.898 | 2.75 | 4.13 | | | |
| PC 38:6 B | 1.973 | 2.00 | 2.18 | 1.960 | 0.41 | 0.35 |
| PC 40:4 | 2.419 | 1.26 | | 2.407 | | |
| PC 40:5 | 2.347 | 1.72 | | 2.336 | | |
| PC 40:6 | 2.188 | 1.63 | 1.88 | 2.174 | 0.51 | |
| PC O-32:0 | 2.370 | 1.54 | | | | |
| PC O-32:1 B | 2.348 | 1.85 | | 2.323 | | |
| PC O-34:1 | 2.384 | 1.47 | | 2.375 | | |
| PC O-34:2 | 2.367 | 1.64 | | 2.187 | | |
| PC O-34:3 | 2.180 | 1.83 | 1.89 | 2.152 | 0.52 | |
| PC O-36:3 | 2.387 | 1.37 | | | | |
| PC O-36:4 | 2.166 | 1.89 | 2.04 | 2.150 | 0.52 | |
| PC O-36:5 B | 2.130 | 2.00 | 2.40 | 2.110 | 0.48 | |
| PC O-38:4 | 2.396 | 1.44 | | 2.379 | | |
| PC O-38:5 A | 2.180 | 1.83 | 1.98 | 2.158 | 0.51 | |
| PC O-38:5 B | 2.351 | 1.79 | | | | |
| PC O-38:6 | 2.118 | 2.00 | | | | |
| PE 31:1-d5 | 1.972 | 1.19 | | 1.955 | 0.58 | |
| PE 33:1-d5 | 2.192 | 1.12 | | 2.171 | 0.53 | |
| PE 35:1-d5 | 2.425 | 1.03 | | 2.401 | 0.62 | |
| PE 37:3-d5 | | | | 2.272 | 0.39 | |
| PE 39:4-d5 | | | | 2.336 | 0.62 | |

| | | | | | | |
|---|---|---|---|---|---|---|
| PE 34:2 | 2.119 | 1.31 | | 2.102 | | |
| PE 36:2 | 2.344 | 1.15 | | 2.324 | 0.53 | |
| PE 36:4 | 2.080 | 1.35 | | 2.064 | | |
| PE 38:4 | 2.310 | 1.38 | | 2.291 | 0.61 | |
| PE 38:6 | 2.019 | 1.31 | | 1.999 | | |
| PE O-38:7 | 2.114 | 1.29 | | 2.090 | 0.59 | |
| PE O-40:7 | 2.337 | 1.23 | | 2.319 | | |
| PE P-34:2 | 2.223 | 1.25 | | | | |
| PE P-36:2 | 2.451 | 1.03 | | 2.428 | 0.67 | |
| PE P-36:4 | 2.182 | 1.19 | | 2.161 | 0.53 | |
| PE P-38:5 | 2.195 | 1.17 | | 2.175 | 0.59 | |
| PI 31:1-d5 | 1.712 | 0.76 | | | | |
| PI 33:1-d5 | 1.909 | 4.14 | | 1.823 | 0.88 | |
| PI 35:1-d5 | 2.122 | 1.35 | | 2.020 | 0.49 | |
| PI 37:3-d5 | 2.005 | 1.06 | | 1.908 | 1.05 | |
| PI 39:4-d5 | 2.072 | 0.97 | | 1.972 | 0.63 | |
| PI 34:2 | 1.848 | | | 1.758 | 0.74 | |
| PI 36:1 | | | | 2.125 | 0.68 | |
| PI 36:2 | | | | 1.951 | 0.58 | 0.60 |
| PI 36:4 | 1.819 | | | 1.741 | 0.78 | |
| PI 38:4 | 2.024 | 1.21 | 1.28 | 1.926 | 0.80 | 0.78 |
| SM d34:2-d9 | 1.789 | 1.07 | | 1.778 | 0.75 | |
| SM d36:2-d9 | 2.011 | 1.92 | | 1.996 | 0.49 | |
| SM d38:2-d9 | 2.229 | 1.73 | | 2.208 | 0.42 | |
| SM d40:2-d9 | 2.449 | 1.39 | | 2.436 | 0.51 | |
| SM d42:2-d9 | 2.674 | 1.43 | | 2.661 | 0.59 | |
| SM d32:1 | 1.758 | 1.09 | 1.18 | 1.737 | 0.95 | |
| SM d33:1 | 1.883 | 1.73 | | 1.847 | 0.67 | |
| SM d34:0 | 2.068 | 1.80 | | 2.052 | | |
| SM d34:1 | 1.981 | 1.80 | 1.89 | 1.968 | 0.43 | 0.39 |
| SM d34:2 | 1.788 | 1.12 | 1.16 | 1.771 | 0.87 | |
| SM d35:1 | 2.097 | 1.95 | | | | |
| SM d35:2 | 1.908 | 1.53 | | | | |
| SM d36:0 | 2.305 | 2.14 | | 2.294 | | |
| SM d36:1 | 2.218 | 1.62 | 1.75 | 2.202 | 0.50 | 0.47 |
| SM d36:2 | 2.013 | 1.93 | 2.08 | 1.995 | 0.49 | |
| SM d38:1 | 2.457 | 1.34 | 1.47 | 2.440 | 0.58 | |
| SM d38:2 | 2.242 | 1.88 | | 2.220 | | |
| SM d39:1 | 2.577 | 0.97 | | 2.559 | 0.62 | |
| SM d40:1 | 2.689 | 1.49 | 1.55 | 2.677 | 0.59 | 0.55 |
| SM d40:2 | 2.467 | 1.44 | 1.57 | 2.452 | 0.50 | |
| SM d40:3 | 2.249 | 1.94 | | | | |
| SM d40:7 | 1.532 | 1.07 | | | | |
| SM d41:1 | 2.806 | 0.97 | 1.18 | 2.789 | 0.84 | |
| SM d41:2 | 2.584 | 1.03 | 1.16 | 2.560 | 0.60 | |
| SM d42:1 | 2.918 | 0.98 | 1.12 | 2.901 | 0.83 | 0.81 |
| SM d42:2 | 2.678 | 1.48 | 1.52 | 2.663 | 0.59 | 0.53 |
| SM d42:3 | 2.474 | 1.49 | 1.61 | 2.454 | 0.51 | 0.50 |
| SM d42:4 | 2.279 | 1.89 | | | | |
| SM d43:2 | 2.770 | 1.02 | | | | |
| TAG 41:0-d5 | 3.449 | 1.17 | | | | |
| TAG 43:1-d5 | 3.452 | 0.87 | 1.16 | | | |
| TAG 45:1-d5 | 3.626 | 0.95 | 1.07 | | | |
| TAG 47:1-d5 | 3.798 | 1.11 | 1.41 | | | |
| TAG 49:1-d5 | 3.948 | 1.25 | 1.79 | | | |
| TAG 51:2-d5 | 3.954 | 1.17 | 1.52 | | | |
| TAG 53:3-d5 | 3.949 | 1.05 | 1.88 | | | |
| TAG 55:4-d5 | 3.962 | 1.14 | | | | |
| TAG 57:4-d5 | 4.070 | 1.00 | 1.31 | | | |

| | | | | |
|---|---|---|---|---|
| TAG 42:0 | 3.564 | 1.09 | | |
| TAG 42:1 | 3.394 | 1.37 | | |
| TAG 44:0 | 3.722 | 1.29 | | |
| TAG 44:1 | 3.568 | 0.84 | | |
| TAG 44:2 | 3.415 | 1.15 | | |
| TAG 46:0 | 3.876 | 0.82 | 0.90 | |
| TAG 46:1 | 3.730 | 1.14 | 1.16 | |
| TAG 46:2 | 3.587 | 0.79 | 0.82 | |
| TAG 46:3 | 3.435 | 1.34 | | |
| TAG 48:1 | 3.882 | 1.14 | 1.14 | |
| TAG 48:2 | 3.745 | 1.19 | 1.31 | |
| TAG 48:3 | 3.600 | 0.83 | | |
| TAG 48:4 | 3.446 | 1.42 | | |
| TAG 49:1 | 3.959 | 0.89 | 0.85 | |
| TAG 49:2 | 3.825 | 0.71 | 0.65 | |
| TAG 50:1 | 4.027 | 1.03 | 1.23 | |
| TAG 50:2 | 3.894 | 1.10 | 1.21 | |
| TAG 50:3 | 3.753 | 1.24 | 1.44 | |
| TAG 50:4 | 3.611 | 0.90 | 1.05 | |
| TAG 50:5 | 3.482 | 1.40 | | |
| TAG 51:1 | 4.101 | 1.25 | 1.32 | |
| TAG 51:2 | 3.967 | 0.99 | 1.19 | |
| TAG 51:3 | 3.833 | 1.00 | 1.24 | |
| TAG 51:4 | 3.695 | 1.21 | | |
| TAG 52:1 | 4.164 | 1.67 | 1.74 | |
| TAG 52:2 | 4.027 | 0.97 | 1.18 | |
| TAG 52:3 | 3.899 | 1.04 | 1.20 | |
| TAG 52:4 | 3.763 | 1.19 | 1.35 | |
| TAG 52:5 | 3.639 | 0.99 | 0.94 | |
| TAG 52:6 | 3.533 | 0.90 | | |
| TAG 53:2 | 4.104 | 1.27 | 1.37 | |
| TAG 53:3 | 3.971 | 1.08 | 1.83 | |
| TAG 53:4 | 3.844 | 1.19 | | |
| TAG 54:1 | 4.298 | 1.01 | | |
| TAG 54:2 | 4.164 | 1.58 | 1.72 | |
| TAG 54:3 | 4.033 | 1.00 | 1.18 | |
| TAG 54:4 | 3.908 | 1.05 | 1.18 | |
| TAG 54:5 | 3.767 | 1.11 | 1.20 | |
| TAG 54:6 | 3.628 | 0.84 | 0.67 | |
| TAG 54:7 A | 3.494 | 1.13 | | |
| TAG 54:7 B | 3.605 | 0.91 | | |
| TAG 56:2 | 4.293 | 1.09 | | |
| TAG 56:3 | 4.165 | 1.67 | | |
| TAG 56:4 | 4.068 | 1.31 | | |
| TAG 56:5 | 3.967 | 1.10 | 1.99 | |
| TAG 56:6 | 3.870 | 1.13 | 1.52 | |
| TAG 56:7 | 3.726 | 1.37 | 1.77 | |
| TAG 56:8 A | 3.565 | 1.13 | | |
| TAG 56:8 B | 3.642 | 1.35 | | |
| TAG 58:6 | 3.965 | 0.95 | | |
| TAG 58:9 | 3.657 | 1.64 | | |

**Table S-3:** Comparison of response factors generated by internal standards (ISTD) and response factors from endogenous lipids measured in NIST SRM 1950.

| Reference lipid | Target lipid | Acquisition mode | RF from NIST SRM 1950 | Structural difference | RF from ISTD |
|---|---|---|---|---|---|
| Cer d41:1 | Cer d42:2 | ESI(+) | 1.03 | +1C+1DB | 1.07 |
| Cer d34:1 | Cer d38:1 | ESI(-) | 1.51 | +4C | 1.41 |
| Cer d38:1 | Cer d42:2 | ESI(-) | 1.25 | +4C+1DB | 1.22 |
| Cer d34:1* | Cer d42:2* | ESI(-) | 1.89 | +8C+1DB | 1.92 |
| LPC 16:0 | LPC 18:0 | ESI(+) | 1.12 | +2C | 1.19 |
| LPC 18:0 | LPC 20:0 | ESI(+) | 0.93 | +2C | 1.19 |
| LPC 20:0 | LPC 22:4 | ESI(+) | 0.86 | +2C+4DB | 1.19 |
| LPC O-16:0 | LPC O-18:0 | ESI(+) | 1.20 | +2C | 1.19 |
| LPC 16:0* | LPC 22:4* | ESI(+) | 1.50 | +6C+4DB | 1.61 |
| LPC 16:0 | LPC 18:0 | ESI(-) | 1.06 | +2C | 1.05 |
| LPE 18:2 | LPE 20:4 | ESI(+) | 1.04 | +2C+2DB | 1.00 |
| LPE 20:4 | LPE 22:6 | ESI(+) | 0.98 | +2C+2DB | 1.00 |
| LPE 18:2* | LPE 22:6* | ESI(+) | 1.02 | +4C+4DB | 1.00 |
| PC 34:0 | PC 36:1 | ESI(+) | 1.02 | +2C+1DB | 1.14 |
| PC 36:1 | PC 36:4 | ESI(+) | 0.93 | +3DB | 1.07 |
| PC 36:4 | PC 38:3 | ESI(+) | 1.17 | +2C-1DB | 1.14 |
| PC 38:3 | PC 38:4 | ESI(+) | 0.86 | +1DB | 1.00 |
| PC O-32:1 | PC O-34:3 | ESI(+) | 0.71 | +2C+2DB | 1.14 |
| PC O-34:3 | PC O-38:5 | ESI(+) | 1.04 | +4C+2DB | 1.31 |
| PC O-38:5 | PC O-40:7 | ESI(+) | 1.04 | +2C+2DB | 1.14 |
| PC 34:0* | PC O-40:7* | ESI(+) | 0.79 | +6C+7DB | 1.39 |
| PC 36:1 | PC 36:5 | ESI(-) | 1.27 | +4DB | 1.11 |
| PC 36:5 | PC 38:3 | ESI(-) | 1.30 | +2C-2DB | 1.23 |
| PC 38:3 | PC 38:4 | ESI(-) | 0.97 | +1DB | 1.00 |
| PC 38:4 | PC 40:4 | ESI(-) | 1.00 | +2C | 1.23 |
| PC 40:4 | PC 40:8 | ESI(-) | 0.82 | +4DB | 1.11 |
| PC O-36:4 | PC O-36:5 | ESI(-) | 0.91 | +1DB | 1.00 |
| PC O-36:5 | PC O-38:5 | ESI(-) | 1.08 | +2C | 1.23 |
| PC 36:1* | PC O-38:5* | ESI(-) | 1.77 | +2C+4DB | 1.37 |
| PE 34:1 | PE 34:2 | ESI(+) | 0.93 | +1DB | 1.00 |
| PE 34:2 | PE 38:4 | ESI(+) | 1.16 | +4C+2DB | 1.19 |
| PE 34:1* | PE 38:4* | ESI(+) | 1.07 | +4C+3DB | 1.30 |
| SM d36:1 | SM d37:1 | ESI(+) | 1.00 | +1C | 1.08 |
| SM d37:1 | SM d38:2 | ESI(+) | 0.96 | +1C+1DB | 1.08 |
| SM d38:2 | SM d40:3 | ESI(+) | 1.02 | +2C+1DB | 1.17 |
| SM d40:3 | SM d41:1 | ESI(+) | 1.28 | +1C-2DB | 1.08 |
| SM d41:1 | SM d42:2 | ESI(+) | 1.00 | +1C+1DB | 1.08 |
| SM d42:2 | SM d43:3 | ESI(+) | 0.95 | +1C+1DB | 1.08 |
| SM d36:1* | SM d43:3* | ESI(+) | 1.68 | +7C+2DB | 1.72 |
| SM d32:1 | SM d34:1 | ESI(-) | 1.32 | +4C | 1.22 |

| | | | | | |
|---|---|---|---|---|---|
| SM d34:1 | SM d36:1 | ESI(-) | 1.21 | +4C | 1.22 |
| SM d36:1 | SM d36:2 | ESI(-) | 0.94 | +1DB | 1.00 |
| SM d36:2 | SM d40:2 | ESI(-) | 1.24 | +4C | 1.29 |
| SM d40:2 | SM d42:2 | ESI(-) | 1.13 | +2C | 1.13 |
| SM d42:2 | SM d42:3 | ESI(-) | 0.90 | +1DB | 1.00 |
| SM d32:1* | SM d42:3* | ESI(-) | 1.88 | +10C+2DB | 2.10 |
| TAG 42:0 | TAG 42:1 | ESI(+) | 0.95 | +1DB | 1.00 |
| TAG 42:1 | TAG 44:0 | ESI(+) | 1.11 | +2C-1DB | 1.00 |
| TAG 44:0 | TAG 46:1 | ESI(+) | 0.99 | +2C+1DB | 1.00 |
| TAG 46:1 | TAG 48:2 | ESI(+) | 0.99 | +2C+1DB | 1.00 |
| TAG 48:2 | TAG 48:3 | ESI(+) | 1.00 | +1DB | 1.00 |
| TAG 48:3 | TAG 49:0 | ESI(+) | 0.98 | +1C-3DB | 1.00 |
| TAG 49:0 | TAG 49:1 | ESI(+) | 0.85 | +1DB | 1.00 |
| TAG 49:1 | TAG 49:2 | ESI(+) | 1.15 | +1DB | 1.00 |
| TAG 49:2 | TAG 49:3 | ESI(+) | 1.06 | +1DB | 1.00 |
| TAG 49:3 | TAG 51:2 | ESI(+) | 0.84 | +2C-1DB | 1.00 |
| TAG 51:2 | TAG 52:1 | ESI(+) | 0.96 | +1C-1DB | 1.00 |
| TAG 52:1 | TAG 53:2 | ESI(+) | 1.08 | +1C+1DB | 1.00 |
| TAG 53:2 | TAG 53:3 | ESI(+) | 0.97 | +1DB | 1.00 |
| TAG 53:3 | TAG 54:4 | ESI(+) | 1.08 | +1C+1DB | 1.00 |
| TAG 54:4 | TAG 54:5 | ESI(+) | 1.10 | +1DB | 1.00 |
| TAG 54:5 | TAG 56:2 | ESI(+) | 0.93 | +2C-3DB | 1.00 |
| TAG 56:2 | TAG 56:4 | ESI(+) | 0.99 | +2DB | 1.00 |
| TAG 56:4 | TAG 56:5 | ESI(+) | 0.94 | +1DB | 1.00 |
| TAG 56:5 | TAG 56:8 | ESI(+) | 1.11 | +3DB | 1.00 |
| TAG 42:0* | TAG 56:8* | ESI(+) | 1.02 | +14C+8DB | 1.00 |

*Indicates the response factor determination for the largest structural difference in a subclass.

**Table S-4:** Comparison of four approaches to quantifying lipids (ng/mL ± SD) using the standard addition of known compounds into human plasma.

| Lipid Name | Acquisition mode | Standard addition concentration (ng/mL) | Subclass-specific matching | Single Point Quant. | RT-based matching | Structure-based matching |
|---|---|---|---|---|---|---|
| CAR 16:0 | ESI (+) | 1.20 | 0.97 ± 0.05 | 0.91 ± 0.02 | 0.91 ± 0.02 | 0.91 ± 0.02 |
| Cer d34:1 | ESI (+) | 24.0 | 25.1 ± 8.7 | 54.6 ± 18.9 | 38.8 ± 13.4 | 25.1 ± 8.7 |
| | ESI (-) | 24.0 | 29.1 ± 4.1 | 57.6 ± 8.2 | 40.5 ± 5.8 | 29.1 ± 4.1 |
| Cer d38:1 | ESI (+) | 24.0 | 24.7 ± 3.9 | 25.9 ± 4.1 | 25.9 ± 4.1 | 24.7 ± 3.9 |
| | ESI (-) | 24.0 | 23.5 ± 4.1 | 29.0 ± 5.0 | 29.0 ± 5.0 | 23.5 ± 4.1 |
| Cer d42:1 | ESI (+) | 24.0 | 23.8 ± 6.0 | 19.5 ± 4.9 | 23.8 ± 6.0 | 23.8 ± 6.0 |
| | ESI (-) | 24.0 | 36.2 ± 6.5 | 33.8 ± 6.1 | 36.2 ± 6.5 | 36.2 ± 6.5 |
| DG 36:1 | ESI (+) | 24.0 | 24.8 ± 5.2 | 26.9 ± 5.7 | 26.9 ± 5.7 | 26.9 ± 5.7 |
| DG 36:2 | ESI (+) | 24.0 | 26.3 ± 13.8 | 38.7 ± 20.4 | 5.0 ± 2.6 | 6.2 ± 3.3 |
| DG 36:4 | ESI (+) | 24.0 | 23.8 ± 4.0 | 138 ± 22.9 | 231 ± 38.4 | 31.9 ± 5.3 |
| DG 36:6 | ESI (+) | 24.0 | 18.3 ± 1.1 | 88.6 ± 7.9 | 151 ± 10.7 | 21.6 ± 1.3 |
| LPC 18:0 | ESI (+) | 24.0 | 24.6 ± 2.5 | 18.9 ± 2.0 | 18.9 ± 2.0 | 27.3 ± 2.8 |
| | ESI (-) | 24.0 | 23.1 ± 3.5 | 23.2 ± 3.5 | 23.2 ± 3.5 | 24.1 ± 3.7 |
| LPC 18:1 | ESI (+) | 24.0 | 46.6 ± 10.0 | 41.6 ± 8.9 | 41.6 ± 8.9 | 85.7 ± 18.4 |
| | ESI (-) | 24.0 | 24.3 ± 1.6 | 23.1 ± 1.6 | 23.1 ± 1.6 | 23.0 ± 1.6 |
| LPC 18:2 | ESI (+) | 24.0 | 26.8 ± 13.0 | 19.0 ± 9.2 | 19.2 ± 9.3 | 49.0 ± 23.7 |
| | ESI (-) | 24.0 | 23.3 ± 4.5 | 24.0 ± 4.6 | 20.3 ± 3.9 | 33.5 ± 6.5 |
| PC 36:0 | ESI (+) | 48.0 | 45.1 ± 3.0 | 45.2 ± 3.0 | 45.2 ± 3.0 | 45.2 ± 3.0 |
| PC 36:1 | ESI (+) | 48.0 | 47.1 ± 10.9 | 47.1 ± 10.9 | 47.1 ± 10.9 | 47.1 ± 10.9 |
| | ESI (-) | 48.0 | 48.5 ± 7.1 | 56.4 ± 8.3 | 56.4 ± 8.3 | 56.4 ± 8.3 |
| PC 36:2 | ESI (+) | 48.0 | 72.0 ± 5.7 | 269 ± 20.4 | 165 ± 12.0 | 75.8 ± 5.7 |
| | ESI (-) | 48.0 | 57.2 ± 11.1 | 145 ± 27.8 | 249 ± 47.8 | 61.5 ± 11.8 |
| PC 36:4 | ESI (+) | 48.0 | 47.0 ± 3.5 | 175 ± 33.9 | 39.5 ± 2.9 | 123 ± 9.1 |
| | ESI (-) | 48.0 | 46.2 ± 7.2 | 40.5 ± 6.3 | 29.1 ± 4.5 | 113 ± 17.6 |
| PC P-32:0 | ESI (+) | 24.0 | 16.8 ± 2.9 | 17.7 ± 3.1 | 17.7 ± 3.1 | 13.0 ± 2.3 |
| | ESI (-) | 24.0 | 24.7 ± 8.0 | 15.5 ± 5.0 | 15.5 ± 5.0 | 15.6 ± 5.0 |
| PC P-40:6 | ESI (+) | 24.0 | 5.9 ± 0.34 | 8.5 ± 0.31 | 6.9 ± 0.39 | 6.9 ± 0.39 |
| PC 21:1;O (POVPC) | ESI (+) | 2.40 | 3.18 ± 0.78 | 4.3 ± 0.99 | 0.98 ± 0.23 | 0.98 ± 0.23 |
| PC 25:1;O (PONPC) | ESI (+) | 2.40 | 2.21 ± 0.51 | 3.5 ± 0.80 | 1.09 ± 0.25 | 1.09 ± 0.25 |
| PE 36:4 | ESI (+) | 24.0 | 17.7 ± 1.3 | 8.4 ± 1.2 | 9.4 ± 1.5 | 8.4 ± 1.2 |
| | ESI (-) | 24.0 | 10.4 ± 1.8 | 7.3 ± 1.1 | 8.8 ± 1.5 | 12.3 ± 2.5 |
| PE 38:4 | ESI (+) | 24.0 | 28.6 ± 2.1 | 12.5 ± 2.4 | 12.5 ± 2.4 | 12.5 ± 2.4 |
| | ESI (-) | 24.0 | 25.6 ± 5.3 | 7.6 ± 1.5 | 19.7 ± 4.1 | 14.6 ± 3.7 |
| SM d34:1 | ESI (+) | 24.0 | 29.7 ± 5.3 | 170 ± 30.4 | 1.4 ± 0.25 | 109 ± 17.1 |
| | ESI (-) | 24.0 | 27.0 ± 7.0 | 69.2 ± 18.0 | 31.1 ± 8.1 | 29.9 ± 7.7 |
| TG 50:2 | ESI (+) | 48.0 | 46.1 ± 10.6 | 63.9 ± 14.7 | 63.9 ± 14.7 | 46.1 ± 10.6 |
| TG 52:2 | ESI (+) | 48.0 | 42.4 ± 9.8 | 19.4 ± 4.5 | 42.8 ± 9.8 | 42.4 ± 9.8 |
| TG 54:1 | ESI (+) | 48.0 | 28.2 ± 6.7 | 32.5 ± 8.0 | 4.5 ± 1.0 | 32.5 ± 8.0 |
| TG 54:2 | ESI (+) | 48.0 | 44.2 ± 10.2 | 73.5 ± 28.9 | 19.9 ± 3.1 | 44.2 ± 10.2 |
| TG 54:4 | ESI (+) | 48.0 | 49.8 ± 13.7 | 101 ± 13.5 | 101 ± 13.5 | 23.4 ± 5.4 |
| TG 56:2 | ESI (+) | 48.0 | 49.1 ± 2.9 | 56.4 ± 3.6 | 15.9 ± 1.9 | 15.9 ± 1.9 |

## Appendix: Additional Projects

In addition to the work presented in the main text, I contributed to other projects in the lab that played a notable role in my graduate studies. My first official project was the nontargeted analysis of mouse tissue samples for the Longevity Consortium. I performed sample preparation, data acquisition, and data curation for nearly 1,000 white adipose tissue samples. This experience, as my initial introduction to nontargeted metabolomics and lipidomics using LC-HRMS/MS, was instrumental in developing my understanding of working with large-scale data. The curation of these datasets as part of the larger consortium study also highlighted the need for further standardization and reproducibility in our workflows, and subsequently inspired my evaluations of adduct formation trends (Chapter 2). Many new skills were developed during this project, including nontargeted data acquisition by HILIC- and RPLC-MS/MS, LC troubleshooting, metabolite identification and annotation, data curation, and batch normalization practices.

Another notable side project was in collaboration with Prof. Enkhmaa Byambaa – the detection and quantification of oxidized phospholipids (OxPL) in lipoprotein (a) (Lp(a)) via nontargeted LC-MS. I played a primary role in preliminary test studies to determine the suitable sample processing for optimal OxPL detection , as well as performed the large-scale study analysis for more than 2,500 purified Lp(a) samples. While I was well-versed in nontargeted analyses by this point, this project still presented new challenges . First, the purification process of Lp(a) resulted in highly variable instrument responses across triplicate samples, raising concerns about its fitness for the intended biological applications. Our efforts to correct for this irreproducibility, led by Dr. Tong Shen, were successful with the normalization of OxPL responses to the total triacylglycerol abundance in each sample. The second challenge arose during the acquisition of the real study samples, with a comparatively higher signal intensity to the original test samples

and a large unknown contaminant eluting with the void volume and into the first several seconds of the analysis. Although we suspected the source of interference to be residual protein, the pre-prepared samples limited our ability to make major adjustments to the analysis. Therefore, I employed a few of strategies to improve data quality: (1) Cold 10-min centrifugation of samples prior to analysis, (2) Adjustment of autosampler needle height, (3) Maintenance of the ESI source (e.g. changing the probe needle, cleaning the ion transfer tube) when more than 20% of the signal intensity was lost. Because of these interventions, we were able to obtain reliable results in batches that could be successfully normalized to meet our data quality standards.

The final contributions I wish to present here are not tied to a specific project, but rather reflect my ongoing collaboration with the West Coast Metabolomics Center core lab to improve our nontargeted workflows. Throughout my Ph.D. training, I focused on curating robust lipidomics data, developing a deep understanding of where errors and inaccuracies can arise in our workflows. This has culminated into regular presentations of data aimed at promoting improved practices for data curation. To highlight a few, I have promoted the evaluation of adduct formation trends and developed guidelines for adduct joining. I have also reviewed our methods for occurrences of isobaric overlap and proposed approaches for identifying and correcting these interferences. Lastly, I have provided guidance on selecting internal standards for the single-point quantification of lipids, based on results from numerous core studies, and proposed confidence thresholds for data reporting. All of these examples, along with those presented in the preceding chapters, reflect my graduate work aimed at process improvement for quantitative reproducibility in nontargeted lipidomics.